catalysts

MDPI

Review

Recent Advances in Endocrine Disrupting Compounds Degradation through Metal Oxide-Based Nanomaterials

Claudio Imparato [1], Aurelio Bifulco [1], Brigida Silvestri [1] and Giuseppe Vitiello [1,2,*]

[1] Department of Chemical, Materials and Production Engineering, University of Naples Federico II, 80125 Naples, NA, Italy; claudio.imparato@unina.it (C.I.); aurelio.bifulco@unina.it (A.B.); brigida.silvestri@unina.it (B.S.)
[2] CSGI, Center for Colloid and Surface Science, Via della Lastruccia 3, 50019 Sesto Fiorentino, FI, Italy
* Correspondence: giuseppe.vitiello@unina.it; Tel.: +39-081-768-5975

Abstract: Endocrine Disrupting Compounds (EDCs) comprise a class of natural or synthetic molecules and groups of substances which are considered as emerging contaminants due to their toxicity and danger for the ecosystems, including human health. Nowadays, the presence of EDCs in water and wastewater has become a global problem, which is challenging the scientific community to address the development and application of effective strategies for their removal from the environment. Particularly, catalytic and photocatalytic degradation processes employing nanostructured materials based on metal oxides, mainly acting through the generation of reactive oxygen species, are widely explored to eradicate EDCs from water. In this review, we report the recent advances described by the major publications in recent years and focused on the degradation processes of several classes of EDCs, such as plastic components and additives, agricultural chemicals, pharmaceuticals, and personal care products, which were realized by using novel metal oxide-based nanomaterials. A variety of doped, hybrid, composite and heterostructured semiconductors were reported, whose performances are influenced by their chemical, structural as well as morphological features. Along with photocatalysis, alternative heterogeneous advanced oxidation processes are in development, and their combination may be a promising way toward industrial scale application.

Keywords: endocrine disruptors; metal oxides; nanomaterials; nanostructured catalysts; photocatalysis; degradation

Citation: Imparato, C.; Bifulco, A.; Silvestri, B.; Vitiello, G. Recent Advances in Endocrine Disrupting Compounds Degradation through Metal Oxide-Based Nanomaterials. *Catalysts* **2022**, *12*, 289. https://doi.org/10.3390/catal12030289

Academic Editor: Adam F. Lee

Received: 5 February 2022
Accepted: 1 March 2022
Published: 3 March 2022

1. Introduction

The growing anthropogenic impact of an exacerbated consumption of products in recent years has induced a continuous discharge into the environment of wastes and new substances which are increasingly harmful to public, animal, and environmental health. Endocrine Disrupting Compounds (EDCs) are inserted in this group of contaminants of emerging concern as recalcitrant and persistent chemicals, which have been widely and increasingly detected in various water matrices, attracting a great attention due to their toxicity and danger for all ecosystems [1–3]. Indeed, EDCs are a large and heterogeneous group of natural or synthetic compounds that are progressively known for their adverse consequences on the endocrine system. They can act as substitutes for the hormones, which are an essential part of the suitable functioning of the human and animal organism, mimicking or inhibiting their effects, thus being able to alter their levels and affect the health of the endocrine system as well as of other systems linked to it [4,5]. Hormonal disturbances caused by EDCs may cause long-lasting and irreversible health problems. Indeed, growing evidence has demonstrated that these compounds contributed to the rapid increase of metabolic syndromes (i.e., insulin resistance, obesity, type 2 and type 1 diabetes, thyroid diseases) and may be associated with an increased incidence of breast cancer, abnormal growth patterns, reproductive abnormalities, and neurodevelopmental delays in children, as well as with changes in immune function [5].

For these reasons, the presence of EDCs in water and wastewater has become a global problem, drawing the attention of international agencies and governments, as well as of an increasing number of research devoted to the identification [2] and abatement/degradation of EDCs present in waters [6]. A great deal of attention has been directed towards the development and application of advanced oxidation processes (AOPs) to eradicate EDCs from various water sources with high efficiency, thus leading to an increase of clean water supply. Compared with conventional technologies, materials nanotechnology offers very flexible and efficient remediation options for water pollutants. Nanostructured materials exhibit a range of features, such as high reactivity, large surface area (surface-to-volume ratio), tunable porosity and surface properties, which make them valuable in fields like catalysis, sensing and biomedicine [7–11]. The growing design of novel nano-catalysts, nano-structured catalytic membranes, and/or nano-sorbents with enhanced efficiency for contaminants removal is a hopeful strategy to contribute solving the worldwide hazardous problem of EDCs water pollution [1,12–15].

In this context, an updated overview on the recently designed (photo)catalytic metal-oxide nanomaterials with highest performances in the EDCs removal appears a useful tool for the scientific community to strategically direct the academic and technological research activities in this field. The proposed review is conceived for this purpose and reports the recent advances, as described by the major publications of the last four years (2018–2021), in the design and application of metal oxide-based nanomaterials in catalytic and photocatalytic degradation processes for the removal from wastewater of the most widespread EDCs belonging to different classes of formulations, such as components and additives of polymeric materials, agricultural chemicals, pharmaceuticals and personal care products.

2. Endocrine Disrupting Compounds (EDCs)

2.1. Historical Definition and Regulatory Evolution

The term "endocrine disruptor" was coined for the first time in 1991 at the Wingspread Conference Center. In 1993, Colborn, T. et al. published a paper [16] focusing on the disrupting role exerted by environmental chemicals on the development of the endocrine system, and on the permanent effects induced by a continuous exposure. In the subsequent years, great attention was addressed to the endocrine disruption by the scientific community [17–19], thus generating consensus statements regarding the hazard from endocrine disruptors, particularly in wildlife and in humans. In 1998, the United States Environmental Protection Agency (US EPA) proposed the first definition of Endocrine Disrupting Compounds (EDCs) as "exogenous agents that interfere with the production, release, transport, metabolism, binding, action, or elimination of the natural hormones in the body responsible for the maintenance of homeostasis and the regulation of developmental processes" [20,21]. In 2002, the World Health Organization (WHO) stated "an endocrine disruptor is an exogenous substance or mixture that alters function(s) of the endocrine system and consequently, causes adverse health effects in an intact organism, or its progeny, or (sub)populations" [20]. In 2013, the WHO and the United Nations Environment Programme released a comprehensive report on EDCs to date, calling for more research to fully understand the associations between EDCs and the risks to health of human and animal life. This work pointed to wide gaps in knowledge and called for more research to obtain a complete depiction of the health and environmental impacts of endocrine disruptors. On October 2020, the European Commission (EU) adopted the "EU Chemicals Strategy for Sustainability" as the first step towards a toxic-free environment under the European Green Deal [22]. This Chemicals Strategy proposes to establish endocrine disruptors as a hazard category in the Classification, Labelling and Packaging (CLP) Regulation. In particular, the Chemicals Strategy set out a vision to ensure that by 2030 a toxic-free environment should be achieved, where chemicals are produced and used in a way that maximizes their contribution to society, while minimizing harm to the planet and current and future generations. On these bases, a growing attention is addressed to reduce the harmful EDCs

impact on the environment and public health, thus defining strategic approaches to realize their removal which is fundamental, together with the reduction of their use, to pursue an environmental sustainability.

2.2. Main Natural and Synthetic EDCs

From a chemical point of view, EDCs are natural or synthetic substances with different structural and functional features. Different lists of substances with confirmed or potential endocrine disrupting activity are available. For example, the European Chemical Agency (ECHA) reports an endocrine disruptor assessment list including the substances undergoing an evaluation under REACH (Registration, Evaluation, Authorization and Restriction of Chemicals) or Biocidal Products Regulations. The U.S. National Institute of Environmental Health Sciences (NIEHS) and US EPA currently conduct research on EDCs and strategies to identify them, in the framework of a National Toxicology Program. However, a widely accepted systematic method to identify EDCs hazards by integrating literature data is still lacking [23]. Therefore, it should be noted that these lists may differ according to the criteria used in their definition, and that they are constantly subject to changes and updates as new evidence is found about the effects of the chemicals concerned. In this review, the most recent sources and literature reports are taken as reference in the selection of compounds considered as certain or potential EDCs; however, it does not intend to provide a complete or definitive list of EDCs.

Natural molecules recognized as EDCs include phytoestrogens, which are plant-derived hormones and are found in widely consumed food and animal products. These are less harmful than synthetic EDCs since they commonly have low affinity for estrogen receptors. At the same time, they exhibit low stability compared to many synthetic substances that are engineered to be stable. However, the potential health risks of phytoestrogens need to be considered, due to elevated levels in some foods and to that they can bind ERs with high affinity [24]. Specifically, daidzein and genistein (Figure 1) are the most abundant natural phytoestrogens detected in all foods. Using an in vitro bioassay, many of these had higher activation of estrogen beta-receptors than estrogen alpha-receptors.

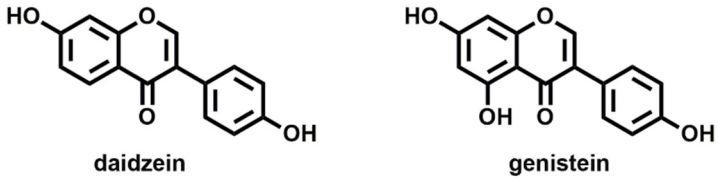

Figure 1. Molecular structures of the most common natural phytoestrogens: daidzein and genistein.

Synthetic EDCs are far more diverse, with several hundred identified and classified as persistent (exhibiting bioaccumulation) or non-persistent in the environment. These compounds are present in many commonly used household and industrial products. They include chemicals used as solvents or lubricants, plasticizers, pesticides [25], fungicides, and pharmaceutical agents, that are present in plastics, detergents, household chemicals and building products, fire retardants, food, medicines, personal care products, perfume, and cosmetics. Dichlorodiphenyltrichloroethane (DDT), polychlorinated biphenyls (PCBs), bisphenol A (BPA), polybrominated diphenyl ethers (PBDEs), perfluoroalkyl compounds, antibacterial triclosan (TCS) which binds with low affinity to both the androgen and estrogen receptors in vitro [26], polycyclic aromatic hydrocarbons (PAHs), and a variety of phthalates are the most detected in people [3,4]. Instead, 17β-estradiol (E2) and ethynyl estradiol (EE2) are the most diffused synthetic hormones. A summary of the main groups of molecules with endocrine disrupting activity is reported in Table 1.

Table 1. Summary of the most used EDCs impacting the immune response.

Endocrine Disrupting Compounds	Main Sources	Description
Bisphenols (e.g., BPA)	Epoxy composites, polyester resins, polycarbonate plastics, conserved food, dental sealants	Highly pervasive, estrogen mimic
Phthalates (e.g., dimethyl phthalate)	Polyvinylchloride (PVC), personal care products, medical devices	Effects on endocrine and reproductive systems
Alkylphenols (e.g., nonylphenol, octylphenol)	Non-ionic surfactants, industrial products, cosmetics	Lipophilic properties, estrogenic activity
Brominated flame retardants (polybrominated diphenyl ethers)	Household products, industrial products	Carcinogenicity
Insecticides (e.g., DDT) Herbicides (e.g., atrazine) Fungicides (e.g., vinclozolin)	Agricultural and household uses	Persistent agents, estrogen mimic
Parabens (e.g., methylparaben)	Common preservatives, food, cosmetics, pharmaceuticals	Estrogenic effect
Antibacterial agents (e.g., triclosan)	Cosmetics, pharmaceuticals	Effects on reproductive hormons
Antibiotics (e.g., cyclines) Anti-inflammatory drugs (e.g., paracetamol, ibuprofen, diclofenac)	Pharmaceutical products	Effects on the level of estrogen hormones
Synthetic hormones (e.g., 17β-estradiol)	Oral contraceptive pills, wastewater contamination	Strong estrogenic behavior

2.3. Main EDC Sources as Risks for Natural Ecosystems

Although many countries and relevant international corporations have put restrictions on the use of many EDCs, the presence of a great amount in the air, soil, and aquatic environments (i.e., drinking water, industrial and urban wastewaters or underground water) is a critical ecological issue which can impact the reproductive performance of the natural ecosystems [27,28]. Nowadays, exposure to EDCs can happen through direct ingestion of contaminated food and water, inhalation of combusted contaminants, and direct contact with a variety of consumer products. Water contamination has been one of the major concerns regarding the overexposure of humans and animals to these compounds. EDCs can reach water bodies through the inadequate disposal of personal care products and medicaments, industrial and agricultural wastewater, in natura sewage containing unused drugs or non-metabolized compounds present in urine and feces. In natural sewage and treated effluents are the main sources of contamination of water bodies [1]. Additionally, given the long-term persistence and high bioaccumulation tendency of EDC pollutants, several efforts have been devoted to defining highly selective and sensitive analytical approaches for the detection of traces of such harmful pollutants in the environment. At the same time, many different treatment methods are being widely investigated for the purification of wastewater from EDCs [29], as described in the following sections.

3. Chemical Degradation Approaches

The strategies for the removal of organic contaminants from water involve physical, chemical, or biological processes. Physical separation of target compounds from solution, e.g., by chemical precipitation or adsorption on a porous material, is a simple approach; however, it implies the issue of the following recovery or disposal of the contaminant. Chemical degradation by oxidative mechanisms is aimed at transforming the contaminant into less hazardous products, and ideally results in its complete mineralization to inorganic compounds such as CO_2 and H_2O. Biological treatments exploiting bacteria or other

microorganisms may also achieve decomposition, nonetheless they usually require strictly controlled operating conditions and offer slow removal kinetics.

Conventional processes carried out in wastewater treatment plants and during the remediation of polluted water show poor efficiency in the elimination of several persistent and recalcitrant organic contaminants, as most EDCs. To supplement the well-established treatment technologies, advanced oxidation processes (AOPs) have emerged in the last three decades as a series of water purification techniques operating at or near ambient temperature and pressure, based on the generation of highly reactive and non-selective species, in particular reactive oxygen species (ROS). The principal ROS are hydroxyl radical (•OH), superoxide radical ($\bullet O_2^-$), hydrogen peroxide (H_2O_2) and singlet oxygen ($^1O_2$). A broader definition of ROS includes ozone (O_3), widely used for water decontamination and disinfection, and organic peroxyl radicals (ROO•). Oxidative processes can also be mediated by other chemical species, among them reactive nitrogen species (e.g., nitric oxide, NO•), sulfate radicals ($SO_4\bullet^-$) and halogen-based oxidants (such as HOCl) [30]. In living organisms, ROS play important physiological roles; on the other hand, an excess in their concentration causes oxidative stress and damage to cells. With the aim of exploiting the oxidative potential of such species against organic pollutants, a variety of methods for their production or activation is available. AOPs include ozonation, sonolysis, Fenton processes, low-temperature plasma oxidation, photochemical degradation. A combination of these techniques is frequently applied to achieve better results, and UV irradiation is a common way to trigger the formation of ROS or enhance their yield, for example together with H_2O_2 and Fe(II) salts (photo-Fenton), O_3 (UV/ozonation) or semiconducting solids (heterogeneous photocatalysis) [1,31].

Most AOPs are homogeneous and require the use of radical precursors, stoichiometric reactants and/or high energy input. Hence, their full-scale implementation is still hindered by some practical limitations, for example the high operation cost, large consumption of reactive compounds, or the sensitivity to various organic and inorganic radical scavengers naturally present in wastewaters (e.g., humic acids, mineral anions) [32]. Heterogeneous water purification processes based on efficient solid catalysts that can be easily separated and reused are considered to offer advantages in terms of environmental sustainability and cost-effectiveness. Their development is therefore sought in view of scale-up and industrialization. Metal oxide semiconductors have acquired huge importance in this field, through photocatalysis as well as different catalytic mechanisms.

3.1. Photocatalytic Processes

Photocatalysis is a low-cost and versatile green technology widely used for the degradation of organic pollutants such as EDCs [33–36]. Photocatalytic processes need a semiconductor acting as photocatalyst that absorbs light radiation in a specific wavelength range, thus resulting in the excitation of electron (e^-) from the valence band (VB) to the conduction band (CB). This jump creates positive holes (h^+) in the VB of the photocatalyst, as shown in Equation (1):

$$\text{photocatalyst} + h\nu \rightarrow {h^+}_{VB} + {e^-}_{CB} \quad (1)$$

The holes in the VB split H_2O molecules thus resulting in the generation of hydroxyl free radicals, while electrons in the CB are trapped by oxygen molecules to form superoxide radicals, as schematized in Equations (2) and (3):

$${h^+}_{VB} + H_2O \rightarrow H^+ + \bullet OH \quad (2)$$

$${e^-}_{CB} + O_2 \rightarrow \bullet O_2^- \quad (3)$$

Other reactions can occur among the various species, producing more •OH radicals, as shown in Equations (4)–(6).

$$\bullet O_2^- + H^+ \rightarrow HO_2\bullet \quad (4)$$

$$2\ HO_2\bullet \rightarrow H_2O_2 + O_2 \quad (5)$$

$$H_2O_2 \rightarrow 2\ \bullet OH \quad (6)$$

The produced hydroxyl radicals can degrade organic pollutants, such as EDCs, which are adsorbed/absorbed on the catalyst surfaces through a series of controlled steps to give CO_2 and H_2O, as schematized in Equation (7):

$$\bullet OH + EDC \rightarrow CO_2 + H_2O \quad (7)$$

In addition to the action of ROS, photogenerated holes may directly react with adsorbed organic targets to produce intermediates that can be eventually oxidized to CO_2 and H_2O.

A huge number of studies have been devoted to the development of efficient and stable photocatalytic materials, starting from the most commonly studied photoactive semiconductors, i.e., titanium dioxide and zinc oxide. Notwithstanding the advancement of both fundamental understanding of photoinduced mechanisms and functional performances of a variety of photocatalysts, there are still important challenges to face, the main being the ineffective use of the solar radiation spectrum and the fast e^-/h^+ recombination, whereby the electrons excited to CB recombine with the separated h^+ in the VB rapidly prior to creation of free radicals. In this view, many flexible strategies can be adopted: the use of specific semiconductors with a low VB-CB band gap energy (E_g), the heterojunction of semiconductors with different E_g, the doping with metal or non-metal elements, the modification with organic molecules or carbon materials as photosensitizers or co-dopants, the engineering of structural defects, such as ion vacancies [35,37–40].

To optimize the decontamination efficiency, photoactive semiconductors can be integrated in a variety of combined water treatment and environmental remediation technologies. Among them, intimate coupling of photocatalysis and biodegradation (ICPB) is a prospective green technique, merging the advantages of both processes without the need for separate reactors. The key principle of ICPB is the transformation of bio-recalcitrant pollutants into biodegradable products by photocatalysis on the surface of porous carriers, which also act as support and protective scaffold for the active microorganisms that can complete the decomposition and mineralization [41,42]. Further examples of combined AOPs are described in the next section.

3.2. Other Heterogeneous Catalytic Processes

Although photocatalysis attracts the broadest interest among AOPs, alternative oxidative processes based on materials which do not need light irradiation are the object of growing research efforts. Such approaches allow overcoming the limitations of photoinduced processes, in particular the use of artificial UV or visible light sources and the constraints in the design of photoreactors to maximize the penetration and absorption of radiation.

A relevant case is the heterogenized Fenton and Fenton-like process. Fenton reaction consists in the oxidation of Fe(II) to Fe(III) inducing the decomposition of H_2O_2 with formation of hydroxyl radicals:

$$Fe^{2+} + H_2O_2 \rightarrow Fe^{3+} + HO^- + \bullet OH \quad (8)$$

Ferric ions can react with H_2O_2 as well, producing hydroperoxyl radicals ($HO_2\bullet$) and ferrous ions, in the so-called Fenton-like reaction:

$$Fe^{3+} + H_2O_2 \rightarrow Fe^{2+} + HO_2\bullet + H^+ \quad (9)$$

This process can be accelerated by coupling with UV irradiation (photo-Fenton) or electrocatalysis (electro-Fenton); nevertheless, shortcomings such as the requested optimum acid pH (around 3), the consumption of reactants, and their separation and subsequent

sludge management limit its large-scale application [43]. Therefore, heterogeneous Fenton catalysts, including iron oxides, zerovalent iron and Fe species supported on a solid matrix, are gaining attention. Some of these materials show a reactivity comparable to homogeneous Fenton in a broad pH range, requiring low amounts of H_2O_2, and ensure high stability (low Fe leaching) [44]. Among iron oxides, magnetite (Fe_3O_4) is the most suitable owing to its structure; however, hematite (α-Fe_2O_3), maghemite (γ-Fe_2O_3) and goethite (α-FeOOH) have been found to be useful as well [43].

A promising alternative to Fenton is represented by AOPs (Advanced Oxidative Processes) based on sulfate radical ($SO_4\bullet^-$), which are emerging in recent years, as testified by the increasing number of related research articles and reviews [45–47]. Compared to •OH, $SO_4\bullet^-$ has a similar or even higher oxidation potential (2.5–3.1 V vs. NHE) and a longer half-life in water (about 30–40 µs vs. 20 ns), so it can migrate longer distances to reach target contaminants. Moreover, sulfate radicals work in aqueous solution on a wider pH range (2–8) and are more selective toward organics containing unsaturated or aromatic bonds [45]. The two major sources of this reactive species are peroxymonosulfate (PMS, HSO_5^-) and persulfate (PS, $S_2O_8^{2-}$) anions. The use of their salts is advantageous because of the low cost, safety and easy transportation and handling, making the in situ chemical oxidation feasible for groundwater and soil remediation [46]. PMS and PS can be activated by various methods, including heating, UV irradiation, ultrasounds, alkaline medium and some transition metals (Fe, Co, Mn, Cu, Ni, Ce, V, Ag), in homogeneous or heterogeneous systems [45]. The activation of PMS and PS by a metal ion (M^{n+}) can be schematized, respectively, as follows:

$$HSO_5^- + M^{n+} \rightarrow M^{(n+1)+} + SO_4\bullet^- + OH^- \quad (10)$$

$$S_2O_8^{2-} + M^{n+} \rightarrow M^{(n+1)+} + SO_4\bullet^- + SO_4^{2-} \quad (11)$$

Oxides of Fe^{2+}, Fe^{3+}, Co^{3+} and Mn^{2+}, often in mixed heterostructures, are the most studied solid catalysts for the generation of sulfate radicals in water treatment strategies [47]. The reaction networks in presence of sulfate radicals can involve the formation of ROS like hydroxyl and superoxide radicals, leading to multifarious oxidation mechanisms [46].

Another attractive strategy to obtain ROS active in the absence of continuous irradiation is the modification of metal oxide semiconductors with suitable organic molecules, forming interfacial charge transfer complexes. These can give the ability to activate molecular O_2 by spontaneous reduction to superoxide, as recently observed for titanium and zirconium oxides with coordinated diketone ligands [48–51]. On the surface of such hybrid materials the generated $\bullet O_2^-$ radicals can be stabilized for exceptionally long times, leading to oxidative degradation of organic water contaminants even in dark conditions [50,52].

Electrocatalysis is a well-known technology applicable to the decomposition of pollutants with relatively high concentration. Nanostructured metal oxides can be employed as electrodes in electrochemical oxidation processes, frequently coupled with light irradiation (photoelectrocatalysis) or other techniques to enhance the efficiency.

An innovative set of AOPs takes advantage of piezoelectric catalysis, or piezocatalysis, a field that has emerged in recent years. It is based on the piezoelectric effect, namely the ability of materials with non-centrosymmetric structure to generate charge separation because of deformation in the presence of external mechanical energy. The possible sources of mechanical energy include ultrasonic cavitation, physical bending, and vortex-induced shearing force. If the potential of the built-in electric field created by the dipole polarization is sufficient, the charge carriers reaching the surface of the materials can accumulate and induce redox reactions, for example generating ROS or directly oxidizing adsorbed molecules. This piezo-catalytic effect was therefore proposed as AOP, either by itself or coupled with irradiation and/or Fenton process [53,54]. Among the piezoelectric ceramics, ZnO and titanates, $BaTiO_3$ and $Pb(Zr,Ti)O_3$, have been successfully tested for the degradation of organic pollutants. 1D and 2D nanomaterials possess high flexibility under mechanical forces and hence are expected to show better piezo-catalytic performances. Beside morphology,

the presence of defects producing free charge carriers should be another crucial factor in driving this kind of catalytic activity [53].

Non-thermal plasma technologies, being able to generate reactive species at relatively low temperature, are emerging as candidates for the treatment of contaminated water. The combination of non-thermal plasma with other AOPs, in particular, heterogeneous catalysis, has been proposed to enhance pollutant degradation performances and reduce the formation of reaction by-products. There are different types of reactor configurations, the most used being the dielectric barrier discharge. Solid (photo)catalysts can be the introduced in various forms, as foam, honeycomb monolith, coating on the reactor walls or electrodes, or as a packed bed [55]. Different metal oxide semiconductors have been integrated in non-plasma systems, improving the degradation efficiency of emerging contaminants and thus making the process more economically sustainable [56]. Another possible advantage is the ability of non-thermal plasma to regenerate the catalyst inserted in the reactor. Finally, metal oxides can also be employed in catalytic wet air (or peroxide) oxidation, where oxygen (or H_2O_2) is dissolved in the liquid phase at high temperatures and pressures. This review focuses on reactions performed at low temperature and ambient pressure, so these treatment techniques are not covered.

The research on efficient oxidative processes based on nanomaterials is constantly evolving, and thus new achievements are expected soon. In the following section, recent results in the application of metal oxide-based (photo)catalysts in the removal of EDCs from water are presented.

4. Metal Oxide-Based Nanomaterials for EDCs Removal

This section reports a selection of recent literature studies on metal oxides and related nanomaterials applied in the heterogeneous degradation of endocrine disruptors in water. The classification is based on the most extensively represented groups of EDCs considered as target contaminants, namely, components and additives of plastic materials, chemicals used in agricultural activities, pharmaceutical, and personal care products and other relevant compounds not included in these categories.

4.1. Photocatalytic and Catalytic Degradation of Plastic Components and Additives

The awareness about plastic and microplastic pollution is finally rising as the adverse effects of many components of common polymeric materials are acknowledged. The massive production and ubiquitous use of plastics (often as disposable items), followed by frequent incorrect disposal, causes the significant presence of these chemicals in sewage. Among EDCs, plasticizers, such as phthalates, chlorinated solvents and additives, and bisphenols (e.g., Bisphenol A (BPA), Bisphenol F (BPF), Bisphenol AF (BPAF) and Bisphenol S (BPS)), the main monomers of epoxy resins (Figure 2), raise large concern. Among the bisphenols, BPA is the most used organic compound in the synthesis and manufacturing of epoxy resins.

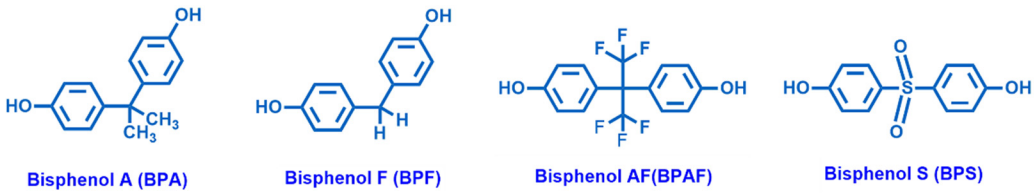

Figure 2. Chemical structures of Bisphenol A (BPA), Bisphenol F (BPF), Bisphenol AF (BPAF) and Bisphenol S (BPS).

BPA is considered an EDC which negatively affects the environment when it is released in water or atmosphere [57] and human health when it enters the body, being able to interfere with the endocrine system, thus possibly causing reproductive and developmental disorders and diseases of the immune and nervous systems [58]. BPA is widely present in the aquatic environment, because it is used in the production of polycarbonate, epoxy

resin and exploited in many plastic products, such as milk packaging and beverage cans in the food industry [59]. Considering human health, the United States Environmental Protection Agency (US EPA) strongly recommended a reference limit dose for oral exposure of 50 μg BPA/kg of body weight/day in 2014 [60]. In view of the above, the removal of BPA from wastewater is a critical issue at present. Phthalic acid esters (PAEs), or phthalates, are typical EDCs and a chemical class of plasticizers used in many plastic products. The ubiquitous presence of PAEs makes them detected everywhere as result of release to water, atmosphere and soil [61]. The scientific community agrees on the role of anthropogenic activities as the primary contributor to the occurrence of bisphenols and phthalate monoesters in lakes, lagoons, and their sediments, caused by the discharge of domestic and industrial waste and wastewater, as well as farming, transportation, etc. [62,63]. The major species detected between the phthalates in the influents of wastewater treatment plants are dimethyl phthalate (DMP), diethyl phthalate (DEP), dibutyl phthalate (DBP) (Figure 3).

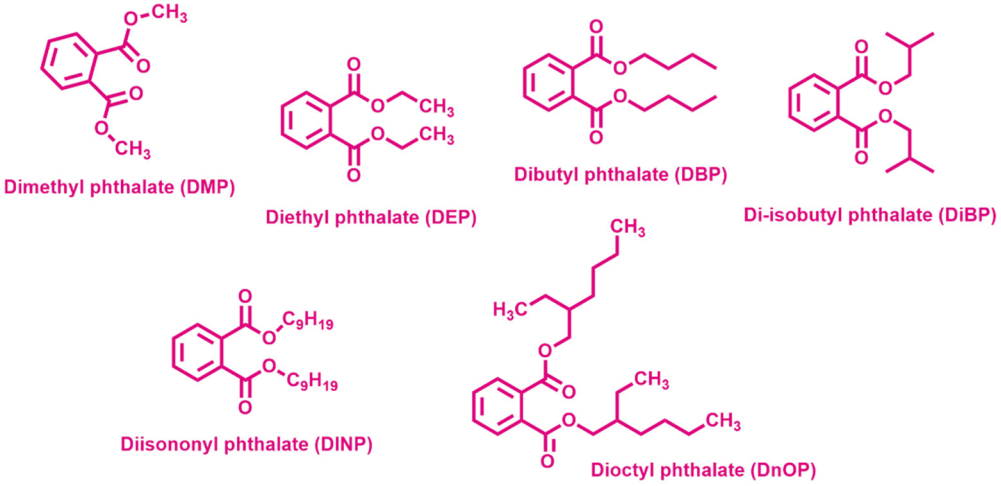

Figure 3. Chemical structures of the most used phthalates.

DBP has been shown to tend to accumulate in the sludge with a maximum detection of 2497 μg/L, exceeding acceptable levels for a safe aquatic environment [64]. Prominent levels of typical phthalates, including di-isobutyl phthalate (DiBP), DBP and di(2-ethylhexyl) phthalate (DEHP) have been found from researchers in both Chinese and French hospitals [65].

The willingness to move toward a more sustainable society and the increasing demand of reducing pollution have boosted the synthesis of new more efficient catalysts and photocatalysts for the degradation of BPA and phthalates. In the recent period, there has been growing interest in the development of doped and hybrid materials based on metal oxides with significant performances in degradation of these plastic derivatives. The main aspects related to oxidative mechanisms as well as chemical features and synthesis of the most representative nanostructured catalysts and photocatalysts are described in the next paragraphs.

4.1.1. Bisphenol A

Among the titanium oxide-based photocatalysts, composites with graphene or reduced graphene oxide (rGO) were intensively investigated. Xu et al. [66] synthetized TiO_{2-x}/rGO nanocomposite via hydrothermal-calcination method, where TiO_2 was self-doped by Ti^{3+} and oxygen vacancies (Ti^{3+}/Ov). The presence of Ti^{3+}/Ov in the oxide lattice led to enhanced visible light harvesting and the chemical bonds (Ti-O-C) between TiO_{2-x} and rGO allowed for an efficient charge separation. Furthermore, the coupling of TiO_{2-x} and rGO prevented the aggregation of TiO_{2-x} particles and thus improved the adsorption of organic pollutants. TiO_{2-x}/rGO exerted a 6.16-, 2.92- and 2.55-fold faster reaction rate for BPA degradation than that of unmodified TiO_2, TiO_2/rGO and TiO_{2-x}, re-

spectively. Chemical analysis showed that $\bullet O_2^-$ radicals were the major oxidizing species, therefore responsible for a maximum of approximately 91% BPA removal after 60 min. Wang et al. [67] synthesized a TiO_2@aspartic acid-β-cyclodextrin@rGO (TiO_2@ACD@rGO) composite photocatalyst by a photochemical method and applied it in the degradation of BPA under UV irradiation. TiO_2@ACD@rGO exhibited higher photocatalytic efficiency than TiO_2 and TiO_2@rGO, resulting in a reaction constant for BPA of 0.739 mg/L·min, which was almost two times its counterparts. The removal efficiency of BPA by TiO_2@ACD@rGO could achieve a value of 85.6% after 60 min under UV irradiation, which is 10% and 24.2% higher than that of BPA by TiO_2@rGO and TiO_2, respectively. TiO_2@ACD@rGO exerted its degradation activity through the release of superoxide radicals and h^+, which was boosted by effective electron and mass transfers at the photocatalyst interface (Figure 4). Moreover, the composite exhibited good stability and reusability after five cycles. The chemical investigation revealed that the modified cyclodextrins strengthens the adsorption of BPA on the photocatalyst surface.

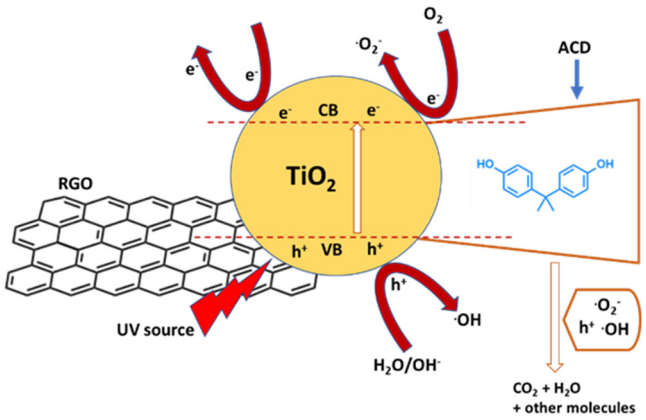

Figure 4. Reaction mechanism of photocatalytic degradation of BPA in the TiO_2@ACD@rGO system, where ACD is aspartic acid–cyclodextrin compound. Adapted and reprinted with permission from [67], Copyright (2021) Elsevier.

On the other hand, Wang et al. [68] synthetized via a hydrothermal approach Fe-doped TiO_2/rGO active under visible light. Fe-TiO_2/rGO nanocomposites exerted high photocatalytic performance for BPA and its analogues (Figure 2), especially when BPA concentration was around 95 ppm and pH in the range 4.5–8.5. The doping Fe as well as GO significantly boosted photocatalytic activity, resulting in an increase of BPA degradation rate compared to pristine samples. The photocatalytic degradation, mainly led by $\bullet O_2^-$ radicals, was promoted by the presence of Ti^{3+} and by the formation of $Fe^+(C_6H_5OH)$ π-complex. Approximately 25% of BPA was adsorbed by Fe-TiO_2/rGO after 30 min in the dark, and BPA was completely removed within 60 min under visible-light irradiation. Additionally, BPF and BPAF were completely degraded after 120 min, and 96% of BPS was removed within 120 min under visible-light irradiation.

Additionally, Garg et al. [69] synthetized via a wet impregnation method TiO_2 co-doped with visible-light photoactive cobalt and nitrogen to enhance pollutants degradation. The photocatalytic activity on the mineralization of BPA under visible-light irradiation was compared to commercial TiO_2 (Degussa P25). In particular, 1.5% Co and 0.5% N co-doped TiO_2 sample showed the highest degradation activity: the complete mineralization of BPA and 97% removal of total organic carbon (TOC) were observed. The performances were associated with alterations in physical properties, crystal structure and energy band gap induced by the dopants. Zhao et al. [70] prepared Fe_3O_4@mTiO_2/C through the combination of mesoporous TiO_2, Fe_3O_4 and carbon. It exhibited intense light response in the visible light region because of the dual sensitization effect and double conductivity, which was beneficial to the transfer and separation of charge carriers, i.e., photogenerated electrons and holes (Figure 5). This double conductive structure of Fe_3O_4@mTiO_2/C

photocatalyst allowed for a significant activity in the complete degradation of BPA in 120 min under visible light and superior stability for its reusability after five cycles.

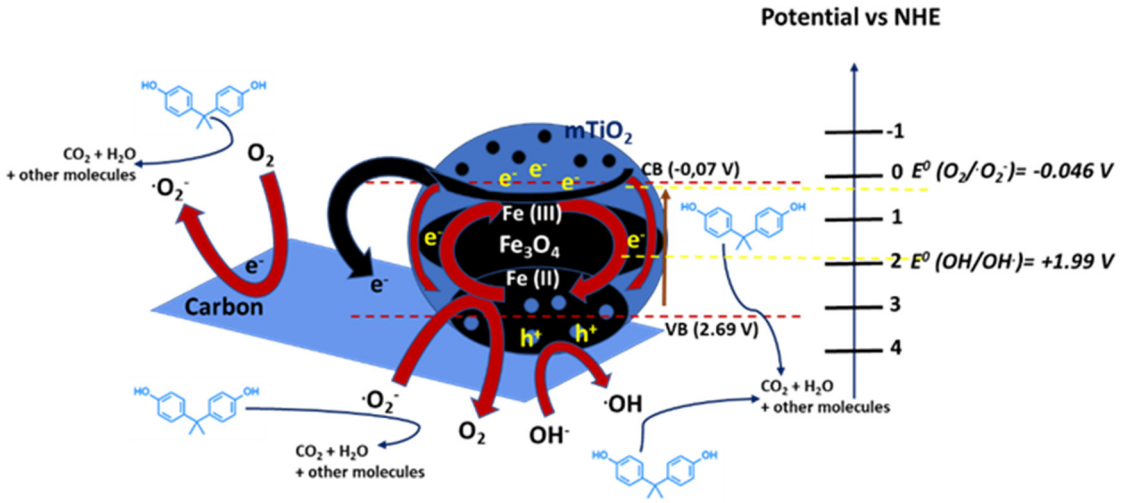

Figure 5. Possible photocatalytic mechanism of the Fe_3O_4@mTiO_2/C sample. Adapted and reprinted with permission from [70], Copyright (2021) Elsevier.

He et al. [71] synthetized a magnetic composite material, Ag/Fe,N-TiO_2/Fe_3O_4@SiO_2 (AgFeNTFS), for the visible-light-driven photocatalytic disinfection of Escherichia coli (*E. coli*) and degradation of BPA. The photocatalyst completely removed BPA (2 mg/L) and showed 6.3-log reduction in cell density of *E. coli* within 120 min. In presence of both BPA and *E. coli* in the treated water sample (i.e., sewage obtained from a wastewater treatment plant), the efficiency of AgFeNTFS in the BPA degradation was dropped by 10%, due to the competition for the same reactive species of O_2 and H_2O_2 between the two contaminants. However, the treated water sample could meet local disinfection discharge standard with a 3-log reduction (99.9%) of *E. coli* after 90 min and a simultaneous complete removal of BPA after 360 min. Ju et al. [72] prepared ZnAlTi layered double oxide (ZnAlTi-LDO)-supported C60@AgCl nanoparticles (C60@AgCl-LDO) for the photo-degradation of BPA under simulated visible-light irradiation. C60@AgCl-LDO showed a characteristic mesoporous structure. The Ag@AgCl heterostructure boosted the near-field for light scattering, reflection, and absorption. Fullerene enhanced the stability of Ag-based phase, so the C60@AgCl reduced the recombination of photo-induced electron–hole pairs, and therefore increased the efficiency of photocatalysis. The chemical investigation showed that photogenerated h^+, superoxide radical, •OH bulk, and singlet oxygen were responsible for the extremely fast photodegradation, allowing a BPA removal of 100% by using C60@AgCl-LDO under ultraviolet light in 5 min. Kumar et al. [73] prepared a graphitic carbon nitride (g-C_3N_4)–$CaTiO_3$ (CTCN) organic–inorganic heterojunction photocatalyst through a mixing methodology and the deposition of calcium titanate (CT) nanoflakes onto the surface of g-C_3N_4 (CN) nanosheets. The CTCN heterojunction with 1:1 ratio of g-C_3N_4/CT exhibited the highest photocatalytic activity under sunlight irradiation, resulting in the 47% degradation of BPA after 120 min. The presence of the two-dimensional (2D) morphology of g-C_3N_4 nanosheets and CT nanoflakes provided a vast number of reaction sites with large surface area, and thus enhanced the overall photocatalytic activity. The chemical analysis of photocatalytic process confirmed that $\bullet O_2^-$ radicals exerted the key role in the degradation of BPA.

Bismuth-based semiconductors are attracting increasing research interest for their tunable properties and wide absorption spectrum. Bismuth mixed metal oxides or oxyhalides are particularly investigated. For example, Ma et al. [74] synthetized a polythiophene (PTh)/$Bi_4O_5I_2$ hybrid by sol–gel. The incorporation of conductive polythiophene enhanced the separation efficiency of photo-charge carriers, boosting the visible light photocatalytic

ability of $Bi_4O_5I_2$. This led to a BPA degradation of 99.2% in 30 min with 0.5 wt% of PTh, with a reaction rate 3.7 times higher than on pristine $Bi_4O_5I_2$. Wu et al. [75] prepared, by a wet-chemical methodology, three BiOI samples with different morphologies (nanoplate, micro-flower, microsphere) and Bi_2WO_6/BiOI microspheres, by a microwave-assisted synthetic method with different ratios of Bi_2WO_6. The chemical investigation proved that BiOI-3 microspheres showed higher photocatalytic activity than other morphologies (BiOI-1 and BiOI-2) in the degradation of BPA and methyl orange, furthermore, Bi_2WO_6/BiOI (BWOI-3) with 3% content of Bi_2WO_6 exhibited the best photocatalytic performance as well as a good durability. Bi_2WO_6/BiOI was highly effective due to a significant production of reactive species (h^+, $\bullet O_2^-$) and a synergistic effect between p-type BiOI and n-type Bi_2WO_6, which could promote the separation of electron–hole pairs. Finally, BWOI-3 showed a photodegradation efficiency up to 95.04% for MO and 86.84% for BPA under visible-light for 60 min and 100 min, respectively. Rao et al. [76] prepared a ternary Pd/PdO/β-Bi_2O_3 composite photocatalyst with different amounts of Pd/PdO by a simple two-step process. The material was characterized by a heterojunction (p-n junction) of PdO/β-Bi_2O_3 and the Schottky barrier of Pd/β-Bi_2O_3, which significantly limited the recombination of photoinduced electron–hole pairs in the composite, increasing visible light absorption and improving charge separation efficiency between Pd, PdO and β-Bi_2O_3. In particular, 1.0 wt% of Pd/PdO/β-Bi_2O_3 showed an excellent photocatalytic activity for BPA degradation and nitric oxide (NO) removal, 97.4% and 47.6%, respectively, within 30 min, outperforming pure β-Bi_2O_3. Both hydroxyl and superoxide radicals were involved in the photocatalytic process. Li et al. [77] synthetized via solvothermal-reduction method $Bi_4O_5Br_2$ nanosheets loaded with Pd nanoparticles for the of BPA. Pd/$Bi_4O_5Br_2$ showed higher photocatalytic activity and photocurrent response than pure $Bi_4O_5Br_2$. In particular, 1.0 wt% loading of Pd was found to be most effective for improving the BPA removal rate constant and achieve a degradation of BPA near to 95.8% after 70 min LED visible-light irradiation. The enhanced performances of Pd/$Bi_4O_5Br_2$ were attributed to the formation of a Schottky barrier between the Pd nanoparticle and the $Bi_4O_5Br_2$ nanosheet, effectively promoting the separation of photogenerated electrons and holes (Figure 6).

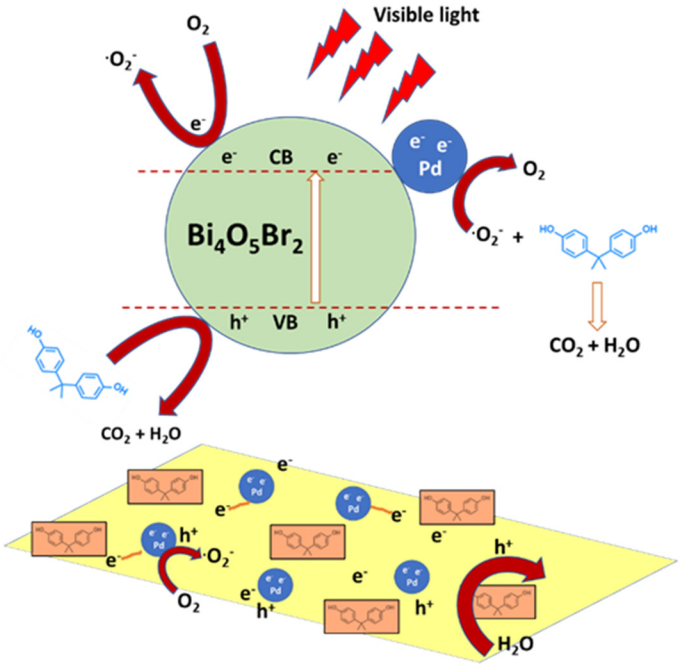

Figure 6. Schematic representation of the photodegradation of BPA over a semiconductor decorated with noble metal nanoparticles, Pd/$Bi_4O_5Br_2$, under visible-light irradiation. Adapted and reprinted with permission from [77], Copyright (2018) Elsevier.

Xu et al. [78] synthetized different Ag_3PO_4 structures to degrade BPA under visible-light irradiation. The degradation of BPA after 30 min was 27% by using cubic Ag_3PO_4, whereas it was almost 100% by the nano-flake Ag_3PO_4 photocatalyst, resulting in a rate constant 9.71 times higher. The performances were attributed to the action of h^+ and $\bullet O_2^-$. The extended light adsorption and accelerated carrier transfer promoted a high photocatalytic activity, where both were accounted for by the increasing number of exposed (111) crystals and catalytic active sites on Ag_3PO_4 nano-flakes. Selvakumar et al. [79] prepared by hydrothermal process a Gd_2WO_6/ZnO/bentonite (GWZB) nanocomposite. It showed a strong decrease in the rate of electron–hole recombination, resulting in a higher photocatalytic activity compared to pure GWZ without bentonite. GWZB was characterized by clustered microsponge-like structure and exerted an effective degradation under visible light of ciprofloxacin (CF) and BPA with good recycling performance. The photodegradation of CF and BPA with 20 mg of GWZB were 97.9 and 98.3% respectively, due to the action of superoxide radicals (Figure 7).

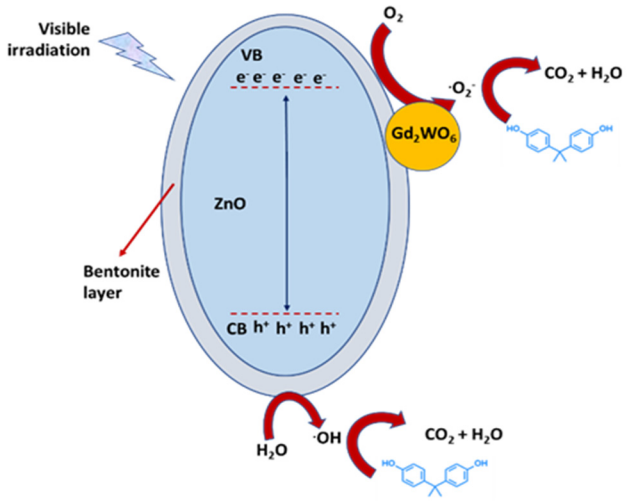

Figure 7. Proposed mechanism for the photodegradation of organic pollutants on a Gd_2WO_6/ZnO/bentonite ternary composite, as described into [79].

Sulfate-based AOPs have become relevant non-photoinduced technologies for the decomposition of emerging contaminants. Fu et al. [80] prepared three novel composites of graphitized hierarchical porous biochar (MX) with magnetic manganese ferrite ($MnFe_2O_4$/MX), which could activate peroxymonosulfate (PMS). The material was aimed at the degradation of a range of contaminants: bisphenol A, orange II, methylene blue, sulfadiazine, and ciprofloxacin. MX included MS, ML, MC synthesized using corn stems (S), leaves (L) and cores (C) as raw waste materials, respectively, possessed hierarchical porous structure, graphitization domains and tremendous surface area. The degradation efficiency was boosted with increasing PMS dose, catalyst dose, reaction temperature, and reducing organic pollutant concentration. Three pathways were involved in the catalytic activity of $MnFe_2O_4$/MS, including radical-induced oxidation attained by surface-bound $SO_4\bullet^-$ and •OH on $MnFe_2O_4$ nanoclusters and hierarchical porous carbon sheets, non-radical pathway ascribed to $\bullet O_2^-$ generated by promoted self-decomposition of PMS, non-radical pathway achieved through electron transfer from organic compounds to PMS mediated by graphitized structures. In addition, $MnFe_2O_4$/MS has the advantages of wide pH usable range. $MnFe_2O_4$/MS and PMS system could degrade orange II/methylene blue, bisphenol A, sulfadiazine, and ciprofloxacin with a removal efficiency of 100%, 95%, 91% and 85%, respectively.

Kong et al. [81] synthetized a stable Cu_2O@β-CD through topotaxial conversion of CuCl assisted by β-CD (β-cyclodextrin) at room temperature. Fenton-like reaction is the most widespread method for removal of organic pollutants, but their reactivity with H_2O_2 may be inhibited by natural organic matter (NOM) due to the competition of hydroxyl

radicals and chelating agents. Covalently linked β-CD could keep humic acid (HA), which is present in the NOM, from interfering catalytic performance of Cu_2O surfaces and inhibited the leaching of copper. Cu_2O@β-cyclodextrin could work in cooperation with Fenton-like catalysis to destruct aromatic pollutants at neutral pH. β-CD with a hydrophobic cavity well anchored on Cu_2O could exhibit selective adsorption to aromatic pollutants including bisphenol A and inhibited HA from bonding with available catalytic (Cu) sites, showing active species •OH on Cu_2O surfaces and 83.7% BPA removal efficiency.

In the emerging branch of piezocatalysis applied to water remediation, coupling with photocatalysis seems extremely promising. ZnO and titanate nanostructures were modified by the formation of heterojunctions or doping to enhance the piezo photocatalytic performances and some of these materials were tested in the removal of EDCs from water, in particular BPA. Zhang et al. coupled ZnO with CdS or BiOI, two semiconductors responsive to visible light, to promote the separation rate of charge carriers in addition to the piezoelectric field produced by ZnO under ultrasonication. ZnO/CdS hierarchical nanofibers with optimal composition could completely remove BPA within 30 min, with a rate of 0.1557 min^{-1}, many-fold improved compared to the sole photocatalytic effect [82]. Among titanate piezoelectric photocatalysts, $SrTiO_3$ inverse opal doped with rhodium was found to give visible-light-driven degradation of BPA under ultrasonic vibration. The 3D ordered inverse opal structure obtained by a hard template method, along with 0.5% Rh doping, contributed to light harvesting, so that almost complete removal of BPA was attained in 30 min [83]. Mixed titanates were also investigated, e.g., $Na_{0.5}Bi_{0.5}TiO_3$ nanowires, synthesized by an efficient templated hydrothermal method, starting from $Na_2Ti_3O_7$ template nanowires subjected to ion-exchange with Bi^{3+} [84]. The piezocatalytic activity of these nanomaterials was tested in the degradation of several organic pollutants, including BPA, tetracycline hydrochloride, phenol, and common dyes.

4.1.2. Phthalates

The removal of various phthalates was investigated principally by means of photocatalytic processes. Jing et al. [85] studied the activity of TiO_2 prepared by sol–gel against dimethyl phthalate (DMP). The photodegradation occurred at the surface of the TiO_2 particles according to Langmuir–Hinshelwood model and the adsorption constant determined from the dark adsorption was lower than the one obtained in light condition. In particular, under the irradiation of UV light, a synergistic mechanism of adsorption and photocatalysis allowed for the DMP degradation, where •OH radicals were the primarily responsible species. By adding foreign Cu^{2+}, the •OH radicals were generated by electrons rather than holes. The highest removal rate of 80.5% was obtained at pH 6–7 after 75 min of irradiation time. Wang et al. [86] investigated the photolysis and photocatalysis of typical phthalic acid esters (dimethyl phthalate, DMP; diethyl phthalate, DEP; dibutyl phthalate, DBP) comparing UV, UV/TiO_2, and UV-Vis/Bi_2WO_6 systems. Both photolysis and photodegradation reaction were performed for 300 min and the different abilities to remove DMP, DEP, and DBP were estimated. The UV/TiO_2 system showed the highest degradation capability, with removal efficiencies of up to 93% in 90 min. On the contrary, the performance of UV-Vis/Bi_2WO_6 was not satisfactory in the removal of DMP and DEP. However, UV, UV/TiO_2, and UV-Vis/Bi_2WO_6 had a strong ability to degrade DBP. The chemical analysis showed that: (i) UV photolysis attacked the carbon branch and produced o-hydroxybenzoates, (ii) the hydroxyl radicals attacked both the carbon branch and the benzene ring. In the case of photocatalytic systems, hydroxylated compounds and ring-opening byproducts were detected. However, UV/TiO_2 system reacted with the pollutants via hydroxyl radicals, whereas UV-Vis/Bi_2WO_6 exerted a direct hole oxidation. You et al. [87] prepared via hydrothermal method Bi_2O_3-TiO_2 composite for the removal of Pb(II) and refractory organic DBP from wastewater under visible-light irradiation. The high efficiency of the photocatalyst was due to the presence of various locations on the composite, which allowed the occurrence of the refractory organic oxidation and heavy metal reduction separately. After 4 h of visible-light irradiation, Bi_2O_3-TiO_2 composite could

effectively perform 40%-Pb(II) reduction and 45%-DBP oxidation. Particularly, Pb(II) could be reduced to Pb(0) on the Bi_2O_3-TiO_2 composite in visible light, because of the energy level adjustment caused by Fermi levels matching at the n–p heterojunction. Additionally, the presence of DBP in the analyzed water sample significantly increased the removal of Pb(II), highlighting that the coupling of the reduction of heavy metals and the oxidation of organics could efficiently enhance the photocatalytic activity of the system.

Meenakshi et al. [88] synthetized through the sol–gel methodology nanorod ZnO/SiC nanocomposite for the UV and visible light photocatalytic degradation of DEP and other toxic organic compounds. The as-prepared materials showed a high degree of porosity, crystallinity, and roughness, and exhibited absorption in the visible light region. A catalyst dosage of 0.5–1.0 mg/mL allowed for 90% DEP degradation at neutral pH conditions under UV and visible-light irradiations. Finally, the nanorod ZnO/SiC nanocomposite could be reused up to three cycles without losing its activity and always following pseudo first-order kinetics. Li et al. [89] prepared a dual Z-scheme heterostructure photocatalyst, composed by mesoporous graphitic carbon nitride (mpg-C_3N_4), BiOBr, polythiophene (PTh), and magnetic iron oxide, for the photocatalytic degradation of DMP in water under visible light. The reaction rate constant was 3.7- and 4.5-fold higher than those of pristine g-C_3N_4 and BiOBr, respectively. The photocatalytic DMP degradation efficiency of mpg-C_3N_4/BiOBr/PTh was 40% and 50% higher than that of pristine g-C_3N_4 and BiOBr, respectively. The enhanced visible-light photocatalytic performance, which followed a pseudo first-order kinetic, was attributed to the dual Z-scheme heterostructure generated between mpg-C_3N_4, PTh, and BiOBr. The chemical investigation revealed that the active species h^+, $\bullet O_2^-$, and •OH coexisted during the photocatalytic reaction process, and that h^+ exerted the main role in the destruction of DMP species (Figure 8).

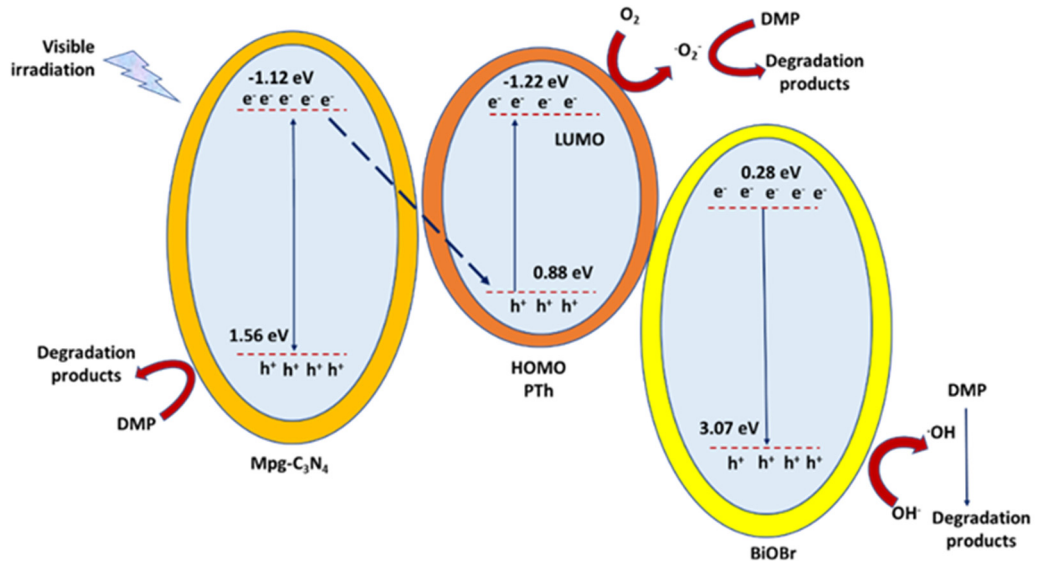

Figure 8. The schematic mechanism for DMP photocatalytic degradation over mpg-C_3N_4/BiOBr/PTh (polythiophene) heterostructure under visible-light irradiation, as described into [89].

Studies on non-irradiated removal of PAEs relied mainly on sulfate-mediated processes. Dong et al. [90] performed the degradation of several phthalates in marine sediments by sodium persulfate ($Na_2S_2O_8$, PS) activated by a series of iron–cerium (Fe-Ce) bimetallic catalysts (FCBCs). With a Fe-Ce molar ratio of 1.5:1 the degradation of DMP, DEP, di-2-ethylhexyl phthalate, dioctyl phthalate and diisononyl phthalate showed the highest value over FCBC and an increase of Ce amount resulted in an improvement in oxygen storage capacity and catalytic activity of bimetallic catalysts. The Fe^{3+}/Fe^{2+} and Ce^{4+}/Ce^{3+} redox couples exerted a synergistic catalytic effect in addition to electron transfer of oxygen vacancies, activated $S_2O_8^{2-}$ to release $\bullet SO_4^-$ and •OH radicals, which were crucial in the oxidative degradation process of PAEs. When the PS and FCBC concentrations were

1.0×10^{-5} M and 1.67 g/L, respectively, the PAE degradation achieved a maximum of 86% at pH 2 and rate constant of 1.5×10^{-1} h^{-1}. The activation of persulfate was reported also using some metal-organic frameworks (MOFs). Ding et al. [91] investigated the adsorptive and catalytic properties of a Fe-based MOF (Fe-MOF-74) for the removal of DMP in water. The adsorption behaviors were evaluated by the Freundlich and pseudo-second-order model. The selective adsorption was crucial in combination with molecular imprinting technique to obtain a 1.5-fold increase in catalytic rate. In particular, DMP was firstly adsorbed on the surface of the material by physical interactions and then $SO_4\bullet^-$ and •OH radicals, generated from PS activation, catalytically oxidized DMP with a degradation rate in water of around 90% after 30 min.

The main outcomes reported in this section highlight that the most representative photocatalysts and catalysts used for the degradation of plastic components are hybrid and/or composite nanomaterials prepared by wet-chemical routes (i.e., sol–gel, hydrothermal or mixed) and composed by metal oxides, M_yO_x, in which M = Ti, Zn, Fe and W are the principal species. High levels of removal were obtained by using visible light and, in some cases, solar irradiation. The chief features and performances of these nanomaterials are summarized in Table 2, including the best achieved removal efficiencies and corresponding rate constants.

Table 2. Summary of representative metal-oxide-based nanomaterials used for the degradation processes of bisphenols and phthalates.

Material	Preparation	Target	Conditions	Results	Ref.
(N, Co)-codoped TiO_2	Wet impregnation method	BPA (20 mg/L)	Visible-light irradiation	97% removal, 0.0195 min^{-1}	[69]
TiO_{2-x}/rGO nanocomposite	Hydrothermal-calcination method	BPA (2.5 mg/L)	Visible-light irradiation (60 min)	91% removal, 0.049 min^{-1}	[66]
TiO_2@ACD@RGO composite	Photochemical method	BPA (20 mg/L)	UV irradiation (60 min)	85.6% removal, 0.739 mg/L·min	[67]
Fe_3O_4@mTiO_2/C	Sol–gel Methodology	BPA	Visible-light irradiation (120 min)	100% removal, 0.01045 min^{-1}	[70]
Ag/Fe,N-TiO_2/Fe_3O_4@SiO_2 (AgFeNTFS)	Sol–gel Methodology	BPA (2 mg/L), *E. coli* (10^6 CFU/mL),	Visible-light irradiation (360 min for BPA, 90 min for *E. coli*)	100% removal	[71]
(g-C_3N_4)–$CaTiO_3$ heterojunction	Mixing methodology	BPA	Sunlight irradiation (120 min)	47% removal	[73]
C60@AgCl-ZnAl LDO	Sol–gel Methodology	BPA (0.5 g/L)	Ultraviolet light (5 min)	100% removal	[72]
Gd_2WO_6/ZnO/bentonite (GWZB) nanocomposite	Hydrothermal process	Ciprofloxacin (CF) (4×10^{-5} M), BPA (4×10^{-5} M)	Visible-light irradiation	Removal 98.3% and 97.9% respectively	[79]
$MnFe_2O_4$/MX magnetic composites	Sol–gel Methodology	BPA (10 mg/L), sulfadiazine (10 mg/L), ciprofloxacin (10 mg/L)	PMS activation	Removal of 95%, 91% and 85%, respectively	[80]

Table 2. *Cont.*

Material	Preparation	Target	Conditions	Results	Ref.
Fe-doped TiO_2/rGO	Hydrothermal process	BPA, Bisphenol F (BPF), Bisphenol AF (BPAF), Bisphenol S (BPS) (20 mg/L)	Visible-light irradiation (60 min for BPA, 120 min for BPF, BPAF and BPS)	Removal of 100%, 100%, 100% and 96% respectively	[68]
Bi_2WO_6/BiOI (BWOI-3 morphology)	Microwave-assisted synthetic method	Methyl orange (MO), BPA	Visible-light irradiation (60 min for MO, 100 min for BPA)	Removal 95.0% and 86.8% respectively, MO: 0.04169 min^{-1}, BPA: 0.01778 min^{-1}	[75]
Polythiophene (PTh)/$Bi_4O_5I_2$	Sol–gel Methodology	BPA	Visible-light irradiation (30 min)	Removal 99.2%, 0.194 min^{-1}	[74]
Pd/PdO/β-Bi_2O_3 composite	Simple two-step Sol–gel-based process	BPA	Visible-light irradiation (30 min)	Removal of 97.4%, 0.1129 min^{-1}	[76]
Pd/$Bi_4O_5Br_2$	Solvothermal-reduction method	BPA (20 mg/L)	LED visible-light irradiation (70 min)	95.8% removal, 0.0548 min^{-1}	[77]
Nano flake Ag_3PO_4	Sol–gel Methodology	BPA (15 mg/L)	Visible-light irradiation (30 min)	100% removal efficiency, 0.6324 min^{-1}	[78]
Cu_2O@β-CD	Topotaxial conversion	BPA (8 mg/L)	Neutral pH	83.7% removal, 0.0196 min^{-1}	[81]
TiO_2	Sol–gel Methodology	DMP (5.16 μM)	UV irradiation (75 min) and pH 6–7	80.5% removal, 0.0768 min^{-1}	[85]
TiO_2	Sol–gel Methodology	DMP, DEP, DBP (6, 6, and 4.128 mg/L)	UV irradiation (90 min)	Removal 93.0, 92.6, 92.5% respectively, 0.025 min^{-1}	[86]
Bi_2O_3-TiO_2 composite	Hydrothermal process	Pb(II), DBP	Visible-light irradiation (4 h)	45%-DBP oxidation, 40%-Pb(II) reduction	[87]
Nanorod ZnO/SiC nanocomposite	Sol–gel Methodology	DEP (5 ppm)	UV and visible light, neutral pH	90% removal, UV: 46.86 × 10^{-3} min^{-1}, Visible: 8.52 × 10^{-3} min^{-1}.	[88]
mpg-C_3N_4/BiOBr/PTh(Z-scheme)	Sol–gel Methodology	DMP (1 g/L)	Visible-light irradiation	Removal efficiency of 40% and 50% higher than g-C_3N_4 and BiOBr, 0.193 h^{-1}.	[89]
Iron–cerium (Fe-Ce) bimetallic catalysts (FCBCs)	Sol–gel Methodology	PAEs (DMP, DEP, DEHP, DINP, DnOP, DIDP)	PS 1.0 × 10^{-5} M, FCBC 1.67 g/L, pH 2	86% removal, 1.5 × 10^{-1} h^{-1}.	[90]

4.2. Photocatalytic and Catalytic Degradation of Agricultural Chemicals

Agricultural chemicals (or agrochemicals) are a variety of synthetic compounds used to protect crops and increase their yield and quality, including mainly pesticides (herbicides, insecticides, fungicides, nematicides, and so forth), but also fertilizers, soil conditioners, and plant growth regulators (Figure 9). Pesticides are meant to eradicate plants, animals, fungi, and microorganisms that are detrimental to cultures, affecting selected functions

in target organisms. Nonetheless, they can also exert toxicity toward humans and wild fauna. The evaluation of these effects is complex, as most toxicity tests are performed in acute rather than long-term experiments, while endocrine disrupting activity often arises upon long-term exposure [25]. The growth of the world's population increases the demand for farming land and productivity, hence the usage of agrochemicals. According to the Food and Agriculture Organization of the United Nations (FAO) the global production of pesticides exceeds 4 million tons per year [92]. These can easily be transferred from soil to surface waters and groundwater and encounter living beings, causing adverse effects. Therefore, pesticides represent a chronic and widespread threat to humans and the ecosystem and their removal from water is a severe concern.

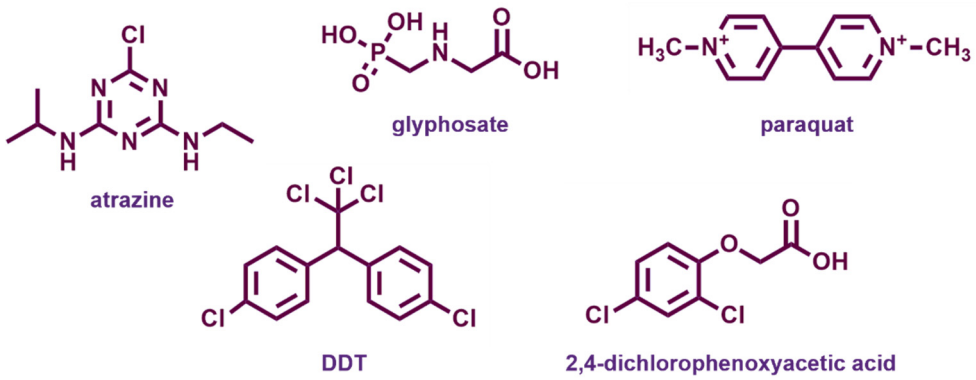

Figure 9. Chemical structures of the most widespread agrochemicals with endocrine disrupting properties.

4.2.1. Atrazine

Atrazine (ATZ) is a chlorinated triazine used as herbicide in the control of broadleaf and grassy weeds, particularly applied in corn cultivation. The triazine ring structure gives high chemical stability and a very long half-life in water, so it can be easily transported through surface water and soil and enter the food chain, becoming a potential threat to human health and animals, connected with reproductive abnormalities and potential carcinogenity. Atrazine has been banned in the European Union since 2004 and has been listed as a prior harmful substance by the U.S. EPA and the Ministry of Ecology and Environment of China. A large number of works have dealt with the removal of this herbicide from water [93].

Noticeable performances in the visible light-driven degradation of atrazine were obtained by coupling two strategies for the modification of TiO_2: co-doping with indium and sulfur and the formation of a heterostructure with rGO [94]. The In,S-TiO_2@rGO nanocomposites were synthesized by an ultrasonic-assisted solvothermal method and the optimized composition yielded complete degradation and 95.5% mineralization of 20 mg/L ATZ within 20 min and good stability with reuse. Titanate semiconductors with peroskite structure are promising photocatalytic materials. Shawky et al. prepared $LaTiO_3$ nanowires modified through the photo-assisted deposition of Ag, which resulted in an improvement of surface texture, light absorption in the visible range, and a reduction of the electron–hole recombination [95]. The Ag/$LaTiO_3$ nanowires (2.5 wt% optimal Ag load) could photodegrade ATZ (50 mg/L initial concentration) under visible light after just 40 min at a catalyst dosage of 1.2 g L^{-1}. Additionally, the same authors synthetized novel spinel-structured $NiCo_2O_4$ nanorods that worked as a visible light photocatalyst upon Ag loading [96]. Particularly, 5 wt% loading of Ag improved the optical and optoelectronic properties of the photocatalyst, resulting in the minimization of the bandgap from 3.6 down to 2.57 eV and in the enhancement of visible light absorption. The Ag/$NiCo_2O_4$ nanorods exhibited a boosted photodegradation of ATZ to completion within 20 min at 2.0 g L^{-1} dosage, with excellent recyclability. Furthermore, in this case, Ag-loaded photocatalyst showed lower electron–hole recombination and outperformed the pristine sample.

Majhi et al. developed though a one-step hydrothermal method bismuth-based ternary heterostructures, CdS/BiOBr/$Bi_2O_2CO_3$, with a controlled morphology and improved visible light absorption [97]. The materials consisted of well dispersed CdS nanoparticles (50–80 nm) anchored over ultrathin BiOBr and $Bi_2O_2CO_3$ nanoplates, which guaranteed a high interfacial contact. The photocatalyst showed significant degradation efficiency (>95% in 30 min) of ATZ herbicide and reduced the cytotoxicity of the treated water solution. Scavenger and radical (•OH and $\bullet O_2^-$) trapping experiments highlighted that the photocatalytic degradation occurred by a double Z-scheme electron transfer mechanism.

The combination of heterogeneous Fenton and photocatalysis was investigated by Yang et al. with a Fe/TiO_2 sol–gel material [98]. Using 1 g/L of catalyst, 1.6 mM H_2O_2 and visible light, 95% degradation of atrazine (10 mg/L initial concentration) was accomplished in 30 min at pH 3, and more than 75% degradation was achieved at up to pH 7. Several intermediate and final products were identified, and the possible degradation mechanism was inferred. Recently, in the field of sulfate-based AOPs, sulfite was proposed as an alternative to the common precursors of sulfate radical. Its activation on zinc-copper ferrites was demonstrated under irradiation by Huang et al. [99]. The $Zn_xCu_{1-x}Fe_2O_4$ mixed oxides, synthesized by a sol–gel combustion method, showed magnetic properties and excellent ability in the removal of ATZ under UV-visible irradiation with the stepwise addition of Na_2SO_3. $Zn_{0.8}Cu_{0.2}Fe_2O_4$ gave the highest activity within 30 min and $SO_4\bullet^-$ was identified as the main reactive species. Moreover, the catalysts could be magnetically separated from the solution for its reuse. The influence of several process parameters was assessed, and a possible reaction pathway was illustrated.

Photoelectrocatalytic systems were also proposed for the degradation of agrochemicals. For example, Xie et al. examined the mechanism of photoelectrochemical removal of ATZ, using typical TiO_2 nanotube arrays obtained by anodization on Ti plates as working photoanode and a wide spectrum Xe lamp [100]. The best removal efficiency reached 96.8% at applied potential of 0.2 V vs. SCE in 2 h, with reaction rate constant of 1.72 h^{-1}. The results indicated that the of optimal bias (requesting a low electric power input) did not change the degradation products of atrazine, but it enhanced the removal rate by affecting the amount and distribution of the ROS generated. Among them, the superoxide radical seemed to play a central role in ATZ dechlorination, possibly because of its nucleophilicity.

The intimate coupling of photocatalysis and biodegradation (ICPB) approach is promising for the treatment of emerging contaminants. A valuable example was reported by Zhang et al., who prepared a heterostructure of Bi_2WO_6 with carbon nitride by hydrothermal method and coated it on a polyurethane sponge cube via powder spraying [101]. A biofilm derived from active sludge was then cultivated in the inner of the macroporous sponge carrier. Under UV-visible light, the Bi_2WO_6/C_3N_4 heterojunction decomposed atrazine into biodegradable intermediates, which were successively mineralized by the microorganisms, increasing the removal of 20% (up to 50% in 8 h with 20 mg/L initial ATZ concentration).

Technologies independent from light irradiation, especially sulfate-based AOPs, are increasingly studied for the decomposition of EDCs. For instance, the activation of persulfate was tested for the removal of atrazine using Fe_3O_4 nanoparticles supported on sepiolite, a hydrated magnesium silicate clay [102]. Magnetite NPs were synthesized in situ and loaded onto fibrous sepiolite via a co-precipitation method. The effective adsorption and alkaline pH values favoured the removal of ATZ, which reached 71.6% after 60 min, with 92 mmol/L of PS and 10 mmol/L initial pesticide concentration). Although TOC removal was merely 21% the identified products were nontoxic, and the nanocomposite maintained structural and functional stability during four consecutive batch runs. Turning to PMS, a heterogeneous Fenton-like system was realized coupling it with the addition of hydroxylamine (HA) in the presence of Fe_3O_4 [103]. HA had a double role, as PMS activator, which accounted for 40% of the observed ATZ decomposition, and also as promoter of the Fe(III)/Fe(II) redox cycle on magnetite surface, which additionally generated •OH radicals. The degradation rate constant of atrazine at near-neutral pH in Fe_3O_4/PMS/HA

system (0.152 min^{-1}) was almost 5 times higher than that in the homogeneous PMS/HA system. PMS was activated also by Cu-doped $LaFeO_3$ perovskites synthesized through a sol–gel method [104]. The sample with $LaFe_{0.8}Cu_{0.2}O_{3-\delta}$ composition exhibited the highest catalytic activity and stability, completely removing ATZ (23 μM) in 60 min, with the use of 0.5 g/L catalyst and 0.5 mM PMS. Both Fe(III)/Fe(II) and Cu(II)/Cu(I) cycles along with surface hydroxyl groups contributed to the degradation in a wide pH range (2–10), leading to different possible reaction pathways. Dong et al. developed a cobalt-nickel mixed oxide supported on diatomite, preparing by co-precipitation 2D $CoNi_3O_4$ nanoribbons which were vertically aligned on diatomite [105]. The topology of the nanoribbons in the composite comprised abundant exposed edges and sharp corners, working as active sites, and open channels, facilitating the migration and reaction of PMS and pollutant molecules. The 30 wt% $CoNi_3O_4$/diatomite/PMS system gave 93% ATZ (5 ppm) removal and 56% TOC decrease after 30 min (rate constant 0.0842 min^{-1}), with 0.1 g/L of catalyst and 0.3 mM PMS. Comparable results were recorded in real water samples. The detection of the involved radicals evidenced that $SO_4\bullet^-$ was the dominant oxidant, while $\bullet O_2^-$ contributed to the reversible redox cycle of Co^{2+}/Co^{3+} and Ni^{2+}/Ni^{3+}, supporting the excellent catalytic efficiency.

Among electrocatalytic processes, a Ti/PbO_2 electrode modified with cobalt and samarium was prepared by one-step electrodeposition on pretreated Ti substrates and used as anode for the electrocatalytic removal of ATZ in wastewater [106]. Co and Sm were proved to enhance the catalytic activity and stability, indeed the Ti/PbO_2–Co-Sm electrode displayed higher oxygen evolution potential, lower charge transfer resistance, longer operative lifetime and higher degradation efficiency compared with bare Ti/PbO_2. 92.6% atrazine removal and 84.5% COD decrease were achieved in 3 h under optimized conditions: current density 20 mA cm^{-2}, pH 5, temperature 35 °C. A particularly interesting three-dimensional electrochemical process, i.e., a system composed of 2D electrode with particulate electrode suspension between the two main electrodes, was investigated by Li et al. [107]. They prepared $CuFe_2O_4$ magnetic nanoparticles by combustion sol–gel method and used them simultaneously as particle electrode and catalyst for PS activation (Figure 10). The best ATZ degradation efficiency (>99%) and TOC removal (22.1%) were achieved after 35 min with solid dosage of 3.0 g/L, 4.0 mM PS, current density of 4 mA/cm^2, and initial pH 6.3. The nanoparticle electrodes maintained stability throughout five consecutive runs, and sulfate radical was identified as the dominant reactive species in the degradation process.

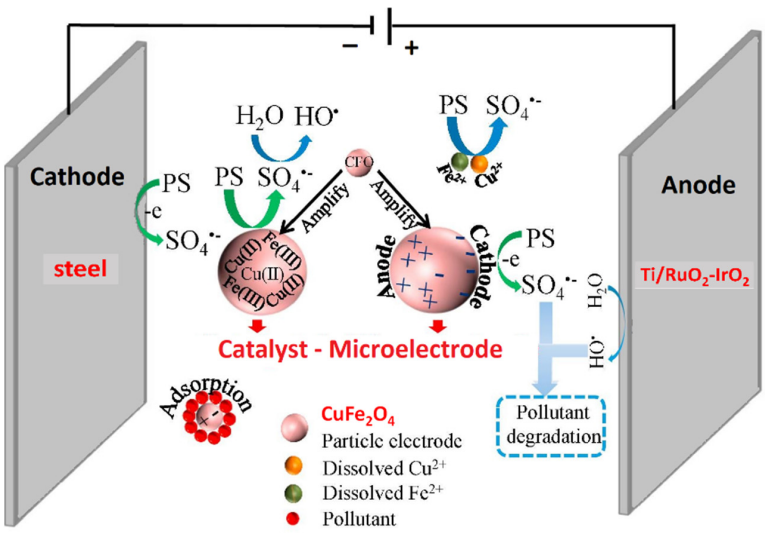

Figure 10. Schematic representation of a 3D electrochemical degradation cell with $CuFe_2O_4$ (CFO) magnetic nanoparticles acting as particle electrodes and catalysts for persulfate (PS) activation. Adapted and reprinted with permission from [107], Copyright (2019) Elsevier.

The most representative reports concerning agrochemicals as endocrine disruptors are summarized in Table 3, including the principal process conditions and results in terms of removal efficiency and rate constant.

Table 3. Summary of representative metal-oxide-based nanomaterials used for the degradation processes of agricultural chemicals atrazine (ATZ), glyphosate (PMG), paraquat, dichlorodiphenyltrichloroethane (DDT), 2,4-dichlorophenoxyacetic acid (2,4-D) and other pesticides.

Material	Preparation	Target	Conditions	Results	Ref.
In,S-TiO_2@rGO	ultrasonic-assisted solvothermal method	ATZ (20 mg/L)	Visible light (20 min)	100% removal, 95.5% mineralization, k = 0.248 min^{-1}	[94]
Fe-TiO_2	Sol–gel method	ATZ (10 mg/L)	Visible light, 1.6 mM H_2O_2 (30 min)	95% degradation at pH 3 k = 0.1021 min^{-1}	[98]
Ag/$LaTiO_3$ nanowires	Hydrothermal method	ATZ (50 mg/L)	Visible light (40 min)	100% removal k = 0.0434 min^{-1}	[95]
Ag/$NiCo_2O_4$ nanorods	Co-precipitation	ATZ (50 mg/L)	Visible light (20 min)	100% removal, k = 0.049 min^{-1}	[96]
CdS/BiOBr/$Bi_2O_2CO_3$	Hydrothermal method	ATZ (50 mg/L)	Visible light (30 min)	95% removal, k = 0.122 min^{-1}	[97]
$Zn_xCu_{1-x}Fe_2O_4$	Sol–gel combustion process	ATZ (4.4 μM)	UV-vis light (30 min), Na_2SO_3 0.5 mM	95% removal, k = 0.195 min^{-1}	[99]
TiO_2 nanotubes	Electrochemical anodization	ATZ (2 mg/L)	UV-vis light, bias 0.2 V vs. SCE (2 h)	96.8% removal, k = 1.72 h^{-1}	[100]
Bi_2WO_6/C_3N_4	Hydrothermal method	ATZ (20 mg/L)	Visible light, biofilm (8 h)	>50% removal	[101]
Fe_3O_4-sepiolite	Co-precipitation	ATZ (10 mM)	PS 92 mM (1 h)	71.6% removal, 21% mineralization k = 0.0108 min^{-1}	[102]
Fe_3O_4	Commercial	ATZ (23 μM)	PMS 0.4 mM hydroxylamine 0.3 mM (15 min)	100% degradation, k = 0.152 min^{-1}	[103]
Cu-doped $LaFeO_3$	Sol–gel method	ATZ (23 μM)	PMS 0.5 mM (1 h)	100% degradation, 52% mineralization k = 0.1406 min^{-1}	[104]
$CoNi_3O_4$ nanoribbons/diatomite	Co-precipitation	ATZ (5 mg/L)	PMS 0.3 mM (30 min)	93% removal, 56% mineralization k = 0.0842 min^{-1}	[105]
Co,Sm-Ti/PbO_2 electrode	Electrochemical deposition	ATZ (20 mg/L)	Current density 20 mA cm^{-2} (3 h)	92.6% removal, 84.5% COD decrease	[106]
Ti/RuO_2-IrO_2 anode, $CuFe_2O_4$ particles	Sol–gel combustion process	ATZ (46 μM)	Current density 20 mA cm^{-2}, PS 4.0 mM (35 min)	99% removal, 22.1% mineralization k = 0.0186 min^{-1}	[107]
Faceted TiO_2	Hydrothermal method	PMG (10 mg/L)	UV light	100% removal in 50 min, k = 3.0 h^{-1} on {201}-TiO_2	[108]
CeO_2 NPs	Solution synthesis	PMG (25 mg/L)	UV or visible light	100% removal in 5 min (UV, k = 0.6601 min^{-1}) or 20 min (visible, 0.3028 min^{-1}) at pH 4	[109]
W/ZnO	Precipitation	PMG (20 mg/L)	Simulated solar light (3 h)	74% removal, 30% mineralization	[110]

Table 3. *Cont.*

Material	Preparation	Target	Conditions	Results	Ref.
$BiOBr/Fe_3O_4$	Solvothermal method	PMG (100 mg/L)	Visible light (1 h)	97% removal	[111]
$MoSe_2/BiVO_4$	Hydrothermal method	PMG (10^{-4} M)	Visible light (3 h)	86.1% removal	[112]
Cu_2S/Bi_2WO_6	Hydrothermal method	PMG (10^{-4} M)	Visible light (3 h)	73.2% removal	[113]
Fe_3CeO_x	Co-precipitation	PMG (100 mg/L)	PMS 0.5 mM (15 min)	100% removal, 85.6 TOC decrease 400 mg L^{-1} h^{-1}	[114]
TiO_2 P25 on SiC	Dip coating	Paraquat (5–40 mg/L)	UV-C light	90% mineralization	[115]
TiO_2 on SBA-16 SiO_2	Sol–gel method	Paraquat (50 mg/L)	UV light (24 h)	70% removal, k = 0.0431 min^{-1}	[116]
N-TiO_2	Hydrothermal method	Paraquat (20 mg/L)	UV or visible light (120 min)	Removal 86% (UV, k = 0.0230 min^{-1}), 62% (visible, k = 0.0074 min^{-1})	[117]
N-TiO_2@SiO_2@Fe_3O_4	Sol–gel method	Paraquat (10–40 mg/L)	Visible light (3 h)	98.7% removal, 84.7% mineralization	[118]
B-TiO_2-SiO_2/$CoFe_2O_4$	Sol–gel, hydrothermal method	Paraquat (300 mg/L COD)	Visible light (3 h)	82% COD removal k = 0.89 h^{-1}	[119]
TiO_2@MIL-101(Cr)@Fe_3O_4	Solution synthesis	Paraquat (20 mg/L)	UV light (45 min)	87% removal, k = 0.0126 min^{-1}	[120]
g-C_3N_4/$Bi_2O_2CO_3$/$CoFe_2O_4$ on biochar	Solution synthesis	Paraquat (20 mg/L)	Visible light, sunlight, photo-ozonation, PMS	99% removal in 1.5 h (vis, 0.0596 min^{-1}), 100% mineralization in 30 min (visible-O_3-PMS)	[121]
CeO_2–Bi_2O_3	Co-precipitation	2,4-D	Visible light (13 h)	90% removal and COD decrease	[122]
Fe_3O_4@WO_3/SBA-15	Co-precipitation hydrothermal method	2,4-D (10^{-6} M)	UV light (4 h)	90.7% removal	[123]
TiO_2 nanotubes	Anodization	2,4-D (10 mg/L)	Simulated sunlight, bias 2.4 V (2 h)	97% removal, k = 0.0295 min^{-1}	[124]
TiO_2-acetylacetone	Sol–gel method	2,4-D, 4-CPA, MCPA, MCPB (≥0.2 mM)	Dark (1 h)	80–90% removal	[50]
Co–Ni@chitosan@Fe_3O_4	Co-precipitation, reduction	2,4-D (100 mg/L)	H_2O_2 1–2 mL	95.5% removal, k = 0.07517 min^{-1}	[125]
polyaniline/SnO_2	Polymerization, precipitation	DDT (100–500 mg/L)	Microwave irradiation (12 min)	80% removal, k = 0.20 min^{-1}	[126]
MnO_2	Oxidation	DDT (0.5 mg/L)	PMS (4 h)	100% removal	[127]
TiO_2,ZnO	Commercial	vinclozoline fenarimol, malathion, fenotrothion, quinalphos, dimethoate (0.3 mg/L)	UV light or sunlight, PS (250 mg/L $Na_2S_2O_8$), 4 h	70–100% removal, except for fenarimol, 0.0018–0.0292 min^{-1} (TiO_2); 0.0023–0.0872 min^{-1} (ZnO)	[128,129]

4.2.2. Glyphosate

Glyphosate, N-(phosphonomethyl)glycine (PMG), an organophosphate compound, is a highly effective broad-spectrum herbicide, such that glyphosate-based herbicides are the most widely used pesticides worldwide. Several studies have put attention on risks related to the possible carcinogenic, neurotoxic, and endocrine-disrupting effects of glyphosate,

and to its impact on the aquatic environment [130], giving rise to a strong controversy from the viewpoint of scientific evaluation and legislation. Disagreements in the assessment of the results are mainly related to methodological differences in the evaluation of the available evidence [131]. In the EU, glyphosate approval has been renewed until December 2022; however, the debate remains open.

Crystalline semiconductors with different exposed facets may show substantial variations in adsorption and photocatalytic efficiency. This was demonstrated for anatase TiO_2 nanomaterials, exposing a high or low fraction of specific facets. The surface energy of different facets dominated the adsorption of PMG, and the highest Langmuir adsorption capacity (0.88 molecules/nm^2) was observed on {201}-TiO_2, with the sample also exhibiting the highest photodegradation reaction constant [108]. The better photoactivity was attributed to a more efficient ROS generation, a larger electron transfer and oxygen reduction reaction (ORR) rate. Two-dimensional correlation spectra (2D-COS) and ATR-FTIR analysis proved that each functional group of PMG adsorbed on TiO_2 underwent a transformation sequence of a different order.

The size of nanoparticles is another factor that can have a great influence on photocatalytic activity, particularly when approaching extremely small sizes. Investigating cerium dioxide nanoparticles with ultrasmall controllable diameter, synthesized with citric acid as capping agent, Wu et al. observed a significantly size-dependent activity in glyphosate degradation [109]. The finest CeO_2 NPs (2.1 nm) provided several times higher degradation rates compared to 4.8 nm NPs, achieving PMG removal in 5 min under UV irradiation and 20 min under visible light, at pH 4. These hybrid CeO_2 nanomaterials exhibited high surface areas, abundant oxygen defects and a good stability of dispersion in water. The excellent photocatalytic efficiency was explained as due not only to the morphology and defectivity, but also on the role of bonded citric acid as electron donor, fostering the regeneration of Ce^{3+} sites by ligand-to-metal charge transfer. On the other hand, W-doped ZnO showing large wurtzite crystallites was prepared by a simple precipitation method and tested in PMG photodegradation under simulated solar light [110]. The optimal doping amount was found to be 1.5 mol%, providing 74% removal and 30% mineralization in 180 min with 1.5 g/L catalyst dosage.

Among the bismuth-based semiconductors emerging as photocatalysts, bismuth vanadate and tungstate possess a relatively low band gap (about 2.4 and 2.7 eV, respectively), resulting in visible light response, and chemical stability against photo-corrosion. Heterojunctions with other semiconductors are frequently examined to enhance their activity. Luo et al. fabricated via a facile two-step hydrothermal method, peanut-like shaped $MoSe_2/BiVO_4$ composites responsive to visible light [112]. The coupling of $MoSe_2$ and $BiVO_4$, forming a heterojunction, enhanced the photocatalytic activity, transfer of photogenerated carriers and the charge separation. The highest photocatalytic performance for the degradation of PMG was observed for $0.15MoSe_2/BiVO_4$ sample, which also presented high stability and good reusability in the photocatalytic reactions among all the as-prepared composites. Cu_2S/Bi_2WO_6 composites synthesized by a three-step route, including hydrothermal treatments for the two semiconductors and a subsequent ultrasound-assisted stage for their coupling, displayed a hierarchical flower-like nanostructure, with Cu_2S nanoparticles deposited on the surface of Bi_2WO_6 nanosheets [113]. These materials proved considerable and stable activity in PMG degradation under visible light, which was explained according to a Z-scheme mechanism that maximizes charge separation, with optimum loading of Cu_2S equal to 1 wt%. Cao et al. prepared magnetic $BiOBr/Fe_3O_4$ nanocomposites photocatalysts via a facile solvothermal process [111]. These catalysts showed excellent photocatalytic activity toward glyphosate degradation in water under visible-light irradiation and magnetic recyclability. The degradation reached 97%, which was higher than that of the pure BiOBr nanosheets (85%) within 60 min. In particular, $BiOBr/Fe_3O_4$ nanocomposites exhibited high reusability, as after five repeated trials, the percent of degradation of PMG was still more than 90%. The higher photocatalytic activity

than that of pure BiOBr was attributed to the efficient separation of photoinduced charge carriers, where h^+ was shown to be the dominant reactive species in the photodegradation.

Electrochemical oxidation systems were also tested for glyphosate decomposition. A TiO_2 photoanode was deposited on boron doped diamond (BDD) by sol–gel coupled with spin coating, using titanium oxysulfate as precursor and obtaining aggregates of anatase nanoparticles [132]. The removal of PMG electrocatalysis in the dark reached 91% in 5 h, with significant TOC and COD abatement. The photoelectrocatalytic performances under UV irradiation were higher, as expected, and allowed a virtually complete PMG removal in less than 4 h with lower current density (3 mA cm^{-2}). Non-irradiated PMS activation was studied on Fe_3CeO_x prepared by a simple co-precipitation procedure, observing rapid and complete degradation of glyphosate (100 mg/L) within 15 min, with 85.6% TOC removal and 80.8% total nitrogen (TN) removal, using 0.5 mM PMS and 3 g/L of catalyst [114]. The outstanding catalytic activity and stability of the material originate from the synergy of iron and cerium, in particular the reductive action of Fe^{2+} and Ce^{3+}. The C–N and C–P bonds of glyphosate appeared susceptible to attack by sulfate and hydroxyl radicals, resulting the formation of aminomethylphosphonic acid (AMPA), a typical by-product, and PO_4^{3-} by dephosphorylation, and ultimately driving mineralization.

4.2.3. Paraquat

Paraquat (also known as methyl viologen) is a bypiridinium compound, widespread as a fast-acting and non-selective herbicide. It exerts significant toxicity in humans and animals, and recent studies have demonstrated adverse effects on the endocrine system of mammals and on neurogenesis (the generation of new neurons), indicating it as an etiological factor of Parkinson's disease [130].

Supported photocatalysts were prepared depositing P25 TiO_2 nanopowder on SiC foam cylinders (16 wt% loading), by repeated dipping and final annealing [115]. Tests of paraquat (5–40 mg/L) degradation were conducted in a photocatalytic tubular reactor equipped with a UV-C lightning system (254 nm), showing improved efficiency of the photocatalytic system compared to photolysis, particularly in the mineralization, which was 90% after 180 min. Carboxylic acids were identified as the main reaction intermediates. TiO_2 was also supported on highly ordered mesoporous silica (SBA-16), preparing nanocomposites with large specific surface area via templated sol–gel route [116]. Batch tests showed that paraquat (50 mg/L) mixed with a dye was adsorbed and gradually decomposed by SBA-16/TiO_2 (0.4 g/L) under UV illumination, reaching 70% removal after a prolonged reaction time of 24 h. Carbon-modified titania nanomaterial synthesized by hydrolytic sol–gel in the presence of coffee extract was tested in the photodegradation of paraquat (5 to 50 mg/L) under UV light, observing a moderate activity with 0.6 g/L of TiO_2/C, which was manifold increased with the addition of 10 mM H_2O_2 [133]. However, the lack of characterization of the materials prevented the evaluation of the influence of the carbonaceous phase on the functionality. In the extensively studied branch of non-metal doping of TiO_2, nitrogen is the reference element, inducing a moderate band gap reduction. N-doped TiO_2 samples with nanorice-like morphology, synthesized via hydrothermal method and calcined at different temperatures, were tested in paraquat (20 mg/L) photodegradation with 1 g/L of catalyst [117]. The removal over the uncalcined sample was about 86% and 62% after 120 min of UV and visible irradiation, respectively. The decrease of the photoactivity with the treatment temperature was explained as due to the gradual reduction of specific surface area and nitrogen content. These results are comparable to those reported for a N-doped TiO_2-based magnetic nanomaterial with a Fe_3O_4 core (N-TiO_2@SiO_2@Fe_3O_4) synthesized by sol–gel and used in paraquat decomposition, showing visible light activity with TOC removal up to 85% in 180 min and good reusability [118]. Boron-doped TiO_2-SiO_2 prepared by sol–gel was coupled with cobalt ferrite nanoparticles through hydrothermal process [119]. The so-obtained magnetically separable composite, B-TiO_2-SiO_2/$CoFe_2O_4$, exhibiting low band gap and long charge carrier lifetime, was applied for the decontamination of real and synthetic wastewaters containing recalcitrant compounds, among them the

pesticides diazinon and paraquat. The latter was completely removed under visible light at the optimized conditions, i.e., COD concentration of 300 mg/L, catalyst loading of 2.5 g/L and pH 3, in 3.5 h, with degradation rate constant 0.89 h^{-1}. Another magnetic photocatalyst was prepared coupling TiO_2 with α-Fe_2O_3 and MIL-101(Cr) metal-organic framework in a three-step solution synthesis procedure [120]. The operating parameters for paraquat photodegradation were optimized, achieving 87% removal at 20 ppm initial concentration with 0.2 g/L of catalyst in 45 min, nonetheless the role of the MOF component was not clearly defined.

Kumar et al. prepared a biochar-supported magnetic ternary heterojunction, g-C_3N_4/$Bi_2O_2CO_3$/$CoFe_2O_4$ (BCBF), through a multistep precipitation–hydrothermal method [121]. The nano-assembly exhibited high quantum efficiency, charge separation and transport and ROS generation, as revealed by photoluminescence and electrochemical analyses, resulting in excellent visible light activity. The degradation of paraquat was tested in various conditions: visible radiation, natural sunlight, photo-ozonation and presence of peroxymonosulfate. The removal of 20 ppm paraquat with 0.5 g/L of BCBF reached 99.3% under visible radiation in 90 min and 92.1% under solar light in 120 min, being manifold faster on the ternary junction than on its single components or binary composites. A combined experiment BCBF/PMS/O_3/visible led to complete mineralization in less than 30 min. Moreover, the absence of cyto-toxicity of the nanomaterial was checked by cell viability assay.

4.2.4. Chlorinated Phenoxyalkanoic Herbicides

Chlorinated phenoxyalkanoic acids are a family of widespread herbicides considered as priority pollutants. Their most common representative is 2,4-dichlorophenoxyacetic acid (2,4-D), an EDC with toxic and carcinogenic effects, whose partial breakdown can originate other harmful compounds, such as 2,4-dichlorophenol. The photodegradation of 2,4-D was tested under UV irradiation over Fe_3O_4@WO_3 nanomaterials supported on mesoporous silica SBA-15, prepared by the co-precipitation, solvothermal and hydrothermal methods [123]. The magnetic photocatalyst with 5% Fe_3O_4@WO_3 loading gave 91% degradation of the herbicide in 4 h. Cerium dioxide and a CeO_2-Bi_2O_3 mixed oxide synthesized through co-precipitation method were tested in the degradation of 2,4-D under visible light [122]. The mixed catalyst with 30 wt% Bi_2O_3 showed slightly increased photodegradation rate, with a removal of the herbicide of 91% after 13 h.

The photoelectrochemical oxidation of 2,4-D was investigated on blue TiO_2 nanotube (TNT) arrays, fabricated via an electrochemical reduction method with formic acid as the electrolyte [124]. These TNT contained Ti^{3+} sites responsible for increased conductivity and visible light absorption. Their use as electrodes under simulated solar radiation gave 2,4-D degradation rate constant (0.0295 min^{-1}) more than twice the sum of the rates of electrocatalytic and photocatalytic processes alone.

TiO_2-based amorphous hybrid materials synthesized by hydrolytic sol–gel route with the addition of a diketone (acetylacetone) were studied by Pirozzi et al. for the catalytic removal of four related chlorinated aromatic herbicides: 2,4-D, MCPA (4-chloro-2-methylphenoxyacetic acid), 4-CPA (4-chlorophenoxyacetic acid), and MCPB (4-(4-chloro-2-methylphenoxy) butanoic acid) [50]. The ligand-to-metal interfacial charge transfer complexes (acetylacetonate-Ti) allowed the generation in ambient conditions of extremely stable superoxide radicals. These ROS induced strong oxidative activity in water in the absence of light irradiation or additional oxidants, also by producing •OH radicals. Removal efficiencies between 80% and 90% were observed in 60 min using 0.2 mM initial herbicide concentration and 1 g/L of catalyst. At higher concentrations some differences in the process rates were observed; however, the removal of all contaminants tended to be completed in short times, leading to a distribution of oxidation by-products and suggesting a consecutive adsorption–degradation process, supported by the good fitting of the concentration decay curves obtained by double-exponential model. •O_2^- radicals were

easily regenerated on the surface of the hybrid catalyst, allowing its efficient reuse. The same catalyst proved effective also in the removal of phenanthrene [50].

The synergy between cobalt and nickel was exploited by Sharma et al., who prepared a bimetallic catalytic system comprising a polymeric chitosan support decorated with redox couple Co–Ni nanoparticles [125]. The magnetically recoverable Co–Ni@CS@Fe_3O_4 nanocomposite was obtained by anchoring Co and Ni catalytic centers onto the surface of chitosan. The bimetallic nanocomposite fostered the in situ generation hydroxyl radical species with the addition of H_2O_2, catalyzing the oxidative degradation of water contaminants, including 2,4-D. In comparison to its monometallic counterparts, the bimetallic nanocomposite resulted in an enhanced degradation efficiency toward 2,4-D (95.50%) and methyl orange dye (93.14%) due to a synergistic effect produced by the combination of two metals, and a significant reusability in eight consecutive cycles.

4.2.5. Other Pesticides

Dichlorodiphenyltrichloroethane (DDT) was an extremely widespread insecticide that was banned in most countries decades ago, because of its environmental and human toxicity, including endocrine disrupting activity and probable carcinogenity. Nonetheless, its production has decreased but not ceased, as DDT is allowed for disease vectors control (like malaria-transmitting mosquitoes) and is still used locally. Moreover, its chemical stability and lipophilicity make it a persistent organic pollutant with high bioaccumulation tendency, still found in waters and soils. In recent years few works have dealt with the heterogeneous chemical degradation of DDT. Tin dioxide was coupled with a conductive polymer, polyaniline (PANI), to enhance its catalytic activity [126]. PANI/SnO_2 nanohybrids with different compositions were prepared via ultrasound-assisted polymerization of aniline in the presence of SnO_2 nanoparticles synthesized by precipitation using Guava extract. Microwave-assisted catalytic degradation of DDT resulted in a fast removal of more than 80% DDT in very short times (12 min of microwave irradiation), even with pollutant concentrations as high as 500 mg/L on PANI/SnO_2-50/50. A variety of by-products was detected, including relatively low molecular weight ones produced by dechlorination. Three different structures of MnO_2 synthesized by an oxidation method in liquid phase were tested in PMS activation for the degradation of DDT [127]. The crystal structure, surface area and Mn(III) content were individuated as the main properties affecting the catalytic activity. α-MnO_2 was the most efficient polymorph, followed by γ-MnO_2 and β-MnO_2. Almost complete removal of DDT (0.5 mg/L) was attained in about 4 h with 0.5 g/L catalyst load, and higher temperature and acidic pH were observed to increase the efficiency. Sulfate radical was confirmed to be the principal oxidant involved in the process and some breakdown products were identified, resulting from dechlorination and hydroxylation.

Some studies have focused on less widely known agrochemicals with ascertained or likely endocrine disrupting effects. TiO_2 and ZnO are still the most studied photocatalysts and the comparison of their efficiency may give variable results, depending on factors like the considered structure and morphology, besides the chosen target substrate and reaction conditions. Vela et al. studied the combination of persulfate with commercial TiO_2 [128] or ZnO [129] in the degradation of two fungicides (vinclozoline and fenarimol) and four insecticides (malathion, fenotrothion, quinalphos, and dimethoate) with endocrine-disrupting activity. After optimizing the process conditions in a lab photoreactor, they tested it in a pilot-scale plant under natural sunlight, using 200 mg/L of photocatalyst, 250 mg/L of $Na_2S_2O_8$ and 0.3 mg/L of each pesticide. In 4 h the target contaminants were in most part removed, except for fenamirol, and a substantial reduction of dissolved organic carbon indicated complete mineralization. The authors reported a higher efficiency of ZnO compared to TiO_2, anyway they did not discuss more in depth the origin of the differences in the behavior of the two materials.

Sharma et al. synthetized porous WO_3/SiO_2 monoliths, by vacuum impregnation of sodium tungstate in silica monoliths and calcination [134]. The composite monoliths

exhibited a connected porous network structure, high surface area and 2.5 eV band gap. Degradation of imidacloprid insecticide (59%) and methylene blue (97%) was recorded under visible-light illumination in 60 min, with good reuse stability.

The problem of the detection of pesticide residuals in liquid matrices was faced by Quan et al., coupling their sensing with the removal [135]. They prepared arrays of 3D tilted ZnO microrods by chemical bath deposition, following by Ag sputtering, which detected small concentrations of pesticides (the fungicide thiram and some methamidophos compounds) in fruit juices by a surface-enhanced Raman spectroscopy (SERS) method. The same ZnO/Ag material revealed promising performance in the degradation of the contaminant under visible irradiation, owing to the Schottky barrier formed by Ag nanoparticles, acting as electron collectors.

4.3. Photocatalytic and Catalytic Degradation of Pharmaceuticals and Personal Care Products

The awareness of the pollution caused by pharmaceuticals and personal care products is growing rapidly, as the negative effects of many active ingredients in drugs or components of the most common personal care products are increasingly being recognized. Massive production and ubiquitous use (often individual use), followed by frequent and incorrect disposal, results in the significant presence of these chemicals in wastewater. Among these classes of EDCs, antimycotic triclosan, parabens, and hormones (Figure 11), as well as other pharmaceuticals, such as anti-inflammatory and antibiotic ones, are of great concern.

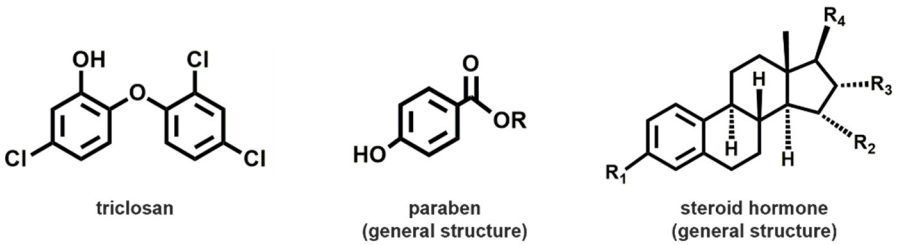

Figure 11. Chemical structures of triclosan, parabens and steroid hormones.

4.3.1. Triclosan

Triclosan (5-Chloro-2-(2,4-dichlorophenoxy) phenol, TCS) is an antimicrobial agent contained in some detergents, toothpastes, and other PCPs. Its use has been restricted in several counties because of concerns about bacterial resistance and endocrine disruption activity. The worries about the environmental consequences of the presence of triclosan (TCS) in water are also related to harmful by-products, such as polychlorinated dibenzodioxins [136].

A TiO_2-rGO composite prepared by hydrothermal method was tested in the photodegradation of triclosan under solar light [137]. At the optimal rGO content of 10 wt%, the catalyst could remove 1 mg/L of triclosan in 24 h exposure to sunlight and performed effectively also in secondary-treated effluent matrix, at ambient pH conditions. Based on scavenging and mineralization experiments the authors proposed a degradation mechanism implying the action of hydroxyl radicals and the removal of chloride. About 85% of TCS degradation was achieved in the secondary effluent, while 100% was obtained in pure water after 16 h of irradiation. A similar nanomaterial produced through a hydrothermal route was proposed by Ojha et al. for triclosan removal [138]. In particular, the authors explored the use of two semiconductor materials (TiO_2 and cadmium sulfide nanoparticles, CdS), connected through a charge transfer system (graphene) with the aim of enhancing photocatalytic degradation. Triclosan was completely degraded after 6.5 h of reaction, followed by an overnight irradiation step. The obtained results were attributed to the enhanced charge transfer as well as separation of the photogenerated charge carriers observed in the ternary CdS@TiO_2-rGO nanocomposite.

A Fe_2O_3-TiO_2/PVP composite layer was prepared by spray coating a mixture of the commercial oxides and polyvinylpyrrolidone on a glass pipe and tested in triclosan degra-

dation under solar light in deionized water and simulated greywater effluent [139]. The authors found this immobilization procedure effective, leading to a removal up to 83%, and proposed a decomposition pathway based on the intermediates detected by LC-MS. A similar spray coating technique was used for the deposition of magnetic composites of iron oxide (α-Fe_2O_3 and Fe_3O_4) and carbon nitride (C_3N_4) synthesized via a microwave-assisted hydrothermal route [140]. Such catalyst showed interesting results in the degradation of triclosan and ethinylestradiol under visible-light irradiation, particularly a TCS was degraded with up to 46% of the initial concentration within 8 h, under visible-light irradiation. A Fe/Nb_2O_5 catalyst, prepared by impregnation of iron (1.5 wt% nominal load) on hydrated niobia and immobilized on calcium alginate spheres, was tested in triclosan degradation in a continuous flow photoreactor, under solar and artificial radiation [136]. The authors showed a promising removal of triclosan and 2,8-dichlorodibenzo-p-dioxin formed as intermediate, with a degradation efficacy up to 80% being achieved in the best operational conditions; however, they recorded a rapid loss of activity and did not investigate the relationships between properties and functionality.

Highly efficient thin film photocatalysts were investigated by Katal et al. [141]. CuO films were developed through rapid thermal annealing and decorated with Pd nanostructures, which considerably increased optical absorption, improving the photocatalytic performance through the enhancement of surface plasmon resonance, ultimately reaching a value of 99% in TCS degradation. Thin film photocatalysts were also synthesized by Tiwari et al. [142]. The authors produced nanocomposite mesoporous Ag(NPs)/TiO_2 thin films through a template assisted synthesis. The oxidative elimination of TCS, under UV-A irradiation, was demonstrated as a function of pH, concentration of triclosan and presence of several co-existing ions. Furthermore, good stability in the multiple use of the obtained nanocomposites was assessed. In addition, the thermal assisted preparation led to a significant enhancement of both charge generation and separation efficiency through improvement of crystallinity and reduction of recombination centers.

Cobalt-doped (Co-TiO_2) and cobalt and nitrogen co-doped (Co-TiO_2-N) anatase nanocatalysts were synthesized by an improved hydrothermal method by Ferreira et al. [143]. The Co-TiO_2-N catalyst displayed the best photocatalytic activity in the degradation of TCS achieving, under UV (365 nm) and Vis (450 nm) LED lights irradiation, nearly complete (>99%) TCS degradation (10 mg/L) in 20 min. The reduction of bandgap energies combined with the electron trapping phenomenon, promoted by both Co^{3+}/Co^{2+} redox pair and the energy level transitions for the nitrogen-related conduction band, improved catalytic performance. In addition, a mechanism involving mineralization of TCS was reported.

Chen et al. successfully synthesized through solution-based oxidation–precipitation and insertion–crystallization processes spinel-type oxide $Co_xMn_{2-x}O_4$ to catalyze peroxymonosulfate in the heterogenous degradation of TCS [144], as schematically described in Figure 12. In addition to sulfate radical, the generation of singlet oxygen from lattice oxygen facilitated the metal redox cycle and promoted the heterogeneous PMS activation in TCS oxidation. At initial pH of 6.8, the authors reported a degradation efficiency up to 96.4% within 30 min of reaction. Furthermore, degradation pathways of TCS which involved the breakage of ether bond or cycloaddition reaction were reported.

A green option for TCS removal was proposed by So et al. using recyclable commercial magnetic nanoparticles, which acted as both adsorbent and catalyst component in a Fenton-like process [145]. PMS was used as source of radicals and the effects of Fe_3O_4 and PMS dosage, adsorption, pH, and catalyst surface charges were studied. Under the optimum conditions, TCS was completely removed in less than 60 min. The same authors implemented their operational conditions avoiding the use of PMS that showed toxic effect on aquatic animals [146]. Indeed, they demonstrated that PMS can be used to pre-activate catalytic $MnFe_2O_4$ nanoparticles, during this activation step Mn^{2+} was altered into manganese oxides which oxidize TCS in the succeeding degradation reactions; hence, the direct addition of PMS is no longer required. The results showed that the preactivated catalyst provides satisfactory results with the total removal of TCS in 20 min at neutral pH.

With a similar purpose, Huang et al. investigated the catalytic performance of CuO loaded halloysite nanotubes to activate persulfate (PS) to degrade and mineralize TCS [147]. Total removal was achieved in 180 min under optimized conditions. The mechanism study demonstrated that even if radical reactions pathway (•OH and $\bullet O_2^-$) existed and the non-radical mechanism ($^1O_2$ and surface electron transport) was dominant to the efficient TCS degradation. A detailed investigation on the degradation intermediates indicated that TCS began to break from the aromatic ring containing monochlorine, and the Cl functional group was gradually substituted. CO_2 and H_2O were generated with breaking of ether bonds. A simultaneous removal of heavy metal, Cr(VI), and TCS was proposed by Song et al. through an Fe_3O_4-activated PS oxidation process [148]. The catalyst was prepared through ultrasonic-assisted reverse coprecipitation, a removal of 87.5% and 99.5% was achieved within 120 min for TCS and Cr(VI), respectively. The proposed degradation pathways indicated that sulfate radicals are the primary radical species responsible for TCS degradation, followed by the breakage of ether bond, de-chlorination, and hydroxylation. The study proved that the Fe_3O_4-activated PS oxidation process could be used as an effective technique for the simultaneous removal of heavy metal and organic pollutants.

Overall, triclosan contamination has recently been treated by sulfate radical generation, in addition to photocatalysis, often relying on iron compounds, as summarized in Table 4.

Table 4. Summary of representative metal-oxide-based nanomaterials used for the degradation processes of triclosan.

Material	Preparation	Target	Conditions	Results	Ref.
TiO_2-rGO	Hydrothermal route	TCS (100 mg/L)	Solar light	85/100% removal 0.251 h^{-1}	[137]
CdS@TiO_2-rGO nanocomposite	Hydrothermal route	TCS (40ppm)	visible light	100% removal 2.7×10^{-3} min^{-1}	[138]
Ag (NPs)/TiO_2 film	Template assisted synthesis	TCS (1.0 mg/L)	UV-A	75% removal 0.992 mg/L/min	[142]
Co,N-codoped TiO_2 nanoparticles	Hydrothermal route	TCS (10mg/L)	UV/Vis LED lights irradiation	>99% removal 0.2340 ± 0.006 min^{-1}	[143]
Fe_2O_3-TiO_2/PVP composite	Spray coating	TCS (1–10 mg/L)	Solar light	83% removal 0.3405–0.0687 min^{-1}	[139]
Fe_3O_4/C_3N_4	Microwave-assisted hydrothermal route	TCS (4×10^{-5} M)	Visible-light	46% removal 2.3×10^{-5} s^{-1}	[140]
Fe/Nb_2O_5	Impregnation	TCS	Solar/artificial irradiation	80% removal	[136]
CuO-loaded halloysite nanotubes	Hydrothermal route	TCS (2 mg/L)	activated PS	100% removal	[147]
$Co_xMn_{2-x}O_4$	Solution-based oxidation/precipitation process	TCS (10 mg/L)	activated PMS	96.4% removal 0.106 min^{-1}	[144]
Fe_3O_4	commercial	TCS (0.03mM)	activated PMS	100% removal	[145]
$MnFe_2O_4$	commercial	TCS (0.03 mM)	activated PMS	100% removal	[146]
Fe_3O_4	Ultrasonic-assisted reverse coprecipitation	TCS (5 mg/L)	activated PS	~88% removal 0.022 min^{-1}	[148]

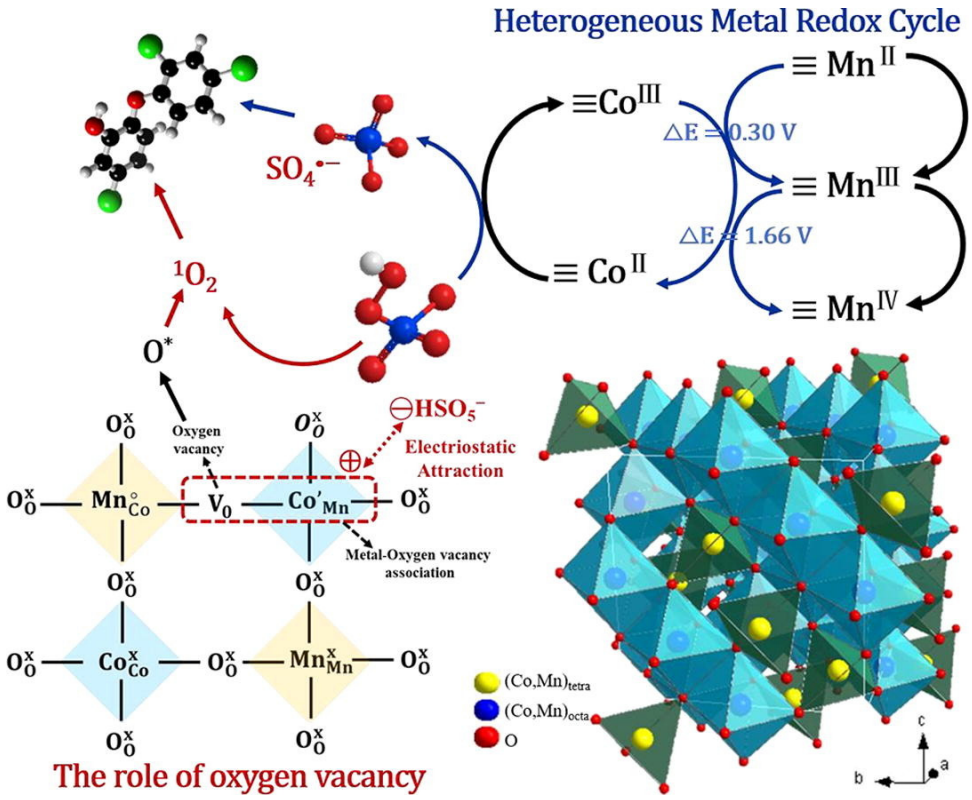

Figure 12. The schematic mechanism of the heterogeneous degradation of triclosan by using spinel-type oxide $Co_xMn_{2-x}O_4$, Adapted and reprinted with permission from [144], Copyright (2020) Elsevier.

4.3.2. Parabens

Parabens are alkyl esters of 4-hydroxybenzoic acid widely used as preservatives in pharmaceutical and personal care products (PCPs) due to their useful properties, such as good water solubility, chemical stability, low production cost combined with antimicrobial activity. The continuous increase in parabens and their metabolites in water bodies cause adverse health effects including inhibition of thyroid gland, hindrance of reproduction, endocrine disruption. Generally, the most used methods of removing parabens from water and wastewaters just transfer them into another medium, without any degradation. In contrast, photocatalysis represents an alternative technique capable of degrading parabens by using cheaply available solar energy and light-sensitive catalysts [149–151].

Foszpańczyk et al. proved that solar energy, instead of expensive UV light, may be applied either as photocatalytic oxidation or as photosensitized oxidation [152]. The efficiency of noble metal-doped TiO_2 nanoparticles in degrading a mixture of parabens (methyl-, ethyl-, propyl, butyl- and benzyl-parabens, MP, EP, PP, BuP and BeP) by simulated and natural sunlight radiation was compared in various water matrixes. They identified the singlet oxygen and hydroxyl radicals as oxidant species for photosensitized and photocatalytic oxidation, respectively. Application of sunlight for both processes led to degradation of parabens which increased with increasing length of the hydrocarbon chain and reached about 90% of degradation efficacy when tap water was used as matrix.

Self-organized TiO_2 supported nanotubes were recently evaluated by Gomes et al. for the photocatalytic degradation of parabens mixtures (MP, EP, PP) [153]. In particular, a one-step anodization method was applied for the TiO_2 systems production with the aim to improve the possibility to easily reuse and recover the catalysts. The photocatalytic oxidation was evaluated using two different irradiation sources, UVA, and sunlight. The sunlight radiation, using the most suitable reactor configuration, accounted for 35% of parabens removal in 60 min. The same authors implemented paraben mixture degradation comparing the ozone-based technologies with photocatalysis [154]. The experiments

involving UVA with ozone should enhance the parabens' degradation leading to a total removal in about 15 min, while photocatalysis only led to a best result of about 50% degradation in 120 min. Methyl and ethyl paraben degradation was investigated by Vela et al. [155], with the purpose of assessing the treatment strategy using commercial TiO_2 nanopowders (P25, Alfa Aesar and Kronos vlp 7000) in tandem with $Na_2S_2O_8$ as electron acceptor under natural sunlight. The degradation rate of the studied EDCs was enhanced compared with photolytic tests. In addition, more than 90% of the TiO_2 nanopowders can be easily recovered through ultrafiltration for reuse in further photocatalytic processes.

A series of $CoO_x/BiVO_4$ catalysts with variable cobalt content were synthesized by Petala et al. [156] and tested for the degradation of PP under simulated solar irradiation. Catalysts were synthesized through wet impregnation method and the cobalt addition improved the absorbance in the visible region of $BiVO_4$. Th efficient electron–hole separation, achieved at the p-n junction formed between the p-type Co_3O_4 and the n-type $BiVO_4$ semiconductors resulted in an impressive enhancement of the photocatalytic performance. The catalyst loaded with 0.5 wt.% Co allowed to obtain an almost complete degradation of PP (97%) after 150 min under simulated solar irradiation.

Porous quaternary titanate nanorods, as efficient catalyst for parabens degradation, were successfully synthesized for the first time by Moschogiannaki at al. [157]. A solution-based method following an ethylene glycol route at room temperature was exploited to produce $Co_xNi_{1-x}TiO_3$ nanorods assessed for the photocatalytic degradation of ethyl paraben under both simulated solar and visible-light irradiation. Again, the reduced recombination rates of the photogenerated electrons and holes, given by the synergy between nickel and cobalt cations, resulted in enhanced degradation activity. All nanorods with $Co_{0.5}Ni_{0.5}TiO_3$ composition were capable of degrading paraben under simulated solar radiation, with the sample exhibiting the best photocatalytic activity: 92% paraben degradation occurred after 5 h of solar irradiation.

To solve the main problem in the photocatalysis processes related to the recombination of the electron–hole pair Sheikhmohammadi et al. investigated the photocatalytic removal of benzylparaben (BzP) using nano-ZnO catalysts in the presence of hydrogen peroxide [158]. H_2O_2 was proposed as exogenous oxidant to generate •OH extra radicals by reacting with e^-. The BzP removal was conducted under UV irradiation and the degradation efficiency was evaluated with and without the presence of H_2O_2. More than 65% of BzP was degraded within 90 min under UV irradiation; under the same operation conditions, the addition of H_2O_2 resulted in 100% degradation efficiency. With the same purpose, Asgari et al. proposed a photocatalytic ozonation treatment of different types of parabens (MP, EP, PP, BuP and BeP) using a combination of ZnO, ozone techniques and UV light source [159]. The results discussed in the study proved that the proposed combined technique, in the best operational condition, enhanced the degradation rate leading to 100% removal for MP, EP, PP, BuP, and 94% for BeP in 20 min.

The main outcomes reported in this section highlight that high percentages of parabens were removed by principally using TiO_2- and ZnO-based nanostructured materials, obtained through different synthetic approaches, and acting under UV and sunlight irradiation. The features and performances of these nanomaterials are summarized in Table 5.

Table 5. Summary of representative metal-oxide-based nanomaterials used for the degradation of parabens.

Material	Preparation	Target	Conditions	Results	Ref.
Ag/Pd/Au/Pt-doped TiO_2	photodeposition/sol–gel method	Paraben mixture MP, EP, PP, BuP, BeP (10 mg/L)	Sunlight	90% removal	[152]
TiO_2 supported nanotubes	one-step anodic oxidation method	Paraben mixture MP, EP, PP (1 mg/L)	UV/Sunlight	35%r emoval	[153]
TiO_2 supported nanotubes	one-step anodic oxidation method	Paraben mixture MP, EP, PP (1 mg/L)	UV/ozone	100% removal	[154]
TiO_2 nanopowder	commercial	MP, EP (300 g/L)	PS, natural sunlight	90% removal (0.006 ± 0.005 min^{-1})	[155]
$CoO_x/BiVO_4$	wet impregnation	PP (200–400 µg/L)	simulated sunlight	97% removal (0.025 ± 0.001 min^{-1})	[156]
$Co_xNi_{1-x}TiO_3$ nanorods	solution-based method	EP (250 g/L)	simulated solar/visible light	92% removal	[157]
nano-ZnO	commercial	BzP (15 mg/L)	UV/H_2O_2	100% removal (0.3305 min^{-1})	[158]
nano-ZnO	commercial	MP, EP, PP, BuP and BeP (10 mg/L)	UV/ozone	100%, 100%, 100%, 100% and 94% removal	[159]

4.3.3. Steroid Hormones

Steroid hormones also directly interact with the normal functioning of endocrine systems. At present, waste generated by pharmaceutical industries and human and animal excretions (urine and feces) represent the major source of hormone pollution. The most common natural and synthetic hormones found in the environment include estrone (E1), 17β-estradiol (E2), estriol (E3), 17α-ethinylestradiol (EE2). All these compounds are constituted by a tetracyclic network consisting of a phenolic, two cyclohexane, and one cyclopentane ring [160].

A new class of 'sea-buckthorn-like' composite material, constituted by amorphous MnO_2 NPs decorated titanate nanotubes (TNTs) was developed by Du et al. and used for 17β-estradiol (E2) degradation [161]. MnO_2 was exploited to pre-activate E2 through one-electron oxidation, while TNTs as the primary photocatalytic center. The synergetic effect of these two processes leads to efficient E2 removal by MnO_2/TNTs under simulated solar light, with a TOC elimination rate of 82.6% in 1 h. In addition, a dual-enhanced mechanism was proposed by the authors to interpret the high degradation efficiency: (1) heterojunction structure of MnO_2 and TNTs inhibited electron−hole recombination and promoted visible-light-driven photocatalytic activity, and (2) synergy of pre-oxidation and photocatalysis led to high reactivity on activated E2 radical and •OH coupling (see Figure 13). MnO_2 nanozyme was also selected by Sun et al. for its intrinsic enzyme-like activity to remove 17β-estradiol [162]. The reported results indicated that the system removed up to 97.3% of E2 at pH 6. In addition, the authors demonstrated that the presence of humic acid, the major component of natural organic matter in aquatic ecosystems, negatively influenced E2 removal. Indeed, humic acid competed with E2 for the catalytic sites of the MnO_2 nanozyme surface and thus decreased the affinity between MnO_2 and E2.

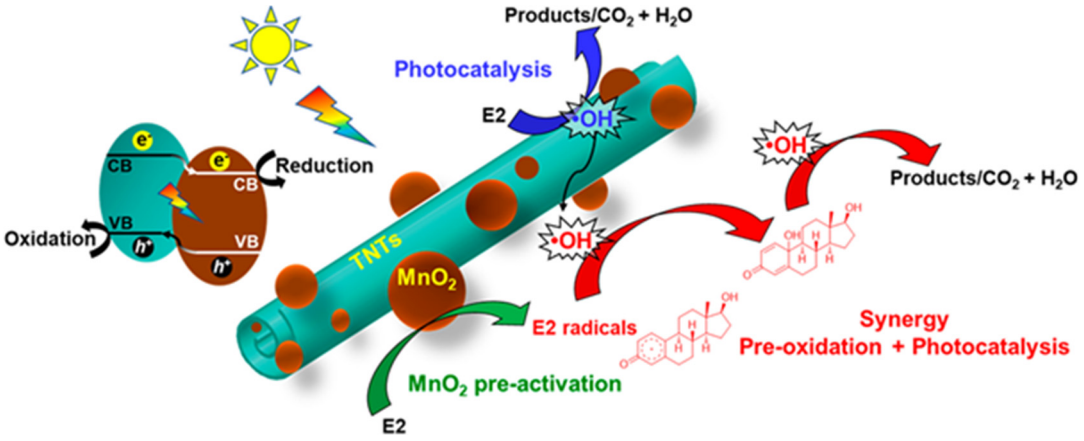

Figure 13. The schematic mechanism of the degradation of E2 by using MnO_2 NPs decorated titanate nanotubes (TNTs). Reprinted with permission from [161], Copyright (2018) American Chemical Society (ACS).

Immobilized titanium oxide-based composites, made by coupling TiO_2 and iron-exchanged zeolite (FeZ) and semiconductor SnS_2, were applied as solar active photocatalysts for the treatment of 17β-estradiol (E2) in water and in the presence of H_2O_2 [163]. The influence of pH, [H_2O_2], and composite formulation on the effectiveness of E2 degradation was deeply investigated. The highest degradation efficacy of 78.1% was achieved by solar/TiO_2-FeZ/H_2O_2 process. In addition, the influence of real water matrix constituents such as natural organic matter, nitrates, and carbonates on the effectiveness of E2 degradation was investigated. The authors found that the removal was enhanced in the presence of natural organic matter, while the inhibitory effect was observed in the case of nitrates and carbonates presence. A novel hybrid photocatalyst, made of zinc oxide functionalized with aluminum and polythiophene (Pth), was proposed by Majumder et al. for the photocatalytic degradation of E2 under UVA irradiation [164]. A removal efficiency of about 96% was achieved in this case. The authors demonstrated that the addition of Pth increased the light-absorbing capacity, while Al doping reduced electron–hole recombination improving the photocatalytic activity. In addition, the choice of the calcination temperature allowed to easily tune crystals size ultimately varying catalyst bandgap.

In the study of Wei et al., a novel synthesis of silver and strontium modified TiO_2 nanocomposite, through a sol–gel method, was proposed [165]. Reported results indicated that co-doping remarkably narrowed the band gap of catalyst and inhibited the recombination of electrons and positive holes, enhancing the visible light degradation of the synthetic estrogen 17α-ethinylestradiol (EE2). A photocatalytic degradation performance of 94% was found, and no decrease in the catalyst activity was observed after four cycles, demonstrating high photocatalytic stability coupled with excellent reusability. TiO_2–ZnO nanocomposites were tested by Menon et al. in the photocatalytic removal of both 17β-estradiol and 17α-ethinylestradiol under UV and visible irradiation [166]. A detailed study of the decomposition of both estrogenic compounds was conducted over a range of different initial ECs concentrations and 100% transformation was obtained in the best conditions under visible irradiation. The authors proved that degradation was accompanied by breakdown of the fused ring structure of E2 and EE2, generating smaller molecular weight by-products. Niobium pentoxide was tested in the UV photodegradation of EE2 and three other pharmaceuticals, acetylsalicylic acid, ibuprofen and paracetamol [167]. The effect of calcination temperature of commercial Nb_2O_5, pH and catalyst dosage were assessed. The higher degradation results were achieved at pH 4, with removal greater than 85% at the end of 120 min of photocatalytic reaction.

A novel catalyst based on the combination of α-FeOOH and MnO_2@$MnCO_3$ was tested for the first time in the photo-Fenton-like degradation of EE2 [168]. α-FeOOH nanoparticles were deposited on the surface of MnO_2@$MnCO_3$ microspheres. The com-

bination of these two components results in a great enhancement of the overall catalytic process, indeed almost total degradation of EE2 hormone was achieved after only 2 min of simulated solar irradiation at neutral pH. The high degradation efficacy was attributed to the larger generation of hydroxyl radicals, the primary mediators of the total oxidation for this hormone.

On the other hand, Zhu et al. developed a bismuth-containing photocatalytic biochar (BiPB) using Bi/Bi_2O_3 for the degradation of estrone (E1) [169]. The reaction rate constant inherent to the degradation process was almost tenfold and more than 20 times than that of biochar without bismuth impregnation and pristine Bi/Bi_2O_3, respectively. The chemical investigation revealed that the photocatalytic performance of BiPB composites could be mainly attributed to generation of •OH, which were effectively stabilized in the hierarchical porous structure of biochar. The pre-concentration of estrone on BiPB was catalyzed by the presence of biochar. This latter also improved the separation and transfer efficiency of charge carriers.

High and low UV irradiation conditions were investigated for the degradation of estriol (E3) using iron doped TiO_2 nanoparticles [170]. Interestingly, the presence of ferric ion (Fe^{3+}), unintentionally added because of the precursors of the synthetic method, played a key role in the photocatalytic generation of hydroxyl radicals (•OH) and estriol (E3) degradation. An efficiency of up to 80% of E3 degradation was achieved in both irradiation regimes [166]. To obtain a fast and efficient degradation of estrone (E1) and 17α-ethinylestradiol (EE2), de Oliveira et al. proposed the use of nanotubular oxide arrays grown on Ti-0.5wt% W under irradiation with ultraviolet (UV) and visible light [171]. The presence of WO_x species and amorphous WO_3 in the oxide layer resulting from the doping of TiO_2 with tungsten allowed to obtain a reduction in charge separation and an extended wavelength range for photoexcitation, ultimately leading to percentage removals of EE2 and E1 were 66% and 53.4%, respectively, after only 2 min of treatment and under UV irradiation.

The application of magnetite nanoparticles coated with polyacrylic acid and immobilized on mesoporous silica matrix support was investigated as alternative catalysts to conventional Fenton processes for the removal of estrogens (E1, E2, EE2) by González-Rodríguez et al. [172]. After the optimization of the operational variables, high removal percentages (above 90%) were obtained. Furthermore, the ease of catalyst recovery, due to their superparamagnetic properties, represented a significant advantage for their separation and reuse in different successive sequential cycles. Bayode et al. proved the efficiency of a new sustainable visible-light active *p-n* heterojunction composite with carbon interlayer from ZnO, GO and *Carica papaya* seeds as carbon source prepared via microwave assisted technique [173]. The degradation of four steroid estrogens, E1, E2, E3 and EE2, was investigated. A degradation efficacy > 89%, as high as 98%, was obtained in single solute systems, while in real wastewater samples, efficiency of 63–78% estrogen removal was achieved. Moreover, the addition of 1% H_2O_2 further raised photodegradation of estrogens to 100% in 10 min.

Finally, WO_3 films, functionalized with silver and platinum metal nanoparticles, were successfully synthesized by a simple drop-casting method by Costa et al. [174]. The photoinduced activity of the obtained systems was investigated for progesterone hormone degradation in aqueous solution under polychromatic irradiation, exploring also electrochemical assisted configuration. Photoelectrochemical characterization showed that the functionalization with metallic NPs accelerates electron transport and increases the separation of the photogenerated electrons and holes. The highest photocatalytic activity, about 27% of degradation efficacy, was obtained for the Pt/WO_3 system in the irradiated electrochemical configuration.

The main outcomes reported in this section highlight that high removal percentages of steroid hormones were obtained under different conditions, in terms of chemical nature and preparation method of Me_xO_y photocatalysts as well as type of irradiation, as schematically reported in Table 6.

Table 6. Summary of representative metal-oxide-based nanomaterials used for the degradation of steroid hormones.

Material	Preparation	Target	Conditions	Results	Ref.
MnO_2 NPs decorated titanate nanotubes	hydrothermal method	E2 (4 μM)	simulated solar light	82.6% removal (0.198 min^{-1})	[161]
MnO_2 nanozyme	commercial	E2 (1 mg/L)	Enzyme-like activity	97.3% removal (0.0131 min^{-1})	[162]
TiO_2-Fe zeolite/SnS_2	Low T/solution method	E2 (5 μM)	Solar light/H_2O_2	78.1% removal (0.01539 min^{-1})	[163]
Al-polythiophene doped ZnO	Co-precipitation	E2 (1 mg/L)	UV-A irradiation	96% removal (0.4451 h^{-1})	[164]
Ag, Sr-modified TiO_2	Sol–gel	EE2 (10 mg/L)	Visible light	94% removal (0.1699 min^{-1})	[165]
Nb_2O_5	commercial	EE2 (10 mg/L)	UV irradiation	85% removal	[167]
a-FeOOH doped MnO_2@$MnCO_3$ microsphere	surface oxidation/hydrothermal reaction	E3 (0.5 mg/L)	simulated solar irradiation	90% removal	[168]
Fe-doped TiO_2	Hydrothermal/sol–gel	E3 (10 μM)	High/low UV irradiation	80% removal (0.009–0.003 min^{-1}/ 0.005–0.016 min^{-1})	[170]
Bi/Bi_2O_3	Impregnation method	E1 (10.4 μmol/L)	UV–vis light irradiation	~95% removal (0.045 min^{-1})	[169]
TiO_2–ZnO nanocomposite	non-aqueous sol–gel process	E2, EE2 (0.05–10 mg/L)	UV and visible irradiation	~100% removal (E2: 0.022 min^{-1}, EE2: 0.013 min^{-1})	[166]
W-doped nanotubular TiO_2	Electrochemical synthesis	E1, EE2 (10 mg/L)	UV and visible light	53.4%, 66% removal (EE2: 0.001215 min^{-1})	[171]
Fe_3O_4 @ SBA15	water-in-oil microemulsion/sol–gel techniques	E1, E2, EE2 (100–500 μg/L)	Fenton-like	~90% removal (E1: 0.160–2.708 h^{-1} E2: 0.228–2.713 h^{-1} EE2: 0.214–3.211 h^{-1})	[172]
(GO)-Carbon-ZnO nanostructures	microwave assisted technique	E1, E2, E3, EE2 (5 mg/L)	visible light	89–98% removal (E1: 0.01019 min^{-1} E2: 0.01236 min^{-1} E3: 0.01286 min^{-1} EE2: 0.01567 min^{-1})	[173]
Ag/Pt functionalized WO_3 films	Drop casting	Progesterone (0.35 mg/L)	polychromatic irradiation, bias +0.7 V vs. Ag/AgCl	~27% removal (Ag/WO_3: 0.001061 min^{-1} Pt/WO_3: 0.001086 min^{-1})	[174]

4.3.4. Other Pharmaceuticals

Pharmaceutical compounds, such as antibiotics, as well as antiviral, anti-inflammatory, analgesic, and hormone drugs, are mostly found in water ecosystems because of their difficult removal through traditional techniques. These classes of drugs are designed to have biological effects, so they the undesired exposure can have serious implications for human health and fauna, including interference with the endocrine system. Another risk related to antibiotics is the development of antibiotic resistance by bacteria and other microorganisms. Sources of environmental contamination by pharmaceuticals include municipal wastewater, improper disposal of drugs, human excretion, livestock farming, hospitals effluents, and pharmaceutical industry [37]. Therefore, these chemicals are widely

studied in terms of toxicological risks, as well as degradation strategies. In recent years, a large number of research works and reviews have been dedicated to the removal of these contaminants from water and wastewater by means of processes based on metal oxide nanomaterials [37,175,176]. Here, an overview is presented with some examples related to drugs of significant concern.

TiO_2-based nanostructured materials and membranes have mostly been applied in photocatalytic systems for the removal of antibiotics, such as amoxicillin [177], erythromycin [178], and tetracycline [179]. However, the degradation of tetracycline has been explored using a variety of other metal oxide nanomaterials, often in photo-responsive heterojunctions, such as those based on ZnO [180,181], tungsten oxides [182,183], or bismuth-molybdenum mixed oxide [184]. Other antibiotics raising interest as water contaminants are levofloxacin [185], nitrofurantoin [186], metronidazole [187], and sulfamethoxazole [188]. Metal oxide nanomaterials have been also used in the catalytic and photocatalytic degradation of several anti-inflammatory and analgesic compounds, such as acetaminophen (well-known as paracetamol) through catalysts based on TiO_2 [189], WO_3 [190], ZnO [191], CuO Fe_xO_y or Co_3O_4 [141,192]. Similarly, TiO_2 and ZnO-based photocatalysts were employed for the degradation of anti-inflammatory compounds diclofenac [193,194] and ibuprofen [195]. In most of these cases, the photocatalytic performances of the oxides were enhanced by doping or coupling with other semiconductors.

4.4. Degradation of Other EDCs

Important groups of EDCs not belonging to the previously presented classes include polyhalogenated biphenyls and diethyl ethers, polyaromatic hydrocarbons and substituted phenols (Figure 14). Polychlorinated biphenyls (PCBs) are a group of environmentally persistent halogenated organic compounds that had been massively produced in past decades for use as insulators, coolants, and lubricants in transformers, capacitors, and other electrical equipment, owing to their chemical stability, low inflammability, and good miscibility. The hazards for human health and the environment related to PCBs and to some carcinogenic derivatives (such as polychlorinated dibenzo-p-dioxins and dibenzofurans) imposed the discontinuance of their production and the disposal within 2028. However, large amounts of PCBs are still used or stored, thus causing severe pollution upon losses, also because of their long half-lives [196,197]. The hydrophobic structure of biphenyls and polyaromatic hydrocarbons hinders their interaction with substantially hydrophilic metal oxide nanomaterials. In fact, in a heterogeneous degradation process, although the ROS generated on the catalyst's surface can diffuse in solution to short distances, allowing oxidation reactions also in homogeneous phase, the adsorption of the target molecule on the surface is generally a fundamental step. The modification of the surface properties to improve its affinity toward the target contaminant is often a fruitful strategy to enhance the process rate and selectivity. To this aim, the use of cyclodextrins has been proposed, since these cyclic oligosaccharides possess a rather lipophilic inner cavity, a hydrophilic outer surface and a truncated-cone shape that enable them to form inclusion complexes with hydrophobic organic pollutants through host-guest interactions. Khammar et al. grafted carboxymethyl-β-cyclodextrin on hydrothermal Fe_3O_4@TiO_2 nanoparticles and evaluated the photocatalytic performance of this hybrid nanomaterial in the removal of PCBs from transformer oil with UV light [196]. Cyclodextrin functionalization promoted the adsorption and successive degradation of PCBs with a yield up to 83% in 16 min, with oil:ethanol ratio of 1:5, and the photocatalyst maintained a sufficient stability in five reuses after a simple regeneration by washing in water. The UV-photoinduced degradation process of planar and non-planar PCBs was studied over TiO_2 and CdS/TiO_2 nanomaterials obtained by Ti(IV) butoxide hydrolysis on CdS quantum dots. Interestingly, some of the PCBs were removed faster by the heterostructure, while others by bare TiO_2, which was explained by the differences in the interactions between the respective radical intermediates and the surface of the photocatalysts [197].

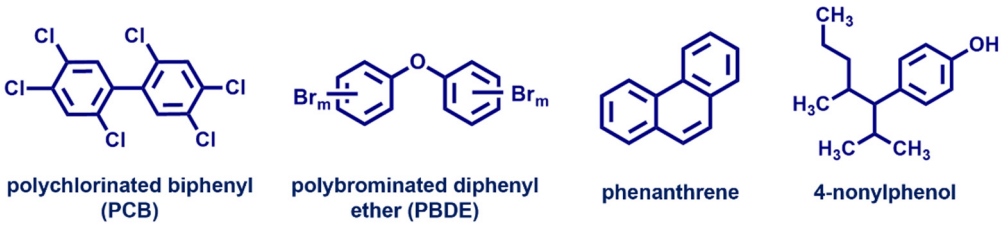

Figure 14. Chemical structures of typical polychlorinated biphenyl, polybrominated diphenyl ether, polycyclic aromatic hydrocarbon (phenanthrene) and alkylphenol.

Plasma treatment was also applied for the removal of polychlorobiphenyls, using an electrode composed of sponge modified by multi-walled carbon nanotubes, on which CuO@Cu and Ag nanowires were attached [198]. The efficiency of the dielectric barrier discharge was improved by the synergistic effects of all components, leading to promising and stable removal efficiency of phenol and 2,4,5-trichlorobiphenyl. The degradation of the latter contaminant reached 65% in 60 min of reaction at an input voltage of 30 V.

It was suggested that in order to push the degradation of recalcitrant pollutants such as halogenated aromatics toward mineralization, oxidative processes should be coupled with reductive ones. A novel method of Advanced Oxidation/Reduction Processes was therefore proposed, relying on the simultaneous generation of both oxidative and reductive agents. For PCBs degradation, sulfite was added together with TiO_2 under UV irradiation to form $SO_3\bullet^-$ reductive radicals. The degradation performances of PCBs (12 mg/L) were improved up to 98.5% degradation in 60 min at pH 7 and at the optimal sulfite/TiO_2 ratio of 1:1 [199].

Polybrominated diphenyl ethers (PBDEs) are a series of aromatic compounds commonly added as flame retardants in the production of electronic equipment, building materials and textiles. The widespread use of PBDEs makes them ubiquitous in the environment. They are classified as persistent organic pollutants and pose health risks related to their bioaccumulation and ability to cause thyroid dysfunctions and developmental neurotoxicity like PCBs. In the challenging decomposition of PBDEs the need for reductive mechanisms seems to acquire great importance, for debromination. A photocatalytic consecutive reduction-oxidation one-pot method was applied by Lei et al. to remove 2,2′,4,4′-tetrabromodiphenyl ether (BDE47) in the presence of a rGO/TiO_2 composite in anoxic conditions (Ar purging) [200]. The reduction became faster in acetonitrile–water solution; however, the key for successful debromination was the addition of a small amount of methanol to the water solution. This system yielded the complete debromination and mineralization of BDE47 within 14 h. Methanol inhibited the recombination of e^-/h^+ pairs, accelerating the formation of hydroxyl radicals by h^+ consumption, thus promoting the direct reduction of BDE47 by photogenerated electrons. The same authors reported complete debromination of BDE47 also without light irradiation, by Cu/TiO_2 in the presence of hydrazine and by 1% Pd/TiO_2 in isopropanol containing NaOH at 40 °C. Metallic Pd activated a catalytic transfer hydrogenation mechanism. Two Br-free products were obtained, diphenyl ether and dibenzofuran, attributed to the hydrogenation and coupling reactions, respectively [201]. A composite photocatalyst with Z-scheme charge transfer was developed through a three-step approach: Cu_2O films prepared by electrochemical deposition were coated with rGO and TiO_2 (P25) [202]. BDE47 reductive removal tested under simulated solar irradiation showed that 1% rGO gave the best enhancement of charge transfer in combination with 70% TiO_2. However, the removal reached only 56% in 3 h, confirming the recalcitrance of PBDEs to degradation.

Polycyclic aromatic hydrocarbons (PAHs) are a large group or molecules generally originated from combustion processes and widely distributed in the environment because of atmospheric transport, wet and dry deposition, and exchange processes between environmental matrices. Other sources of contamination include oil spills and water production. Acute or chronic exposure to PAHs causes risks to humans, animals, and plants, including

inflammatory response, carcinogenity, endocrine and reproductive disorders [203]. The high stability of PAHs makes them recalcitrant to biological degradation and also hampers their chemical degradation. In recent years, an increasing number of works have dealt with photocatalytic removal of PAHs from water or soil samples, using mainly modified TiO_2 or ZnO [204]. ZnO-based nanocomposites were prepared by one-pot co-precipitation with small fractions of MnO (a p-type semiconductor), obtaining p-n junctions, as demonstrated by a thorough electrochemical characterization, which evidenced changes in the flat band potential of ZnO and an increase in the transient time constant related to the electron transport [205]. Photodegradation tests of anthracene in alkaline ethanol–water solution under UV irradiation showed a fast removal with the optimal MnO content (2.25 wt%), although anthraquinone was identified as the main product, indicating only partial degradation. The adsorption of PAHs can be greatly promoted by the presence of graphene or similar structures, owing to π-π interactions. For instance, ZnO/Ag/GO nanocomposite obtained by precipitation of Ag and ZnO in a graphene oxide suspension adsorbed naphthalene with a remarkable adsorption capacity, estimated as 500 mg g^{-1}. In a successive stage under visible-light irradiation, adsorbed naphthalene was photodegraded, resulting in a high removal of the pollutant (50 mg/L) with a relatively low dosage of nanomaterial (0.25 g/L) [206].

Metal hexacyanoferrates (HCF), with general formula $M_k[Fe(CN)_6]\cdot xH_2O$, have been proposed as photocatalytic compounds, coupled with oxide semiconductors. For example, Rachna et al. prepared nanocomposites of encapsulated TiO_2, ZnO or Fe_2O_3 nanoparticles with ZnHFC nanocubes, adopting simple precipitation procedures assisted by plant extracts [207,208]. These materials were found effective in the degradation and mineralization of 3-, 4- and 5-cyclic aromatic hydrocarbons, such as chrysene, benzanthracene and benzopyrene, under sunlight exposure for 24 h. The enhanced photocatalytic activity was attributed to the reduced band gap, increased surface area and enhanced charge separation in the formed heterostructures. Interestingly, a significant activity was also detected in the dark, which was not further examined by the authors. A catalytic system composed of Fe_3O_4 particles incorporated into wood biomass and added persulfate was tested for the remediation of real sediments contaminated with 16 different PAHs [209]. The oxidation efficiency was related to the number of rings in their structure, and the faster removal of high-ring PAHs (with four to six rings) was attributed to their stronger affinity for biochar.

The intimate coupling of photocatalysis and biodegradation approach was also applied for the decontamination of water from PAHs. The investigation of Cu/N-codoped TiO_2 nanoparticles prepared by a sol–gel method and coated on PTFE carriers along with a suitable bacterial consortium [210] showed a slight contribution of biodegradation in the conversion and mineralization of pyrene under UV and visible irradiation and revealed alterations the composition and structure of the bacterial community during the process, especially with UV light. Composites of manganese oxide nanosheets with cubic silver orthophosphate (Mn_3O_4/MnO_2-Ag_3PO_4), prepared by precipitation, exhibited high photocatalytic activity in the degradation of phenanthrene under visible-light irradiation [211]. The efficiency was improved applying ICPB systems fabricated by coating polyurethane porous carriers with the photocatalyst and then forming biofilms from an activated sludge (Figure 15).

Alkylphenols, especially 4-nonylphenol (4-NP), are strong endocrine disruptors with estrogen-like action. They are often found in water as breakdown product of alkylphenol ethoxylates, nonionic surfactants with wide domestic, industrial, and agricultural use [212]. In the case of nonylphenol removal, a viable approach to improve the affinity of the catalyst surface toward the target is the functionalization with non-polar groups, as demonstrated by Tang et al., who obtained hydrophobic titanium oxide nanotubes by reaction with perfluorooctyl triethoxysilane [213]. The introduction of exposed perfluorooctyl groups induced an increase of the water contact angle on the surface from 21.1° to 128.4°. The adsorption rate of the hydrophobic 4-NP on the modified TiO_2 nanotubes was 4 times higher than on bare ones, which resulted in a moderate increase of photodegradation

efficiency of about 15%. The degradation performances were also tested in the presence of other hydrophilic pollutants, namely atrazine, paraquat and potassium butylxanthate, to compare the results and check the interference effects, confirming the efficiency of the modified photocatalyst. The molecular imprinting approach was adopted in the design of a tin (IV) oxide electrode exposing high-energy facets for 4-NP electrocatalytic oxidation [214]. 4-NP molecules were immobilized on carboxylated SiO_2 and then immersed in a SnO_2 sol derived from $SnCl_4$. After hydrothermal process etching of SiO_2 and calcination at 400 °C, the obtained SnO_2 nanoparticles were coated on FTO. Such electrode effectively removed 4-NP from industrial wastewater at applied potential of 1.8 V, suppressing human estrogenic activity and enhancing the biodegradability of the treated water. Nonylphenol, being more persistent, lipophilic, and toxic than the parent chemicals, is often found in rivers and lakes and is an indicator of contamination of sediments [215]. The treatment of real river sediments containing 4-NP was studied using Fe_3O_4 particles deposited by co-precipitation on a bio-derived support, bamboo biochar, and sodium persulfate. The catalytic performance of the system was highly dependent on pH and catalyst dosage: 85% degradation of 4-NP was achieved at pH 3 using a load of 3.33 g/L, 2.3×10^{-5} M PS and equimolar initial concentration (2.3×10^{-5} M) of the contaminant. An analogous system (Fe_3O_4 particles supported on wood biomass used with PS) was tested in similar conditions for the removal of 16 PAHs from real sediments [209].

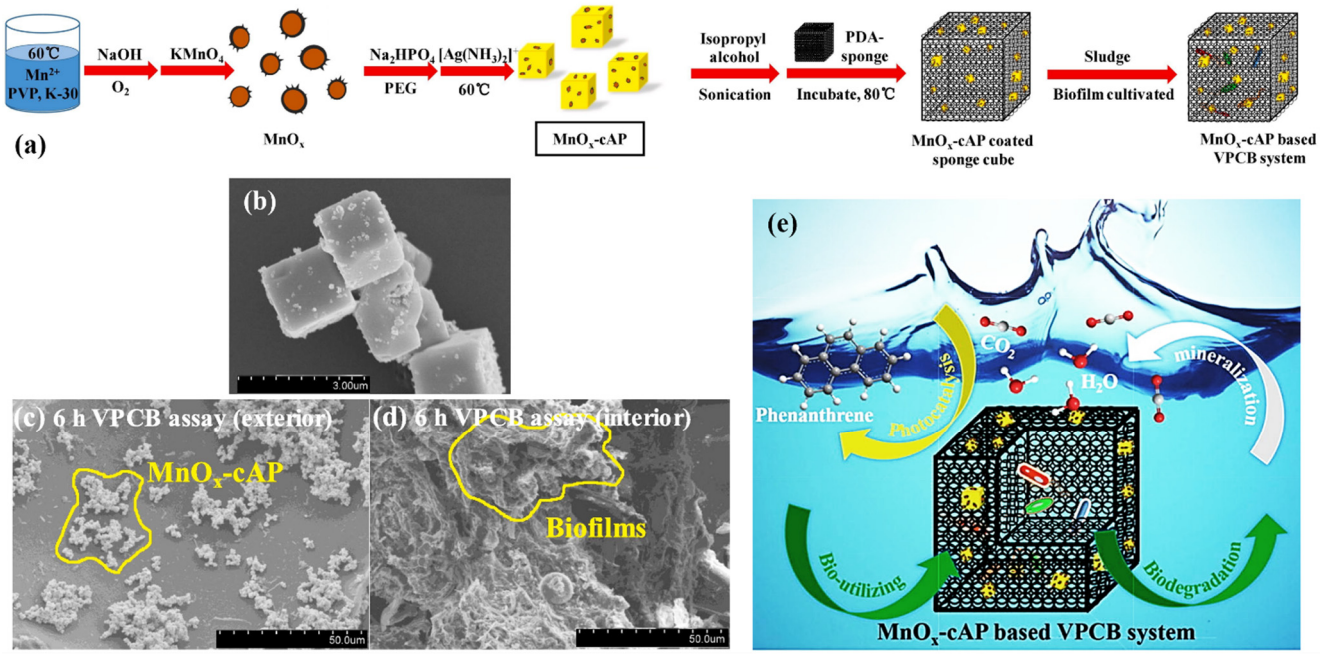

Figure 15. Sketch of the preparation of MnO_x on Ag_3PO_4 cubes (MnO_x-cAP), followed by coating on polyurethane sponge (**a**); SEM micrograph of the MnO_x-cAP isolated (**b**) and coated (**c**), along with the biofilm (**d**); scheme of the coupled visible light photocatalysis and biodegradation (VPCB) process (**e**). Adapted with permission from [211], Copyright (2019), Elsevier.

An interdisciplinary study [216] focused on the effects of typical nanomaterials employed in water treatment, i.e., Fe_2O_3 and Fe_3O_4 nanoparticles and multi-wall carbon nanotubes, on the degradation of 4-NP at the water-sediment interface and on the functions of the natural bacterial communities in sediments. It demonstrated that iron oxides promoted the direct 4-NP degradation, moreover their incorporation by bacteria enhanced the biodegradation processes by bacterial enzymes. Therefore, the presence of biocompatible inorganic nanomaterials can reveal a synergistic effect in the decontamination, promoting the microbial activity. This kind of study evidences the limited knowledge currently available on the fate of nanomaterials accidentally released in water and on their interactions with

the biosphere, suggesting a direction for future research integrating chemistry, material science, and environmental science.

5. Conclusions and Perspectives

Endocrine Disrupting Compounds (EDCs) comprise a lot of chemicals such as sex-steroid hormone mimics, pesticides, fertilizers, medicinal drugs, plasticizers, derived from the waste of industries, agriculture, pharmaceutics, and sewage treatment plants. The rising concerns of worldwide use of EDCs and their dangerous effects on human health are continuously attracting increasing attention due to their gradual accumulation and persistence in the environment. Therefore, the issues originating from the contamination of water resources (freshwater, seawater, wastewater and drinking water) are stimulating several research groups to define and develop strategies for an effective removal of EDCs from water. The main ones include physical, chemical, or biological processes. Among them, chemical degradation, which is based on oxidative mechanisms, is aimed at transforming the organic pollutants in less hazardous products and ideally arises in its complete mineralization to H_2O, CO_2 and other inorganic molecules. In this context, photocatalysis has emerged as a fascinating process for the removal of EDCs from wastewater. However, other heterogeneous catalytic processes were also defined for their degradation, such as those founded on Fenton reaction, generation of sulfate radicals, electrochemical and piezocatalytic processes. Further techniques to enhance the production of ROS include low temperature plasma, ozonation and the use of radical precursors.

In all cases, a key role is played by the designed materials employed as catalysts. Research on the design and use of new and effective nanostructured materials aimed at EDCs decontamination has prospered because of the growing awareness of this problem. From the outline offered in this review on metal oxide-based nanomaterials reported in recent years, it emerges that beside the well-studied TiO_2, ZnO, suitably modified by doping or coupling with other semiconductors, relatively innovative materials such as WO_3, Cu_xO, MnO_x, and bismuth oxides are gaining attention, especially as photocatalysts, and frequently mixed as heterojunctions, allowing for a wider visible light absorption and more effective charge separation. On the other hand, iron oxides and other redox-active semiconductors show remarkable results in non-irradiated AOPs, e.g., Fenton-like mechanism and the activation of persulfate or peroxymonosulfate, that make it possible to overcome the restrictions related to photoreactors. The synthesis procedure and conditions have a crucial role in determining the structure and functional properties of complex nanomaterials. Wet chemical methods, in particular, hydrothermal and sol–gel, offer great flexibility and as a result are the most widely applied.

Although many advances have been made by virtue of the design and use of these new nanostructured materials based on hybrid, composite or co-doped metal oxides, some questions remain open yet. Therefore, the enhancement of nanomaterial stability and the feasibility of (photo)catalysts separation and reuse are both challenging tasks to improve their use and potential commercialization for this aim. Indeed, large investments are necessary to produce these semiconductor metal oxide-based nanomaterials for their application in large-scale processes of water treatment. Consequently, important goals should be to define useful and sustainable strategies to prepare low-cost nanomaterials through simple steps, following the principles of green chemistry, as well as to recuperate and regenerate the (photo)catalysts for subsequent reuses. Indeed, the dispersed form of the nanostructures in water is highly appreciable for degradation, then the immediate separation of used nanomaterials by centrifugation or filtration after EDCs degradation is recommended to avoid long-term contact with decontaminated water. Anyway, such separation steps can be expensive or difficult to operate on a large scale; therefore, the fabrication of catalysts supported on suitable scaffolds or coated on reactive surfaces and membranes, assuring an optimal dispersion of the active phase may result advantageous, even though it may decrease the catalytic efficiency.

Moreover, a growing number of works deal with the mechanism, pathway, and by-products of the contaminant degradation process. These key aspects should always be considered to understand the relationships between the properties and activity and to evaluate the environmental impact of the treatment, aiming to maximize the mineralization of the pollutants, avoiding the risk of secondary contamination by harmful or unknown products. Such a holistic approach may assist the development of materials optimized either for specific target contaminants or for the removal of wide range of undesired species. It is envisioned that in the future, more research will be devoted to the combination of different AOPs, boosting the overall efficiency and facilitating the integration of these steps in water treatment plants or water remediation systems. Such combined systems should be designed so to enhance the synergism between their components. The achievement of these goals should not be separated from the optimized design of the (photo)reactors, which is decisive for efficient catalytic and photocatalytic degradation processes, preferably exploiting as well as possible the energy of natural sunlight. For these reasons, future works should be more focused on a complete assessment of the water treatment issue and on the prospective technological implementation, and the collaborative efforts between chemists, environmental scientists, material scientists and chemical engineers could pave and manage the way in this direction.

Author Contributions: Conceptualization, C.I. and G.V.; writing—original draft preparation, C.I., A.B., B.S. and G.V.; writing—review and editing, C.I. and G.V.; supervision, G.V.; project administration, G.V. All authors have read and agreed to the published version of the manuscript.

Funding: This research received no external funding.

Conflicts of Interest: The authors declare no conflict of interest.

References

1. Vieira, W.T.; De Farias, M.B.; Spaolonzi, M.P.; Da Silva, M.G.C.; Vieira, M.G.A. Latest Advanced Oxidative Processes Applied for the Removal of Endocrine Disruptors from Aqueous Media—A Critical Report. *J. Environ. Chem. Eng.* **2021**, *9*, 105748. [CrossRef]
2. Vieira, W.T.; De Farias, M.B.; Spaolonzi, M.P.; Da Silva, M.G.C.; Vieira, M.G.A. Endocrine-Disrupting Compounds: Occurrence, Detection Methods, Effects and Promising Treatment Pathways—A Critical Review. *J. Environ. Chem. Eng.* **2021**, *9*, 104558. [CrossRef]
3. Pironti, C.; Ricciardi, M.; Proto, A.; Bianco, P.M.; Montano, L.; Motta, O. Endocrine-Disrupting Compounds: An Overview on Their Occurrence in the Aquatic Environment and Human Exposure. *Water* **2021**, *13*, 1347. [CrossRef]
4. Kabir, E.R.; Rahman, M.S.; Rahman, I. A Review on Endocrine Disruptors and Their Possible Impacts on Human Health. *Environ. Toxicol. Pharmacol.* **2015**, *40*, 241–258. [CrossRef] [PubMed]
5. Schjenken, J.E.; Green, E.S.; Overduin, T.S.; Mah, C.Y.; Russell, D.L.; Robertson, S.A. Endocrine Disruptor Compounds—A Cause of Impaired Immune Tolerance Driving Inflammatory Disorders of Pregnancy? *Front. Endocrinol.* **2021**, *12*, 4. [CrossRef] [PubMed]
6. Gao, X.; Kang, S.; Xiong, R.; Chen, M. Environment-Friendly Removal Methods for Endocrine Disrupting Chemicals. *Sustainability* **2020**, *12*, 7615. [CrossRef]
7. Medhi, R.; Marquez, M.D.; Lee, T.R. Visible-Light-Active Doped Metal Oxide Nanoparticles: Review of Their Synthesis, Properties, and Applications. *ACS Appl. Nano Mater.* **2020**, *3*, 6156–6185. [CrossRef]
8. Yoon, Y.; Truong, P.L.; Lee, D.; Ko, S.H. Metal-Oxide Nanomaterials Synthesis and Applications in Flexible and Wearable Sensors. *ACS Nanosci. Au* **2021**. [CrossRef]
9. Singh, K.R.; Nayak, V.; Singh, J.; Singh, A.K.; Singh, R.P. Potentialities of Bioinspired Metal and Metal Oxide Nanoparticles in Biomedical Sciences. *RSC Adv.* **2021**, *11*, 24722–24746. [CrossRef]
10. Costantini, A.; Venezia, V.; Pota, G.; Bifulco, A.; Califano, V.; Sannino, F. Adsorption of Cellulase on Wrinkled Silica Nanoparticles with Enhanced Inter-Wrinkle Distance. *Nanomaterials* **2020**, *10*, 1799. [CrossRef]
11. Selvaraj, M.; Hai, A.; Banat, F.; Haija, M.A. Application and Prospects of Carbon Nanostructured Materials in Water Treatment: A Review. *J. Water Process Eng.* **2020**, *33*, 100996. [CrossRef]
12. Ojha, A.; Tiwary, D.; Oraon, R.; Singh, P. Degradations of Endocrine-Disrupting Chemicals and Pharmaceutical Compounds in Wastewater with Carbon-Based Nanomaterials: A Critical Review. *Environ. Sci. Pollut. Res.* **2021**, *28*, 30573–30594. [CrossRef] [PubMed]
13. Lu, F.; Astruc, D. Nanocatalysts and Other Nanomaterials for Water Remediation from Organic Pollutants. *Coord. Chem. Rev.* **2020**, *408*, 213180. [CrossRef]

14. Bilal, M.; Rasheed, T.; Mehmood, S.; Tang, H.; Ferreira, L.F.R.; Bharagava, R.N.; Iqbal, H.M.N. Mitigation of Environmentally-Related Hazardous Pollutants from Water Matrices Using Nanostructured Materials—A Review. *Chemosphere* **2020**, *253*, 126770. [CrossRef] [PubMed]
15. González-González, R.B.; Parra-Arroyo, L.; Parra-Saldívar, R.; Ramirez-Mendoza, R.A.; Iqbal, H.M.N. Nanomaterial-Based Catalysts for the Degradation of Endocrine-Disrupting Chemicals—A Way Forward to Environmental Remediation. *Mater. Lett.* **2022**, *308*, 131217. [CrossRef]
16. Colborn, T.; vom Saal, F.S.; Soto, A.M. Developmental Effects of Endocrine-Disrupting Chemicals in Wildlife and Humans. *Environ. Health Perspect.* **1993**, *101*, 378–384. [CrossRef]
17. Dirac, P.; Kapitza, P.; Zichichi, A. Statement from the Work Session on Environmental Endocrine-Disrupting Chemical: Neural, Endocrine and Behavioral Effects. *Toxicol. Ind. Health* **1998**, *14*, 1–8.
18. Short, P. Statement from the Work Session on Health Effects of Contemporary-Use Pesticides: The Wildlife/Human Connection. *Toxicol. Ind. Health* **1999**, *15*, 1–5. [CrossRef]
19. Colborn, T.; Clement, C. *Chemically-Induced Alterations in Sexual and Functional Development*; Princeton Scientific Pub. Co.: Princeton, NJ, USA, 1992.
20. Thomas Zoeller, R.; Brown, T.R.; Doan, L.L.; Gore, A.C.; Skakkebaek, N.E.; Soto, A.M.; Woodruff, T.J.; Vom Saal, F.S. Endocrine-Disrupting Chemicals and Public Health Protection: A Statement of Principles from the Endocrine Society. *Endocrinology* **2012**, *153*, 4097–4110. [CrossRef]
21. Register-Notices. Available online: https://Www.Epa.Gov/Endocrine-Disruption/Endocrine-Disruptor-Screening-Program-Edsp-1998-Federal (accessed on 28 December 2021).
22. *Chemicals Strategy for Sustainability towards a Toxic-Free Environment*; European Commision: Brussels, Belgium, 2020.
23. La Merrill, M.A.; Vandenberg, L.N.; Smith, M.T.; Goodson, W.; Browne, P.; Patisaul, H.B.; Guyton, K.Z.; Kortenkamp, A.; Cogliano, V.J.; Woodruff, T.J.; et al. Consensus on the Key Characteristics of Endocrine-Disrupting Chemicals as a Basis for Hazard Identification. *Nat. Rev. Endocrinol.* **2020**, *16*, 45–57. [CrossRef]
24. Liu, Z.H.; Kanjo, Y.; Mizutani, S. A Review of Phytoestrogens: Their Occurrence and Fate in the Environment. *Water Res.* **2010**, *44*, 567–577. [CrossRef] [PubMed]
25. Combarnous, Y. Endocrine Disruptor Compounds (EDCs) and Agriculture: The Case of Pesticides. *C. R. Biol.* **2017**, *340*, 406–409. [CrossRef] [PubMed]
26. González-Davis, O.; Chauhan, K.; Zapian-Merino, S.J.; Vazquez-Duhalt, R. Bi-Enzymatic Virus-like Bionanoreactors for the Transformation of Endocrine Disruptor Compounds. *Int. J. Biol. Macromol.* **2020**, *146*, 415–421. [CrossRef] [PubMed]
27. Dichiarante, V.; Cavallo, G.; Metrangolo, P. Endocrine-Disrupting Pollutants Properties Affecting Their Bioactivity, Remediation, and Detection. *Curr. Opin. Green Sustain. Chem.* **2021**, *30*, 100485. [CrossRef]
28. Barra, R.O.; Chiang, G.; Saavedra, M.F.; Orrego, R.; Servos, M.R.; Hewitt, L.M.; McMaster, M.E.; Bahamonde, P.; Tucca, F.; Munkittrick, K.R. Endocrine Disruptor Impacts on Fish from Chile: The Influence of Wastewaters. *Front. Endocrinol.* **2021**, *12*, 208. [CrossRef]
29. Al Sharabati, M.; Abokwiek, R.; Al-Othman, A.; Tawalbeh, M.; Karaman, C.; Orooji, Y.; Karimi, F. Biodegradable Polymers and Their Nano-Composites for the Removal of Endocrine-Disrupting Chemicals (EDCs) from Wastewater: A Review. *Environ. Res.* **2021**, *202*, 111694. [CrossRef]
30. Wang, J.; Wang, S. Reactive Species in Advanced Oxidation Processes: Formation, Identification and Reaction Mechanism. *Chem. Eng. J.* **2020**, *401*, 126158. [CrossRef]
31. Serpone, N.; Artemev, Y.M.; Ryabchuk, V.K.; Emeline, A.V.; Horikoshi, S. Light-Driven Advanced Oxidation Processes in the Disposal of Emerging Pharmaceutical Contaminants in Aqueous Media: A Brief Review. *Curr. Opin. Green Sustain. Chem.* **2017**, *6*, 18–33. [CrossRef]
32. Rizzo, L.; Malato, S.; Antakyali, D.; Beretsou, V.G.; Đolić, M.B.; Gernjak, W.; Heath, E.; Ivancev-Tumbas, I.; Karaolia, P.; Lado Ribeiro, A.R.; et al. Consolidated vs New Advanced Treatment Methods for the Removal of Contaminants of Emerging Concern from Urban Wastewater. *Sci. Total Environ.* **2019**, *655*, 986–1008. [CrossRef]
33. Canle, M.; Fernández Pérez, M.I.; Santaballa, J.A. Photocatalyzed Degradation/Abatement of Endocrine Disruptors. *Curr. Opin. Green Sustain. Chem.* **2017**, *6*, 101–138. [CrossRef]
34. Ushavipinachandran, V.; Rajendran, S.; Badagoppam Haroon, K.H.; Ashokan, I.; Mondal, A.; Bhunia, S.K. Detoxification of Endocrine Disruptors in Water Using Visible-Light-Active Nanostructures: A Review. *ACS Appl. Nano Mater.* **2020**, *3*, 11659–11687. [CrossRef]
35. Wang, R.; Ma, X.; Liu, T.; Li, Y.; Song, L.; Tjong, S.C.; Cao, L.; Wang, W.; Yu, Q.; Wang, Z. Degradation Aspects of Endocrine Disrupting Chemicals: A Review on Photocatalytic Processes and Photocatalysts. *Appl. Catal. A Gen.* **2020**, *597*, 117547. [CrossRef]
36. Kumar, A.; Sharma, V.; Kumar, A.; Krishnan, V. Nanomaterials for Photocatalytic Decomposition of Endocrine Disruptors in Water. In *Nanostructured Materials for Environmental Applications*; Springer International Publishing: Berlin/Heidelberg, Germany, 2021; pp. 299–320.
37. Velempini, T.; Prabakaran, E.; Pillay, K. Recent Developments in the Use of Metal Oxides for Photocatalytic Degradation of Pharmaceutical Pollutants in Water—A Review. *Mater. Today Chem.* **2021**, *19*, 100380. [CrossRef]
38. Luciani, G.; Imparato, C.; Vitiello, G. Photosensitive Hybrid Nanostructured Materials: The Big Challenges for Sunlight Capture. *Catalysts* **2020**, *10*, 103. [CrossRef]

39. Zhan, C.; Li, Y.; Sharma, P.R.; He, H.; Sharma, S.K.; Wang, R.; Hsiao, B.S. A Study of TiO_2 Nanocrystal Growth and Environmental Remediation Capability of TiO_2/CNC Nanocomposites. *RSC Adv.* **2019**, *9*, 40565–40576. [CrossRef] [PubMed]
40. Sharma, P.R.; Sharma, S.K.; Antoine, R.; Hsiao, B.S. Efficient Removal of Arsenic Using Zinc Oxide Nanocrystal-Decorated Regenerated Microfibrillated Cellulose Scaffolds. *ACS Sustain. Chem. Eng.* **2019**, *7*, 6140–6151. [CrossRef]
41. Zhang, C.; Li, Y.; Shen, H.; Shuai, D. Simultaneous Coupling of Photocatalytic and Biological Processes: A Promising Synergistic Alternative for Enhancing Decontamination of Recalcitrant Compounds in Water. *Chem. Eng. J.* **2021**, *403*, 126365. [CrossRef]
42. Yu, M.; Wang, J.; Tang, L.; Feng, C.; Liu, H.; Zhang, H.; Peng, B.; Chen, Z.; Xie, Q. Intimate Coupling of Photocatalysis and Biodegradation for Wastewater Treatment: Mechanisms, Recent Advances and Environmental Applications. *Water Res.* **2020**, *175*, 115673. [CrossRef]
43. Scaria, J.; Gopinath, A.; Nidheesh, P.V. A Versatile Strategy to Eliminate Emerging Contaminants from the Aqueous Environment: Heterogeneous Fenton Process. *J. Clean. Prod.* **2021**, *278*, 124014. [CrossRef]
44. Kumar, A.; Rana, A.; Sharma, G.; Naushad, M.; Dhiman, P.; Kumari, A.; Stadler, F.J. Recent Advances in Nano-Fenton Catalytic Degradation of Emerging Pharmaceutical Contaminants. *J. Mol. Liq.* **2019**, *290*, 111177. [CrossRef]
45. Xiao, S.; Cheng, M.; Zhong, H.; Liu, Z.; Liu, Y.; Yang, X.; Liang, Q. Iron-Mediated Activation of Persulfate and Peroxymonosulfate in Both Homogeneous and Heterogeneous Ways: A Review. *Chem. Eng. J.* **2020**, *384*, 123265. [CrossRef]
46. Duan, X.; Yang, S.; Wacławek, S.; Fang, G.; Xiao, R.; Dionysiou, D.D. Limitations and Prospects of Sulfate-Radical Based Advanced Oxidation Processes. *J. Environ. Chem. Eng.* **2020**, *8*, 103849. [CrossRef]
47. Xia, X.; Zhu, F.; Li, J.; Yang, H.; Wei, L.; Li, Q.; Jiang, J.; Zhang, G.; Zhao, Q. A Review Study on Sulfate-Radical-Based Advanced Oxidation Processes for Domestic/Industrial Wastewater Treatment: Degradation, Efficiency, and Mechanism. *Front. Chem.* **2020**, *8*, 592056. [CrossRef]
48. Sannino, F.; Pirozzi, D.; Vitiello, G.; D'Errico, G.; Aronne, A.; Fanelli, E.; Pernice, P. Oxidative Degradation of Phenanthrene in the Absence of Light Irradiation by Hybrid ZrO_2-Acetylacetonate Gel-Derived Catalyst. *Appl. Catal. B Environ.* **2014**, *156–157*, 101–107. [CrossRef]
49. Sannino, F.; Pernice, P.; Imparato, C.; Aronne, A.; D'Errico, G.; Minieri, L.; Perfetti, M.; Pirozzi, D. Hybrid TiO_2-Acetylacetonate Amorphous Gel-Derived Material with Stably Adsorbed Superoxide Radical Active in Oxidative Degradation of Organic Pollutants. *RSC Adv.* **2015**, *5*, 93831–93839. [CrossRef]
50. Pirozzi, D.; Imparato, C.; D'Errico, G.; Vitiello, G.; Aronne, A.; Sannino, F. Three-Year Lifetime and Regeneration of Superoxide Radicals on the Surface of Hybrid TiO_2 Materials Exposed to Air. *J. Hazard. Mater.* **2020**, *387*, 121716. [CrossRef]
51. Imparato, C.; Passaro, J.; Bifulco, A.; Branda, F.; Pirozzi, D.; Aronne, A. Development of Hybrid Titanium Oxide-Based Systems for the Surface Stabilization of Reactive Oxygen Radicals. *Chem. Eng. Trans.* **2021**, *84*, 139–144. [CrossRef]
52. Ritacco, I.; Imparato, C.; Falivene, L.; Cavallo, L.; Magistrato, A.; Caporaso, L.; Farnesi Camellone, M.; Aronne, A. Spontaneous Production of Ultrastable Reactive Oxygen Species on Titanium Oxide Surfaces Modified with Organic Ligands. *Adv. Mater. Interfaces* **2021**, *8*, 2100629. [CrossRef]
53. Liang, Z.; Yan, C.F.; Rtimi, S.; Bandara, J. Piezoelectric Materials for Catalytic/Photocatalytic Removal of Pollutants: Recent Advances and Outlook. *Appl. Catal. B Environ.* **2019**, *241*, 256–269. [CrossRef]
54. Nie, G.; Yao, Y.; Duan, X.; Xiao, L.; Wang, S. Advances of Piezoelectric Nanomaterials for Applications in Advanced Oxidation Technologies. *Curr. Opin. Chem. Eng.* **2021**, *33*, 100693. [CrossRef]
55. Russo, M.; Iervolino, G.; Vaiano, V.; Palma, V. Non-Thermal Plasma Coupled with Catalyst for the Degradation of Water Pollutants: A Review. *Catalysts* **2020**, *10*, 1438. [CrossRef]
56. Nam, S.-N.; Choong, C.E.; Hoque, S.; Farouk, T.I.; Cho, J.; Jang, M.; Snyder, S.A.; Meadows, M.E.; Yoon, Y. Catalytic Non-Thermal Plasma Treatment of Endocrine Disrupting Compounds, Pharmaceuticals, and Personal Care Products in Aqueous Solution: A Review. *Chemosphere* **2022**, *290*, 133395. [CrossRef] [PubMed]
57. Staples, C.A.; Dorn, P.B.; Klecka, G.M.; O'Block, S.T.; Harris, L.R. A Review of the Environmental Fate, Effects, and Exposures of Bisphenol A. *Chemosphere* **1998**, *36*, 2149–2173. [CrossRef]
58. Ismail, N.A.H.; Wee, S.Y.; Aris, A.Z. Multi-Class of Endocrine Disrupting Compounds in Aquaculture Ecosystems and Health Impacts in Exposed Biota. *Chemosphere* **2017**, *188*, 375–388. [CrossRef] [PubMed]
59. Bhatnagar, A.; Anastopoulos, I. Adsorptive Removal of Bisphenol A (BPA) from Aqueous Solution: A Review. *Chemosphere* **2017**, *168*, 885–902. [CrossRef] [PubMed]
60. Careghini, A.; Mastorgio, A.F.; Saponaro, S.; Sezenna, E. Bisphenol A, Nonylphenols, Benzophenones, and Benzotriazoles in Soils, Groundwater, Surface Water, Sediments, and Food: A Review. *Environ. Sci. Pollut. Res.* **2015**, *22*, 5711–5741. [CrossRef]
61. Rastkari, N.; Jeddi, M.Z.; Yunesian, M.; Ahmadkhaniha, R. Effect of Sunlight Exposure on Phthalates Migration from Plastic Containers to Packaged Juices. *J. Environ. Health Sci. Eng.* **2018**, *16*, 27–33. [CrossRef]
62. Russo, G.; Laneri, S.; di Lorenzo, R.; Ferrara, L.; Grumetto, L. The Occurrence of Selected Endocrine-Disrupting Chemicals in Water and Sediments from an Urban Lagoon in Southern Italy. *Water Environ. Res.* **2021**, *93*, 1944–1958. [CrossRef]
63. Jiang, J.; Mu, D.; Ding, M.; Zhang, S.; Zhang, H.; Hu, J. Simultaneous Determination of Primary and Secondary Phthalate Monoesters in the Taihu Lake: Exploration of Sources. *Chemosphere* **2018**, *202*, 17–24. [CrossRef]
64. Salaudeen, T.; Okoh, O.; Agunbiade, F.; Okoh, A. Phthalates Removal Efficiency in Different Wastewater Treatment Technology in the Eastern Cape, South Africa. *Environ. Monit. Assess.* **2018**, *190*, 299. [CrossRef]
65. Wang, Y.; Qian, H. Phthalates and Their Impacts on Human Health. *Healthcare* **2021**, *9*, 603. [CrossRef] [PubMed]

66. Xu, L.; Yang, L.; Johansson, E.M.J.; Wang, Y.; Jin, P. Photocatalytic Activity and Mechanism of Bisphenol a Removal over TiO_{2-x}/RGO Nanocomposite Driven by Visible Light. *Chem. Eng. J.* **2018**, *350*, 1043–1055. [CrossRef]
67. Wang, G.; Dai, J.; Luo, Q.; Deng, N. Photocatalytic Degradation of Bisphenol A by TiO_2@aspartic Acid-β-Cyclodextrin@reduced Graphene Oxide. *Sep. Purif. Technol.* **2021**, *254*, 117574. [CrossRef]
68. Wang, H.; Zhang, N.; Cheng, G.; Guo, H.; Shen, Z.; Yang, L.; Zhao, Y.; Alsaedi, A.; Hayat, T.; Wang, X. Preparing a Photocatalytic Fe Doped TiO_2/RGO for Enhanced Bisphenol A and Its Analogues Degradation in Water Sample. *Appl. Surf. Sci.* **2020**, *505*, 144640. [CrossRef]
69. Garg, A.; Singhania, T.; Singh, A.; Sharma, S.; Rani, S.; Neogy, A.; Yadav, S.R.; Sangal, V.K.; Garg, N. Photocatalytic Degradation of Bisphenol-A Using N,Co Codoped TiO_2 Catalyst under Solar Light. *Sci. Rep.* **2019**, *9*, 765. [CrossRef]
70. Zhao, X.; Wang, R.; Lu, Z.; Wang, W.; Yan, Y. Dual Sensitization Effect and Conductive Structure of Fe_3O_4@mTiO_2/C Photocatalyst towards Superior Photodegradation Activity for Bisphenol A under Visible Light. *J. Photochem. Photobiol. A Chem.* **2019**, *382*, 111902. [CrossRef]
71. He, J.; Zeng, X.; Lan, S.; Lo, I.M.C. Reusable Magnetic Ag/Fe, N-TiO_2/Fe_3O_4@SiO_2 Composite for Simultaneous Photocatalytic Disinfection of *E. Coli* and Degradation of Bisphenol A in Sewage under Visible Light. *Chemosphere* **2019**, *217*, 869–878. [CrossRef]
72. Ju, L.; Wu, P.; Yang, Q.; Ahmed, Z.; Zhu, N. Synthesis of ZnAlTi-LDO Supported C_{60}@AgCl Nanoparticles and Their Photocatalytic Activity for Photo-Degradation of Bisphenol A. *Appl. Catal. B Environ.* **2018**, *224*, 159–174. [CrossRef]
73. Kumar, A.; Schuerings, C.; Kumar, S.; Kumar, A.; Krishnan, V. Perovskite-Structured $CaTiO_3$ Coupled with g-C_3N_4 as a Heterojunction Photocatalyst for Organic Pollutant Degradation. *Beilstein J. Nanotechnol.* **2018**, *9*, 671–685. [CrossRef]
74. Ma, Y.; Xu, Y.; Ji, X.; Xie, M.; Jiang, D.; Yan, J.; Song, Z.; Xu, H.; Li, H. Construction of Polythiophene/$Bi_4O_5I_2$ Nanocomposites to Promote Photocatalytic Degradation of Bisphenol a. *J. Alloys Compd.* **2020**, *823*, 153773. [CrossRef]
75. Wu, R.; Song, H.; Luo, N.; Sheng, Y.; Ji, G. Microwave-Assisted Preparation and Enhanced Photocatalytic Activity of Bi_2WO_6/BiOI Heterojunction for Organic Pollutants Degradation under Visible-Light Irradiation. *Solid State Sci.* **2019**, *87*, 101–109. [CrossRef]
76. Rao, F.; Zhu, G.; Wang, M.; Zubairu, S.M.; Peng, J.; Gao, J.; Hojamberdiev, M. Constructing the Pd/PdO/β-Bi_2O_3 Microspheres with Enhanced Photocatalytic Activity for Bisphenol A Degradation and NO Removal. *J. Chem. Technol. Biotechnol.* **2020**, *95*, 862–874. [CrossRef]
77. Li, N.; Zhu, G.; Hojamberdiev, M.; Zhu, R.; Chang, J.; Gao, J.; Guo, Q.; Liu, P. Pd Nanoparticle-Decorated $Bi_4O_5Br_2$ Nanosheets with Enhanced Visible-Light Photocatalytic Activity for Degradation of Bisphenol A. *J. Photochem. Photobiol. A Chem.* **2018**, *356*, 440–450. [CrossRef]
78. Xu, Y.; Zhang, X.; Zhang, Y.; Zhu, J.; Zhu, R. Nano Flake Ag_3PO_4 Enhanced Photocatalytic Activity of Bisphenol A under Visible Light Irradiation. *Colloids Interface Sci. Commun.* **2020**, *37*, 100277. [CrossRef]
79. Karuppaiah, S.; Annamalai, R.; Muthuraj, A.; Kesavan, S.; Palani, R.; Ponnusamy, S.; Nagarajan, E.R.; Meenakshisundaram, S. Efficient Photocatalytic Degradation of Ciprofloxacin and Bisphenol A under Visible Light Using Gd_2WO_6 Loaded ZnO/Bentonite Nanocomposite. *Appl. Surf. Sci.* **2019**, *481*, 1109–1119. [CrossRef]
80. Fu, H.; Ma, S.; Zhao, P.; Xu, S.; Zhan, S. Activation of Peroxymonosulfate by Graphitized Hierarchical Porous Biochar and $MnFe_2O_4$ Magnetic Nanoarchitecture for Organic Pollutants Degradation: Structure Dependence and Mechanism. *Chem. Eng. J.* **2019**, *360*, 157–170. [CrossRef]
81. Kong, L.; Fang, G.; Kong, Y.; Xie, M.; Natarajan, V.; Zhou, D.; Zhan, J. Cu_2O@B-Cyclodextrin as a Synergistic Catalyst for Hydroxyl Radical Generation and Molecular Recognitive Destruction of Aromatic Pollutants at Neutral PH. *J. Hazard. Mater.* **2018**, *357*, 109–118. [CrossRef]
82. Zhang, C.; Li, N.; Chen, D.; Xu, Q.; Li, H.; He, J.; Lu, J. The Ultrasonic-Induced-Piezoelectric Enhanced Photocatalytic Performance of ZnO/CdS Nanofibers for Degradation of Bisphenol A. *J. Alloys Compd.* **2021**, *885*, 160987. [CrossRef]
83. Zhou, Q.; Shi, Q.; Li, N.; Chen, D.; Xu, Q.; Li, H.; He, J.; Lu, J. Environmental Science Nano Rh-Doped $SrTiO_3$ Inverse Opal with Piezoelectric Effect for Enhanced Visible-Light-Driven Photodegradation of Bisphenol A. *Environ. Sci. Nano* **2020**, *7*, 2267. [CrossRef]
84. Huang, R.; Wu, J.; Lin, E.; Kang, Z.; Qin, N.; Bao, D. A New Strategy for Large-Scale Synthesis of $Na_{0.5}Bi_{0.5}TiO_3$ Nanowires and Their Application in Piezocatalytic Degradation. *Nanoscale Adv.* **2021**, *3*, 3159–3166. [CrossRef]
85. Jing, W.W.; Li, D.Q.; Li, J.; Li, X.F.; Wu, Z.H.; Liu, Y.L. Photodegradation of Dimethyl Phthalate (DMP) by UV–TiO_2 in Aqueous Solution: Operational Parameters and Kinetic Analysis. *Int. J. Environ. Sci. Technol.* **2018**, *15*, 969–976. [CrossRef]
86. Wang, C.; Zeng, T.; Gu, C.; Zhu, S.; Zhang, Q.; Luo, X. Photodegradation Pathways of Typical Phthalic Acid Esters Under UV, UV/TiO_2, and UV-Vis/Bi_2WO_6 Systems. *Front. Chem.* **2019**, *7*, 852. [CrossRef] [PubMed]
87. You, S.; Hu, Y.; Liu, X.; Wei, C. Synergetic Removal of Pb(II) and Dibutyl Phthalate Mixed Pollutants on Bi_2O_3-TiO_2 Composite Photocatalyst under Visible Light. *Appl. Catal. B Environ.* **2018**, *232*, 288–298. [CrossRef]
88. Meenakshi, G.; Sivasamy, A. Nanorod ZnO/SiC Nanocomposite: An Efficient Catalyst for the Degradation of an Endocrine Disruptor under UV and Visible Light Irradiations. *J. Environ. Chem. Eng.* **2018**, *6*, 3757–3769. [CrossRef]
89. Li, S.; Lai, C.; Li, C.; Zhong, J.; He, Z.; Peng, Q.; Liu, X.; Ke, B. Enhanced Photocatalytic Degradation of Dimethyl Phthalate by Magnetic Dual Z-Scheme Iron Oxide/Mpg-C_3N_4/BiOBr/Polythiophene Heterostructure Photocatalyst under Visible Light. *J. Mol. Liq.* **2021**, *342*, 116947. [CrossRef]
90. di Dong, C.; Huang, C.P.; Nguyen, T.B.; Hsiung, C.F.; Wu, C.H.; Lin, Y.L.; Chen, C.W.; Hung, C.M. The Degradation of Phthalate Esters in Marine Sediments by Persulfate over Iron–Cerium Oxide Catalyst. *Sci. Total Environ.* **2019**, *696*, 133973. [CrossRef]

91. Ding, S.; Wan, J.; Ma, Y.; Wang, Y.; Li, X.; Sun, J.; Pu, M. Targeted Degradation of Dimethyl Phthalate by Activating Persulfate Using Molecularly Imprinted Fe-MOF-74. *Chemosphere* **2021**, *270*, 128620. [CrossRef]
92. FAO. Available online: https://www.fao.org/faostat/ (accessed on 31 January 2022).
93. Rostami, S.; Jafari, S.; Moeini, Z.; Jaskulak, M.; Keshtgar, L.; Badeenezhad, A.; Azhdarpoor, A.; Rostami, M.; Zorena, K.; Dehghani, M. Current Methods and Technologies for Degradation of Atrazine in Contaminated Soil and Water: A Review. *Environ. Technol. Innov.* **2021**, *24*, 102019. [CrossRef]
94. Khavar, A.H.C.; Moussavi, G.; Mahjoub, A.R.; Satari, M.; Abdolmaleki, P. Synthesis and Visible-Light Photocatalytic Activity of In,S-TiO_2@rGO Nanocomposite for Degradation and Detoxification of Pesticide Atrazine in Water. *Chem. Eng. J.* **2018**, *345*, 300–311. [CrossRef]
95. Shawky, A.; Mohamed, R.M.; Mkhalid, I.A.; Youssef, M.A.; Awwad, N.S. Visible Light-Responsive Ag/$LaTiO_3$ Nanowire Photocatalysts for Efficient Elimination of Atrazine Herbicide in Water. *J. Mol. Liq.* **2020**, *299*, 112163. [CrossRef]
96. Shawky, A.; Alhaddad, M.; Mohamed, R.M.; Awwad, N.S.; Ibrahium, H.A. Magnetically Separable and Visible Light-Active Ag/$NiCo_2O_4$ Nanorods Prepared by a Simple Route for Superior Photodegradation of Atrazine in Water. *Prog. Nat. Sci. Mater. Int.* **2020**, *30*, 160–167. [CrossRef]
97. Majhi, D.; Das, K.; Mishra, A.; Dhiman, R.; Mishra, B.G. One Pot Synthesis of CdS/BiOBr/$Bi_2O_2CO_3$: A Novel Ternary Double Z-Scheme Heterostructure Photocatalyst for Efficient Degradation of Atrazine. *Appl. Catal. B Environ.* **2020**, *260*, 118222. [CrossRef]
98. Yang, N.; Liu, Y.; Zhu, J.; Wang, Z.; Li, J. Study on the Efficacy and Mechanism of Fe-TiO_2 Visible Heterogeneous Fenton Catalytic Degradation of Atrazine. *Chemosphere* **2020**, *252*, 126333. [CrossRef]
99. Huang, Y.; Han, C.; Liu, Y.; Nadagouda, M.N.; Machala, L.; O'Shea, K.E.; Sharma, V.K.; Dionysiou, D.D. Degradation of Atrazine by $Zn_xCu_{1-x}Fe_2O_4$ Nanomaterial-Catalyzed Sulfite under UV–Vis Light Irradiation: Green Strategy to Generate SO_4^-. *Appl. Catal. B Environ.* **2018**, *221*, 380–392. [CrossRef]
100. Xie, S.; Tang, C.; Shi, H.; Zhao, G. Highly Efficient Photoelectrochemical Removal of Atrazine and the Mechanism Investigation: Bias Potential Effect and Reactive Species. *J. Hazard. Mater.* **2021**, *415*, 125681. [CrossRef]
101. Zhang, L.; Zhang, Y.; Xiao, K.; Shi, J.; Du, X.; Wang, L.; Wu, X. The Intimate Coupling of Photocatalysis and Biodegradation for the Degradation and Mineralization of Atrazine in Water. *New J. Chem.* **2021**, *45*, 13029–13039. [CrossRef]
102. Xu, X.; Chen, W.; Zong, S.; Ren, X.; Liu, D. Atrazine Degradation Using Fe_3O_4-Sepiolite Catalyzed Persulfate: Reactivity, Mechanism and Stability. *J. Hazard. Mater.* **2019**, *377*, 62–69. [CrossRef]
103. Li, J.; Wan, Y.; Li, Y.; Yao, G.; Lai, B. Surface Fe(III)/Fe(II) Cycle Promoted the Degradation of Atrazine by Peroxymonosulfate Activation in the Presence of Hydroxylamine. *Appl. Catal. B Environ.* **2019**, *256*, 117782. [CrossRef]
104. Wang, G.; Cheng, C.; Zhu, J.; Wang, L.; Gao, S.; Xia, X. Enhanced Degradation of Atrazine by Nanoscale $LaFe_{1-x}Cu_xO_{3-\delta}$ Perovskite Activated Peroxymonosulfate: Performance and Mechanism. *Sci. Total Environ.* **2019**, *673*, 565–575. [CrossRef]
105. Dong, X.; Ren, B.; Zhang, X.; Liu, X.; Sun, Z.; Li, C.; Tan, Y.; Yang, S.; Zheng, S.; Dionysiou, D.D. Diatomite Supported Hierarchical 2D $CoNi_3O_4$ Nanoribbons as Highly Efficient Peroxymonosulfate Catalyst for Atrazine Degradation. *Appl. Catal. B Environ.* **2020**, *272*, 118971. [CrossRef]
106. Chen, S.; He, P.; Wang, X.; Xiao, F.; Zhou, P.; He, Q.; Jia, L.; Dong, F.; Zhang, H.; Jia, B.; et al. Co/Sm-Modified Ti/PbO_2 Anode for Atrazine Degradation: Effective Electrocatalytic Performance and Degradation Mechanism. *Chemosphere* **2021**, *268*, 128799. [CrossRef] [PubMed]
107. Li, J.; Yan, J.; Yao, G.; Zhang, Y.; Li, X.; Lai, B. Improving the Degradation of Atrazine in the Three-Dimensional (3D) Electrochemical Process Using $CuFe_2O_4$ as Both Particle Electrode and Catalyst for Persulfate Activation. *Chem. Eng. J.* **2019**, *361*, 1317–1332. [CrossRef]
108. Yang, Y.; Deng, Q.; Zhang, Y. Comparative Study of Low-Index {1 0 1}-TiO_2, {0 0 1}-TiO_2, {1 0 0}-TiO_2 and High-Index {2 0 1}-TiO_2 on Glyphosate Adsorption and Photo-Degradation. *Chem. Eng. J.* **2019**, *360*, 1247–1254. [CrossRef]
109. Wu, H.; Sun, Q.; Chen, J.; Wang, G.Y.; Wang, D.; Zeng, X.F.; Wang, J.X. Citric Acid-Assisted Ultrasmall CeO_2 Nanoparticles for Efficient Photocatalytic Degradation of Glyphosate. *Chem. Eng. J.* **2021**, *425*, 130640. [CrossRef]
110. Russo, M.; Iervolino, G.; Vaiano, V. W-Doped ZnO Photocatalyst for the Degradation of Glyphosate in Aqueous Solution. *Catalysts* **2021**, *11*, 234. [CrossRef]
111. Cao, L.; Ma, D.; Zhou, Z.; Xu, C.; Cao, C.; Zhao, P.; Huang, Q. Efficient Photocatalytic Degradation of Herbicide Glyphosate in Water by Magnetically Separable and Recyclable BiOBr/Fe_3O_4 Nanocomposites under Visible Light Irradiation. *Chem. Eng. J.* **2019**, *368*, 212–222. [CrossRef]
112. Luo, X.L.; Chen, Z.Y.; Yang, S.Y.; Xu, Y.H. Two-Step Hydrothermal Synthesis of Peanut-Shaped Molybdenum Diselenide/Bismuth Vanadate ($MoSe_2$/$BiVO_4$) with Enhanced Visible-Light Photocatalytic Activity for the Degradation of Glyphosate. *J. Colloid Interface Sci.* **2018**, *532*, 456–463. [CrossRef]
113. Tang, Q.Y.; Chen, W.F.; Lv, Y.R.; Yang, S.Y.; Xu, Y.H. Z-Scheme Hierarchical Cu_2S/Bi_2WO_6 Composites for Improved Photocatalytic Activity of Glyphosate Degradation under Visible Light Irradiation. *Sep. Purif. Technol.* **2020**, *236*, 116243. [CrossRef]
114. Xue, L.; Hao, L.; Ding, H.; Liu, R.; Zhao, D.; Fu, J.; Zhang, M. Complete and Rapid Degradation of Glyphosate with $Fe_3Ce_1O_x$ Catalyst for Peroxymonosulfate Activation at Room Temperature. *Environ. Res.* **2021**, *201*, 111618. [CrossRef]
115. Marien, C.B.D.; le Pivert, M.; Azaïs, A.; M'Bra, I.C.; Drogui, P.; Dirany, A.; Robert, D. Kinetics and Mechanism of Paraquat's Degradation: UV-C Photolysis vs UV-C Photocatalysis with TiO_2/SiC Foams. *J. Hazard. Mater.* **2019**, *370*, 164–171. [CrossRef]

116. Vanichvattanadecha, C.; Jaroenworaluck, A.; Henpraserttae, P.; Wimuktiwan, P.; Manpetch, P.; Singhapong, W. Ordered Mesoporous Silica (SBA-16) Supporting Titania (TiO_2) Nanoparticles for Photodegradation of Paraquat (PQ) Herbicide. *J. Porous Mater.* **2021**, *28*, 1137–1153. [CrossRef]
117. Suwannaruang, T.; Kamonsuangkasem, K.; Kidkhunthod, P.; Chirawatkul, P.; Saiyasombat, C.; Chanlek, N.; Wantala, K. Influence of Nitrogen Content Levels on Structural Properties and Photocatalytic Activities of Nanorice-like N-Doped TiO_2 with Various Calcination Temperatures. *Mater. Res. Bull.* **2018**, *105*, 265–276. [CrossRef]
118. Pourzad, A.; Sobhi, H.R.; Behbahani, M.; Esrafili, A.; Kalantary, R.R.; Kermani, M. Efficient Visible Light-Induced Photocatalytic Removal of Paraquat Using N-Doped TiO_2@SiO_2@Fe_3O_4 Nanocomposite. *J. Mol. Liq.* **2020**, *299*, 112167. [CrossRef]
119. Zangeneh, H.; Zinatizadeh, A.A.; Feyzi, M.; Zinadini, S.; Bahnemann, D.W. Photomineralization of Recalcitrant Wastewaters by a Novel Magnetically Recyclable Boron Doped-TiO_2-SiO_2 Cobalt Ferrite Nanocomposite as a Visible-Driven Heterogeneous Photocatalyst. *J. Environ. Chem. Eng.* **2018**, *6*, 6370–6381. [CrossRef]
120. Khodkar, A.; Khezri, S.M.; Pendashteh, A.R.; Khoramnejadian, S.; Mamani, L. A Designed Experimental Approach for Photocatalytic Degradation of Paraquat Using α-Fe_2O_3@MIL-101(Cr)@TiO_2 Based on Metal–Organic Framework. *Int. J. Environ. Sci. Technol.* **2019**, *16*, 5741–5756. [CrossRef]
121. Kumar, A.; Kumar, A.; Sharma, G.; Al-Muhtaseb, A.H.; Naushad, M.; Ghfar, A.A.; Guo, C.; Stadler, F.J. Biochar-Templated g-C_3N_4/$Bi_2O_2CO_3$/$CoFe_2O_4$ Nano-Assembly for Visible and Solar Assisted Photo-Degradation of Paraquat, Nitrophenol Reduction and CO_2 Conversion. *Chem. Eng. J.* **2018**, *339*, 393–410. [CrossRef]
122. Mary Nisha, U.; Umapathy, M.J.; Sivasamy, A. Effective Degradation of 2,4-Dichlorophenoxy Acetic Acid Endocrine Disruptor Using CeO_2–Bi_2O_3 Mixed Metal Oxide Photocatalyst under Visible Light Irradiation. *J. Mater. Sci. Mater. Electron.* **2021**, *32*, 14791–14800. [CrossRef]
123. Lima, M.S.; Cruz-Filho, J.F.; Noleto, L.F.G.; Silva, L.J.; Costa, T.M.S.; Luz, G.E. Synthesis, Characterization and Catalytic Activity of Fe_3O_4@WO_3/SBA-15 on Photodegradation of the Acid Dichlorophenoxyacetic (2,4-D) under UV Irradiation. *J. Environ. Chem. Eng.* **2020**, *8*, 104145. [CrossRef]
124. Xu, X.; Cai, J.; Zhou, M.; Du, X.; Zhang, Y. Photoelectrochemical Degradation of 2,4-Dichlorophenoxyacetic Acid Using Electrochemically Self-Doped Blue TiO_2 Nanotube Arrays with Formic Acid as Electrolyte. *J. Hazard. Mater.* **2020**, *382*, 121096. [CrossRef]
125. Sharma, R.K.; Arora, B.; Sharma, S.; Dutta, S.; Sharma, A.; Yadav, S.; Solanki, K. In Situ Hydroxyl Radical Generation Using the Synergism of the Co–Ni Bimetallic Centres of a Developed Nanocatalyst with Potent Efficiency for Degrading Toxic Water Pollutants. *Mater. Chem. Front.* **2020**, *4*, 605–620. [CrossRef]
126. Riaz, U.; Zia, J. Microwave-Assisted Rapid Degradation of DDT Using Nanohybrids of PANI with SnO_2 Derived from Psidium Guajava Extract. *Environ. Pollut.* **2020**, *259*, 113917. [CrossRef] [PubMed]
127. Liu, J.; An, F.; Zhu, C.; Zhou, D. Efficient Transformation of DDT with Peroxymonosulfate Activation by Different Crystallographic MnO_2. *Sci. Total Environ.* **2021**, *759*, 142864. [CrossRef] [PubMed]
128. Vela, N.; Calín, M.; Yáñez-Gascón, M.J.; Garrido, I.; Pérez-Lucas, G.; Fenoll, J.; Navarro, S. Photocatalytic Oxidation of Six Pesticides Listed as Endocrine Disruptor Chemicals from Wastewater Using Two Different TiO_2 Samples at Pilot Plant Scale under Sunlight Irradiation. *J. Photochem. Photobiol. A Chem.* **2018**, *353*, 271–278. [CrossRef]
129. Vela, N.; Calín, M.; Yáñez-Gascón, M.J.; el Aatik, A.; Garrido, I.; Pérez-Lucas, G.; Fenoll, J.; Navarro, S. Removal of Pesticides with Endocrine Disruptor Activity in Wastewater Effluent by Solar Heterogeneous Photocatalysis Using ZnO/$Na_2S_2O_8$. *Water Air Soil Pollut.* **2019**, *230*, 134. [CrossRef]
130. Rossetti, M.F.; Stoker, C.; Ramos, J.G. Agrochemicals and Neurogenesis. *Mol. Cell. Endocrinol.* **2020**, *510*, 110820. [CrossRef]
131. Kalofiri, P.; Balias, G.; Tekos, F. The EU Endocrine Disruptors' Regulation and the Glyphosate Controversy. *Toxicol. Rep.* **2021**, *8*, 1193–1199. [CrossRef]
132. Alulema-Pullupaxi, P.; Fernández, L.; Debut, A.; Santacruz, C.P.; Villacis, W.; Fierro, C.; Espinoza-Montero, P.J. Photoelectrocatalytic Degradation of Glyphosate on Titanium Dioxide Synthesized by Sol-Gel/Spin-Coating on Boron Doped Diamond (TiO_2/BDD) as a Photoanode. *Chemosphere* **2021**, *278*, 130488. [CrossRef]
133. Phuinthiang, P.; Kajitvichyanukul, P. Degradation of Paraquat from Contaminated Water Using Green TiO_2 Nanoparticles Synthesized from *Coffea arabica* L. in Photocatalytic Process. *Water Sci. Technol.* **2018**, *79*, 905–910. [CrossRef]
134. Sharma, S.; Basu, S. Highly Reusable Visible Light Active Hierarchical Porous WO_3/SiO_2 Monolith in Centimeter Length Scale for Enhanced Photocatalytic Degradation of Toxic Pollutants. *Sep. Purif. Technol.* **2020**, *231*, 115916. [CrossRef]
135. Quan, Y.; Yao, J.; Yang, S.; Chen, L.; Liu, Y.; Lang, J.; Zeng, H.; Yang, J.; Gao, M. Detect, Remove and Re-Use: Sensing and Degradation Pesticides via 3D Tilted ZMRs/Ag Arrays. *J. Hazard. Mater.* **2020**, *391*, 122222. [CrossRef]
136. Fidelis, M.Z.; Abreu, E.; Josué, T.G.; de Almeida, L.N.B.; Lenzi, G.G.; Santos, O.A.A. dos Continuous Process Applied to Degradation of Triclosan and 2.8-Dichlorodibenzene-p-Dioxin. *Environ. Sci. Pollut. Res.* **2021**, *28*, 23675–23683. [CrossRef] [PubMed]
137. Kaur, H.; Dahake, R.; Maddigapu, P.R.; Hippargi, G.; Pophali, G.R.; Bansiwal, A. Enhanced Photocatalytic Degradation of Antimicrobial Triclosan Using RGO–TiO_2 Composite under Natural Solar Illumination. *J. Mater. Sci. Mater. Electron.* **2020**, *31*, 6045–6058. [CrossRef]
138. Ojha, A.; Singh, P.; Tiwary, D. Photocatalytic Degradation of Triclosan in Visible-Light-Induced via CdS@TiO_2-RGO Nanocomposite. *Surf. Topogr.: Metrol. Prop.* **2021**, *9*, 035032. [CrossRef]

139. Chandra Pragada, S.; Thalla, A.K. Polymer-Based Immobilized Fe_2O_3–TiO_2/PVP Catalyst Preparation Method and the Degradation of Triclosan in Treated Greywater Effluent by Solar Photocatalysis. *J. Environ. Manag.* **2021**, *296*, 113305. [CrossRef]
140. Köwitsch, I.; Mehring, M. Coatings of Magnetic Composites of Iron Oxide and Carbon Nitride for Photocatalytic Water Purification. *RSC Adv.* **2021**, *11*, 14053–14062. [CrossRef]
141. Katal, R.; Panah, S.M.; Saeedikhani, M.; Kosari, M.; Sheng, C.C.; Leong, O.S.; Xiao, G.; Jiangyong, H. Pd-Decorated CuO Thin Film for Photodegradation of Acetaminophen and Triclosan under Visible Light Irradiation. *Adv. Mater. Interfaces* **2018**, *5*, 1801440. [CrossRef]
142. Tiwari, A.; Shukla, A.; Lalliansanga; Tiwari, D.; Lee, S.M. Synthesis and Characterization of Ag^0(NPs)/TiO_2 Nanocomposite: Insight Studies of Triclosan Removal from Aqueous Solutions. *Environ. Technol.* **2020**, *41*, 3500–3514. [CrossRef]
143. Ferreira, O.; Monteiro, O.C.; do Rego, A.M.B.; Ferraria, A.M.; Batista, M.; Santos, R.; Monteiro, S.; Freire, M.; Silva, E.R. Visible Light-Driven Photodegradation of Triclosan and Antimicrobial Activity against Legionella Pneumophila with Cobalt and Nitrogen Co-Doped TiO_2 Anatase Nanoparticles. *J. Environ. Chem. Eng.* **2021**, *9*, 106735. [CrossRef]
144. Chen, Z.; Bi, S.; Zhao, G.; Chen, Y.; Hu, Y. Enhanced Degradation of Triclosan by Cobalt Manganese Spinel-Type Oxide Activated Peroxymonosulfate Oxidation Process via Sulfate Radicals and Singlet Oxygen: Mechanisms and Intermediates Identification. *Sci. Total Environ.* **2020**, *711*, 134715. [CrossRef]
145. So, H.L.; Lin, K.Y.; Chu, W. Triclosan Removal by Heterogeneous Fenton-like Process: Studying the Kinetics and Surface Chemistry of Fe_3O_4 as Catalyst. *J. Environ. Chem. Eng.* **2019**, *7*, 103432. [CrossRef]
146. So, H.L.; Lin, K.Y.; Chu, W.; Gong, H. Degradation of Triclosan by Recyclable $MnFe_2O_4$-Activated PMS: Process Modification for Reduced Toxicity and Enhanced Performance. *Ind. Eng. Chem. Res.* **2020**, *59*, 4257–4264. [CrossRef]
147. Huang, Z.; Lin, Q.; Cai, N.; Weng, Q.; Xu, J.; Gan, S.; Chen, C.; Zhong, Q.; Fu, H.; Xia, Y.; et al. Coexistence of Free Radical and Nonradical Mechanisms for Triclosan Degradation by CuO/HNTs. *Sep. Purif. Technol.* **2021**, *276*, 119318. [CrossRef]
148. Song, X.; Ren, C.; Zhao, Q.; Su, B. Simultaneous Removal of Cr(VI) and Triclosan from Aqueous Solutions through Fe_3O_4 Magnetic Nanoscale-Activated Persulfate Oxidation. *Chem. Eng. J.* **2020**, *381*, 122586. [CrossRef]
149. Ajiboye, T.O.; Oyewo, O.A.; Onwudiwe, D.C. Photocatalytic Removal of Parabens and Halogenated Products in Wastewater: A Review. *Environ. Chem. Lett.* **2021**, *19*, 3789–3819. [CrossRef]
150. de Jesus, R.A.; de Assis, G.C.; de Oliveira, R.J.; Costa, J.A.S.; da Silva, C.M.P.; Bilal, M.; Iqbal, H.M.N.; Ferreira, L.F.R.; Figueiredo, R.T. Environmental Remediation Potentialities of Metal and Metal Oxide Nanoparticles: Mechanistic Biosynthesis, Influencing Factors, and Application Standpoint. *Environ. Technol. Innov.* **2021**, *24*, 101851. [CrossRef]
151. Ngigi, E.M.; Nomngongo, P.N.; Ngila, J.C. Recent Methods Used in Degradation of Parabens in Aqueous Solutions: A Review. *Int. J. Environ. Sci. Technol.* **2022**, *19*, 2139–2154. [CrossRef]
152. Foszpańczyk, M.; Bednarczyk, K.; Drozdek, E.; Martins, R.C.; Ledakowicz, S.; Gmurek, M. Comparison of Photocatalytic and Photosensitized Oxidation of Paraben Aqueous Solutions Under Sunlight. *Water Air Soil Pollut.* **2018**, *229*, 362. [CrossRef]
153. Gomes, J.; Lincho, J.; Domingues, E.; Gmurek, M.; Mazierski, P.; Zaleska-Medynska, A.; Klimczuk, T.; Quinta-Ferreira, R.M.; Martins, R.C. TiO_2 Nanotube Arrays-Based Reactor for Photocatalytic Oxidation of Parabens Mixtures in Ultrapure Water: Effects of Photocatalyst Properties, Operational Parameters and Light Source. *Sci. Total Environ.* **2019**, *689*, 79–89. [CrossRef]
154. Lincho, J.; Gomes, J.; Kobylanski, M.; Bajorowicz, B.; Zaleska-Medynska, A.; Martins, R.C. TiO_2 Nanotube Catalysts for Parabens Mixture Degradation by Photocatalysis and Ozone-Based Technologies. *Process Saf. Environ. Prot.* **2021**, *152*, 601–613. [CrossRef]
155. Vela, N.; Calín, M.; Yáñez-Gascón, M.J.; Garrido, I.; Pérez-Lucas, G.; Fenoll, J.; Navarro, S. Solar Reclamation of Wastewater Effluent Polluted with Bisphenols, Phthalates and Parabens by Photocatalytic Treatment with TiO_2/$Na_2S_2O_8$ at Pilot Plant Scale. *Chemosphere* **2018**, *212*, 95–104. [CrossRef]
156. Petala, A.; Noe, A.; Frontistis, Z.; Drivas, C.; Kennou, S.; Mantzavinos, D.; Kondarides, D.I. Synthesis and Characterization of CoO_x/$BiVO_4$ Photocatalysts for the Degradation of Propyl Paraben. *J. Hazard. Mater.* **2019**, *372*, 52–60. [CrossRef] [PubMed]
157. Moschogiannaki, M.; Frontistis, Z.; Kiriakidis, G.; Mantzavinos, D.; Binas, V. Porous $Co_xNi_{1-x}TiO_3$ Nanorods for Solar Photocatalytic Degradation of Ethyl Paraben. *J. Mater.* **2020**, *6*, 788–799. [CrossRef]
158. Sheikhmohammadi, A.; Nourmoradi, H.; Manshouri, M.; Asgari, E. Performance Intensification of BzP Photo-Catalytic Degradation through Adding Exogenous Oxidant. *Optik* **2020**, *202*, 163571. [CrossRef]
159. Asgari, E.; Esrafili, A.; Rostami, R.; Farzadkia, M. O_3, O_3/UV and O_3/UV/ZnO for Abatement of Parabens in Aqueous Solutions: Effect of Operational Parameters and Mineralization/Biodegradability Improvement. *Process Saf. Environ. Prot.* **2019**, *125*, 238–250. [CrossRef]
160. Pratush, A.; Ye, X.; Yang, Q.; Kan, J.; Peng, T.; Wang, H.; Huang, T.; Xiong, G.; Hu, Z. Biotransformation Strategies for Steroid Estrogen and Androgen Pollution. *Appl. Microbiol. Biotechnol.* **2020**, *104*, 2385–2409. [CrossRef]
161. Du, P.; Chang, J.; Zhao, H.; Liu, W.; Dang, C.; Tong, M.; Ni, J.; Zhang, B. Sea-Buckthorn-Like MnO_2 Decorated Titanate Nanotubes with Oxidation Property and Photocatalytic Activity for Enhanced Degradation of 17β-Estradiol under Solar Light. *ACS Appl. Energy Mater.* **2018**, *1*, 2123–2133. [CrossRef]
162. Sun, K.; Liu, Q.; Li, S.; Qi, Y.; Si, Y. MnO_2 Nanozyme-Driven Polymerization and Decomposition Mechanisms of 17β-Estradiol: Influence of Humic Acid. *J. Hazard. Mater.* **2020**, *393*, 122393. [CrossRef]
163. Kovacic, M.; Kopcic, N.; Kusic, H.; Bozic, A.L. Solar Driven Degradation of 17β-Estradiol Using Composite Photocatalytic Materials and Artificial Irradiation Source: Influence of Process and Water Matrix Parameters. *J. Photochem. Photobiol. A Chem.* **2018**, *361*, 48–61. [CrossRef]

164. Majumder, A.; Gupta, A.K. Enhanced Photocatalytic Degradation of 17β-Estradiol by Polythiophene Modified Al-Doped ZnO: Optimization of Synthesis Parameters Using Multivariate Optimization Techniques. *J. Environ. Chem. Eng.* **2020**, *8*, 104463. [CrossRef]
165. Wei, X.; Li, J.; Liu, Z.; Yang, X.; Naraginti, S.; Xu, X.; Wang, X. Visible Light Photocatalytic Mineralization of 17α-Ethinyl Estradiol (EE2) and Hydrogen Evolution over Silver and Strontium Modified TiO_2 Nanoparticles: Mechanisms and Phytotoxicity Assessment. *RSC Adv.* **2018**, *8*, 4329–4339. [CrossRef]
166. Menon, N.G.; George, L.; Tatiparti, S.S.V.; Mukherji, S. Efficacy and Reusability of Mixed-Phase TiO_2–ZnO Nanocomposites for the Removal of Estrogenic Effects of 17β-Estradiol and 17α-Ethinylestradiol from Water. *J. Environ. Manag.* **2021**, *288*, 112340. [CrossRef] [PubMed]
167. Abreu, E.; Fidelis, M.Z.; Fuziki, M.E.; Malikoski, R.M.; Mastsubara, M.C.; Imada, R.E.; Diaz de Tuesta, J.L.; Gomes, H.T.; Anziliero, M.D.; Baldykowski, B.; et al. Degradation of Emerging Contaminants: Effect of Thermal Treatment on nb_2o_5 as Photocatalyst. *J. Photochem. Photobiol. A Chem.* **2021**, *419*, 113484. [CrossRef]
168. Villa, K.; Parmar, J.; Vilela, D.; Sánchez, S. Core-Shell Microspheres for the Ultrafast Degradation of Estrogen Hormone at Neutral pH. *RSC Adv.* **2018**, *8*, 5840–5847. [CrossRef]
169. Zhu, N.; Li, C.; Bu, L.; Tang, C.; Wang, S.; Duan, P.; Yao, L.; Tang, J.; Dionysiou, D.D.; Wu, Y. Bismuth Impregnated Biochar for Efficient Estrone Degradation: The Synergistic Effect between Biochar and Bi/Bi_2O_3 for a High Photocatalytic Performance. *J. Hazard. Mater.* **2020**, *384*, 121258. [CrossRef] [PubMed]
170. Ramírez-Sánchez, I.M.; Bandala, E.R. Photocatalytic Degradation of Estriol Using Iron-Doped TiO_2 under High and Low UV Irradiation. *Catalysts* **2018**, *8*, 625. [CrossRef]
171. Escudeiro de Oliveira, M.; Barroso, B.L.; de Almeida, J.; Moraes, M.L.L.; de Arruda Rodrigues, C. Photoelectrocatalytic Degradation of 17α-Ethinylestradiol and Estrone under UV and Visible Light Using Nanotubular Oxide Arrays Grown on Ti-0.5wt%W. *Environ. Res.* **2020**, *191*, 110044. [CrossRef]
172. González-Rodríguez, J.; Gamallo, M.; Conde, J.J.; Vargas-Osorio, Z.; Vázquez-Vázquez, C.; Piñeiro, Y.; Rivas, J.; Feijoo, G.; Moreira, M.T. Exploiting the Potential of Supported Magnetic Nanomaterials as Fenton-like Catalysts for Environmental Applications. *Nanomaterials* **2021**, *11*, 2902. [CrossRef]
173. Bayode, A.A.; Vieira, E.M.; Moodley, R.; Akpotu, S.; de Camargo, A.S.S.; Fatta-Kassinos, D.; Unuabonah, E.I. Tuning ZnO/GO p-n Heterostructure with Carbon Interlayer Supported on Clay for Visible-Light Catalysis: Removal of Steroid Estrogens from Water. *Chem. Eng. J.* **2021**, *420*, 127668. [CrossRef]
174. Joseita dos Santos Costa, M.; dos Santos Costa, G.; Estefany Brandão Lima, A.; Eduardo da Luz Júnior, G.; Longo, E.; Santos Cavalcante, L.; da Silva Santos, R. Photocurrent Response and Progesterone Degradation by Employing WO_3 Films Modified with Platinum and Silver Nanoparticles. *ChemPlusChem* **2018**, *83*, 1153–1161. [CrossRef]
175. Maniakova, G.; Kowalska, K.; Murgolo, S.; Mascolo, G.; Libralato, G.; Lofrano, G.; Sacco, O.; Guida, M.; Rizzo, L. Comparison between Heterogeneous and Homogeneous Solar Driven Advanced Oxidation Processes for Urban Wastewater Treatment: Pharmaceuticals Removal and Toxicity. *Sep. Purif. Technol.* **2020**, *236*, 116249. [CrossRef]
176. Fanourakis, S.K.; Peña-Bahamonde, J.; Bandara, P.C.; Rodrigues, D.F. Nano-Based Adsorbent and Photocatalyst Use for Pharmaceutical Contaminant Removal during Indirect Potable Water Reuse. *NPJ Clean Water* **2020**, *3*, 1. [CrossRef]
177. Salimi, M.; Behbahani, M.; Sobhi, H.R.; Gholami, M.; Jonidi Jafari, A.; Rezaei Kalantary, R.; Farzadkia, M.; Esrafili, A. A New Nano-Photocatalyst Based on Pt and Bi Co-Doped TiO_2 for Efficient Visible-Light Photo Degradation of Amoxicillin. *New J. Chem.* **2019**, *43*, 1562–1568. [CrossRef]
178. Thakur, A.; Kumar, P.; Kaur, D.; Devunuri, N.; Sinha, R.K.; Devi, P. TiO_2 Nanofibres Decorated with Green-Synthesized PAu/Ag@CQDs for the Efficient Photocatalytic Degradation of Organic Dyes and Pharmaceutical Drugs. *RSC Adv.* **2020**, *10*, 8941–8948. [CrossRef]
179. Song, J.; Wu, X.; Zhang, M.; Liu, C.; Yu, J.; Sun, G.; Si, Y.; Ding, B. Highly Flexible, Core-Shell Heterostructured, and Visible-Light-Driven Titania-Based Nanofibrous Membranes for Antibiotic Removal and *E. Coil* Inactivation. *Chem. Eng. J.* **2020**, *379*, 122269. [CrossRef]
180. Islam, S.E.; Hang, D.R.; Chen, C.H.; Sharma, K.H. Facile and Cost-Efficient Synthesis of Quasi-0D/2D ZnO/MoS_2 Nanocomposites for Highly Enhanced Visible-Light-Driven Photocatalytic Degradation of Organic Pollutants and Antibiotics. *Chem. Eur. J.* **2018**, *24*, 9305–9315. [CrossRef]
181. Lwin, H.M.; Zhan, W.; Song, S.; Jia, F.; Zhou, J. Visible-Light Photocatalytic Degradation Pathway of Tetracycline Hydrochloride with Cubic Structured ZnO/SnO_2 Heterojunction Nanocatalyst. *Chem. Phys. Lett.* **2019**, *736*, 136806. [CrossRef]
182. Ghoreishian, S.M.; Raju, G.S.R.; Pavitra, E.; Kwak, C.H.; Han, Y.K.; Huh, Y.S. Ultrasound-Assisted Heterogeneous Degradation of Tetracycline over Flower-like $RGO/CdWO_4$ Hierarchical Structures as Robust Solar-Light-Responsive Photocatalysts: Optimization, Kinetics, and Mechanism. *Appl. Surf. Sci.* **2019**, *489*, 110–122. [CrossRef]
183. Chen, W.; Chang, L.; Ren, S.B.; He, Z.C.; Huang, G.B.; Liu, X.H. Direct Z-Scheme 1D/2D $WO_{2.72}/ZnIn_2S_4$ Hybrid Photocatalysts with Highly-Efficient Visible-Light-Driven Photodegradation towards Tetracycline Hydrochloride Removal. *J. Hazard. Mater.* **2020**, *384*, 121308. [CrossRef]
184. Kandi, D.; Behera, A.; Sahoo, S.; Parida, K. CdS QDs Modified $BiOI/Bi_2MoO_6$ Nanocomposite for Degradation of Quinolone and Tetracycline Types of Antibiotics towards Environmental Remediation. *Sep. Purif. Technol.* **2020**, *253*, 117523. [CrossRef]

185. Kumar, A.; Rana, A.; Sharma, G.; Naushad, M.; Al-Muhtaseb, A.H.; Guo, C.; Iglesias-Juez, A.; Stadler, F.J. High-Performance Photocatalytic Hydrogen Production and Degradation of Levofloxacin by Wide Spectrum-Responsive Ag/Fe_3O_4 Bridged $SrTiO_3$/g-C_3N_4 Plasmonic Nanojunctions: Joint Effect of Ag and Fe_3O_4. *ACS Appl. Mater. Interfaces* **2018**, *10*, 40474–40490. [CrossRef]
186. Szabó-Bárdos, E.; Cafuta, A.; Hegedűs, P.; Fónagy, O.; Kiss, G.; Babić, S.; Škorić, I.; Horváth, O. Photolytic and Photocatalytic Degradation of Nitrofurantoin and Its Photohydrolytic Products. *J. Photochem. Photobiol. A Chem.* **2020**, *386*, 112093. [CrossRef]
187. Devi, M.; Das, B.; Barbhuiya, M.H.; Bhuyan, B.; Dhar, S.S.; Vadivel, S. Fabrication of Nanostructured NiO/WO_3 with Graphitic Carbon Nitride for Visible Light Driven Photocatalytic Hydroxylation of Benzene and Metronidazole Degradation. *New J. Chem.* **2019**, *43*, 14616–14624. [CrossRef]
188. Zhu, W.; Li, Z.; He, C.; Faqian, S.; Zhou, Y. Enhanced Photodegradation of Sulfamethoxazole by a Novel WO_3-CNT Composite under Visible Light Irradiation. *J. Alloys Compd.* **2018**, *754*, 153–162. [CrossRef]
189. Katal, R.; Davood Abadi Farahani, M.H.; Jiangyong, H. Degradation of Acetaminophen in a Photocatalytic (Batch and Continuous System) and Photoelectrocatalytic Process by Application of Faceted-TiO_2. *Sep. Purif. Technol.* **2020**, *230*, 115859. [CrossRef]
190. Namshah, K.S.; Mohamed, R.M. WO3–TiO_2 Nanocomposites for Paracetamol Degradation under Visible Light. *Appl. Nanosci.* **2018**, *8*, 2021–2030. [CrossRef]
191. Ranjith Kumar, D.; Ranjith, K.S.; Haldorai, Y.; Kandasami, A.; Rajendra Kumar, R.T. Nitrogen-Implanted ZnO Nanorod Arrays for Visible Light Photocatalytic Degradation of a Pharmaceutical Drug Acetaminophen. *ACS Omega* **2019**, *4*, 11973–11979. [CrossRef]
192. Palas, B.; Ersöz, G.; Atalay, S. Bioinspired Metal Oxide Particles as Efficient Wet Air Oxidation and Photocatalytic Oxidation Catalysts for the Degradation of Acetaminophen in Aqueous Phase. *Ecotoxicol. Environ. Saf.* **2019**, *182*, 109367. [CrossRef]
193. Sacco, O.; Murcia, J.J.; Lara, A.E.; Hernández-Laverde, M.; Rojas, H.; Navío, J.A.; Hidalgo, M.C.; Vaiano, V. Pt–TiO_2–Nb_2O_5 Heterojunction as Effective Photocatalyst for the Degradation of Diclofenac and Ketoprofen. *Mater. Sci. Semicond. Process.* **2020**, *107*, 104839. [CrossRef]
194. Vitiello, G.; Iervolino, G.; Imparato, C.; Rea, I.; Borbone, F.; de Stefano, L.; Aronne, A.; Vaiano, V. F-Doped ZnO Nano- and Meso-Crystals with Enhanced Photocatalytic Activity in Diclofenac Degradation. *Sci. Total Environ.* **2021**, *762*, 143066. [CrossRef]
195. Yilmaz, E.; Salem, S.; Sarp, G.; Aydin, S.; Sahin, K.; Korkmaz, I.; Yuvali, D. TiO_2 Nanoparticles and C-Nanofibers Modified Magnetic Fe_3O_4 Nanospheres (TiO_2@Fe_3O_4@C–NF): A Multifunctional Hybrid Material for Magnetic Solid-Phase Extraction of Ibuprofen and Photocatalytic Degradation of Drug Molecules and Azo Dye. *Talanta* **2020**, *213*, 120813. [CrossRef]
196. Khammar, S.; Bahramifar, N.; Younesi, H. Preparation and Surface Engineering of CM-β-CD Functionalized Fe_3O_4@TiO_2 Nanoparticles for Photocatalytic Degradation of Polychlorinated Biphenyls (PCBs) from Transformer Oil. *J. Hazard. Mater.* **2020**, *394*, 122422. [CrossRef] [PubMed]
197. Gorbunova, T.I.; Kozhevnikova, N.S.; Vorokh, A.S.; Enyashin, A.N.; Pervova, M.G.; Zapevalov, A.Y.; Saloutin, V.I.; Chupakhin, O.N. Photolysis of Polychlorobiphenyls in the Presence of Nanocrystalline TiO_2 and CdS/TiO_2. *React. Kinet. Mech. Catal.* **2019**, *126*, 1115–1134. [CrossRef]
198. Zhang, Y.; Nie, J.; Yuan, C.; Long, Y.; Chen, M.; Tao, J.; Wang, Q.; Cong, Y. CuO@Cu/Ag/MWNTs/Sponge Electrode-Enhanced Pollutant Removal in Dielectric Barrier Discharge (DBD) Reactor. *Chemosphere* **2019**, *229*, 273–283. [CrossRef] [PubMed]
199. Entezari, M.; Godini, H.; Sheikhmohammadi, A.; Esrafili, A. Enhanced Degradation of Polychlorinated Biphenyls with Simultaneous Usage of Reductive and Oxidative Agents over UV/Sulfite/TiO_2 Process as a New Approach of Advanced Oxidation/Reduction Processes. *J. Water Process Eng.* **2019**, *32*, 100983. [CrossRef]
200. Lei, M.; Wang, N.; Guo, S.; Zhu, L.; Ding, Y.; Tang, H. A One-Pot Consecutive Photocatalytic Reduction and Oxidation System for Complete Debromination of Tetrabromodiphenyl Ether. *Chem. Eng. J.* **2018**, *345*, 586–593. [CrossRef]
201. Lei, M.; Wang, Z.; Tang, Y.; Wang, H.; Zhu, L.; Tang, H. Peculiar and Full Debromination of Tetrabromodiphenyl Ether on Pd/TiO_2: A Competing Route through Hydro-Debromination and Coupling-Debromination. *Appl. Catal. B Environ.* **2020**, *275*, 119093. [CrossRef]
202. Chen, K.; Wang, X.; Xia, P.; Xie, J.; Wang, J.; Li, X.; Tang, Y.; Li, L. Efficient Removal of 2,2′,4,4′-Tetrabromodiphenyl Ether with a Z-Scheme Cu_2O-(RGO-TiO_2) Photocatalyst under Sunlight Irradiation. *Chemosphere* **2020**, *254*, 126806. [CrossRef]
203. Zhang, Y.; Dong, S.; Wang, H.; Tao, S.; Kiyama, R. Biological Impact of Environmental Polycyclic Aromatic Hydrocarbons (EPAHs) as Endocrine Disruptors. *Environ. Pollut.* **2016**, *213*, 809–824. [CrossRef]
204. Nguyen, V.-H.; Phan Thi, L.-A.; van Le, Q.; Singh, P.; Raizada, P.; Kajitvichyanukul, P. Tailored Photocatalysts and Revealed Reaction Pathways for Photodegradation of Polycyclic Aromatic Hydrocarbons (PAHs) in Water, Soil and Other Sources. *Chemosphere* **2020**, *260*, 127529. [CrossRef]
205. Martínez-Vargas, B.L.; Cruz-Ramírez, M.; Díaz-Real, J.A.; Rodríguez-López, J.L.; Bacame-Valenzuela, F.J.; Ortega-Borges, R.; Reyes-Vidal, Y.; Ortiz-Frade, L. Synthesis and Characterization of N-ZnO/p-MnO Nanocomposites for the Photocatalytic Degradation of Anthracene. *J. Photochem. Photobiol. A Chem.* **2019**, *369*, 85–96. [CrossRef]
206. Mukwevho, N.; Gusain, R.; Fosso-Kankeu, E.; Kumar, N.; Waanders, F.; Ray, S.S. Removal of Naphthalene from Simulated Wastewater through Adsorption-Photodegradation by ZnO/Ag/GO Nanocomposite. *J. Ind. Eng. Chem.* **2020**, *81*, 393–404. [CrossRef]
207. Rachna; Rani, M.; Shanker, U. Sunlight Mediated Improved Photocatalytic Degradation of Carcinogenic Benz[a]Anthracene and Benzo[a]Pyrene by Zinc Oxide Encapsulated Hexacyanoferrate Nanocomposite. *J. Photochem. Photobiol. A Chem.* **2019**, *381*, 111861. [CrossRef]

208. Rachna; Rani, M.; Shanker, U. Enhanced Photocatalytic Degradation of Chrysene by Fe_2O_3@ZnHCF Nanocubes. *Chem. Eng. J.* **2018**, *348*, 754–764. [CrossRef]
209. Dong, C.-D.; Chen, C.-W.; Kao, C.-M.; Chien, C.-C.; Hung, C.-M. Wood-Biochar-Supported Magnetite Nanoparticles for Remediation of PAH-Contaminated Estuary Sediment. *Catalysts* **2018**, *8*, 73. [CrossRef]
210. Qin, Z.; Zhao, Z.; Jiao, W.; Han, Z.; Xia, L.; Fang, Y.; Wang, S.; Ji, L.; Jiang, Y. Coupled Photocatalytic-Bacterial Degradation of Pyrene: Removal Enhancement and Bacterial Community Responses. *Environ. Res.* **2020**, *183*, 109135. [CrossRef]
211. Cai, H.; Sun, L.; Wang, Y.; Song, T.; Bao, M.; Yang, X. Unprecedented Efficient Degradation of Phenanthrene in Water by Intimately Coupling Novel Ternary Composite Mn_3O_4/MnO_2-Ag_3PO_4 and Functional Bacteria under Visible Light Irradiation. *Chem. Eng. J.* **2019**, *369*, 1078–1092. [CrossRef]
212. Guan, S.H.; Zhao, K.F.; Tong, Q.; Rao, Q.X.; Cheng, L.; Song, W.; Zhang, Q.C.; Wang, X.L.; Song, W.G. A Review of Photocatalytic Materials Application on Nonylphenol Degradation. *Environ. Chall.* **2021**, *4*, 100172. [CrossRef]
213. Tang, C.; Huang, X.; Wang, H.; Shi, H.; Zhao, G. Mechanism Investigation on the Enhanced Photocatalytic Oxidation of Nonylphenol on Hydrophobic TiO_2 Nanotubes. *J. Hazard. Mater.* **2020**, *382*, 121017. [CrossRef]
214. Niu, B.; Cai, J.; Song, W.; Zhao, G. Novel Electrochemical Pretreatment for Preferential Removal of Nonylphenol in Industrial Wastewater: Biodegradability Improvement and Toxicity Reduction. *Environ. Sci. Technol.* **2020**, *54*, 1258–1266. [CrossRef]
215. Dong, C.-D.; Chen, C.-W.; Tsai, M.-L.; Chang, J.-H.; Lyu, S.-Y.; Hung, C.-M. Degradation of 4-Nonylphenol in Marine Sediments by Persulfate over Magnetically Modified Biochars. *Bioresour. Technol.* **2019**, *281*, 143–148. [CrossRef]
216. Xu, P.; Chen, M.; Lai, C.; Zeng, G.; Huang, D.; Wang, H.; Gong, X.; Qin, L.; Liu, Y.; Mo, D.; et al. Effects of Typical Engineered Nanomaterials on 4-Nonylphenol Degradation in River Sediment: Based on Bacterial Community and Function Analysis. *Environ. Sci. Nano* **2019**, *6*, 2171–2184. [CrossRef]